Tribological Properties of Ultrananocrystalline Diamond Films at High Temperature and Controlled Atmosphere

By

REVATI RANI
Enrolment No: PHYS 02 2016 04 002

Indira Gandhi Centre for Atomic Research, Kalpakkam

A thesis submitted to the
Board of Studies in Physical Sciences

In partial fulfillment of requirements
for the Degree of

DOCTOR OF PHILOSOPHY
of
HOMI BHABHA NATIONAL INSTITUTE

December, 2019

Homi Bhabha National Institute

Recommendations of the Viva Voce Committee

As members of the Viva Voce Committee, we certify that we have read the dissertation prepared by **REVATI RANI** entitled **"Tribological Properties of Ultrananocrystalline Diamond Films at High Temperature and Controlled Atmosphere"** and recommend that it may be accepted as fulfilling the thesis requirement for the award of Degree of Doctor of Philosophy.

N.V. Chandra Shekr 29-6-2020

Chairman - Dr. N. V. Chandra Shekar **Date:**

28/6/'20

Guide / Convener - Dr. M. Kamruddin **Date:**

* Aug. 6, 2020

Examiner - Prof. Noritsugu Umehara **Date:**

Member 1- Dr. T. R. Ravindran **Date:** 29/6/2020.

TRRavindran

Member 2- Dr. B. Sundaravel **Date:**

B. Sundaravel 29/6/2020

Member 3- Dr. Shaju K Albert **Date:** 29/6/2020.

Final approval and acceptance of this thesis is contingent upon the candidate's submission of the final copies of the thesis to HBNI.

I/We hereby certify that I/we have read this thesis prepared under my/our direction and recommend that it may be accepted as fulfilling the thesis requirement.

* The viva voce exam was conducted in video conference mode. Subsequently the signature was obtained from the external examiner.

Date: 28/6/'20

Place: Kalpakkam

Dr. M. Kamruddin
(Guide)

STATEMENT BY AUTHOR

This dissertation has been submitted in partial fulfillment of requirements for an advanced degree at Homi Bhabha National Institute (HBNI) and is deposited in the library to be made available to borrowers under rules of the HBNI.

Brief quotations from this dissertation are allowable without special permission, provided that accurate acknowledgement of source is made. Requests for permission for extended quotation from or reproduction of this manuscript in whole or in part may be granted by the Competent Authority of HBNI when in his or her judgment the proposed use of the material is in the interests of scholarship. In all other instances, however, permission must be obtained from the author.

Revati Rani

(Revati Rani)
Ph.D Candidate

DECLARATION

I, hereby declare that the investigation presented in the thesis has been carried out by me. The work is original and has not been submitted earlier as a whole or in part for a degree / diploma at this or any other Institution / University.

Revati Rani

(Revati Rani)

Ph.D Candidate

LIST OF PUBLICATIONS

Journals:

1) **Revati Rani**, K.J. Sankaran, K. Panda, N. Kumar, K. Ganesan, S. Chakravarty, I-Nan Lin; Tribofilm formation in ultrananocrystalline diamond film, **Diamond Relat. Mater.** 78 (**2017**) 12–23.
2) **Revati Rani,** K. Panda, N. Kumar, K.A. Titovich, K.V. Ivanovich, S.A. Vyacheslavovich, I-Nan Lin; Tribological properties of ultrananocrystalline diamond films: Mechanochemical transformation of sliding interfaces, **Sci. Rep.** 8 **(2018)** 283−298.
3) **Revati Rani,** K. Panda, N. Kumar, K.J. Sankaran, R. Pandian, M. Ficek, R. Bogdanowicz, K. Haenen, I-Nan Lin; Triboenvironment dependent chemical modification of sliding interfaces in ultrananocrystalline diamond nanowall film: Correlation with friction and wear, **J. Phys. Chem. C** 122 **(2018)** 945−956.
4) **Revati Rani,** K. Panda, N. Kumar, K.J. Sankaran, K. Ganesan, I-Nan Lin; Tribological properties of ultrananocrystalline diamond films in inert and reactive tribo-atmospheres: XPS depth-resolved chemical analysis, **J. Phys. Chem. C** 122 **(2018)** 8602−8613.

Conferences:

1) **Revati Rani**, N. Kumar, I-Nan Lin; Tribological properties of ultrananocrystalline diamond nanowire thin film: Influence of sliding counterbodies, International Conference on Thin Films **ICTF-2017**, 13–17 Nov, 2017 at NPL-CSIR, New Delhi, India. [**Oral** presentation]
2) **Revati Rani**, N. Kumar, I-Nan Lin; Ultrananocrystalline diamond film: Tribological studies against metal and ceramic balls, 9th International Conference on Industrial Tribology **ICIT-2017**, 6–9 Dec, 2017, Kolkata, India. [**Oral** presentation]
3) **Revati Rani**, N. Kumar, I-Nan Lin; Ultrahigh wear resistance of ultrananocrystalline diamond nanowall thin film, International Nanotribology Forum: Nanoscale Effects in Macrotribology **INF NanoGoa-2018**, 8–12 Jan, 2018 at Dona Sylvia Beach Resort, Goa, India. [**Poster** presentation & awarded **full scholarship (~1500USD)** for conference participation]

4) **Revati Rani**, N. Kumar, I-Nan Lin; Tribological properties of ultrananocrystalline diamond thin films: Role of intrinsic hydrogen, International Conference on Nano Science and Technology **ICONSAT-2018**, 21–23 March, 2018 at IISc, Bengaluru, India organised by CeNS, Bengaluru. [**Poster** presentation]

5) **Revati Rani**, N. Kumar, I-Nan Lin; Smart ultrananocrystalline diamond thin films for tribological applications, 5th International Conference on Nanoscience and Nanotechnology **ICONN-2019**, 28–30 January, 2019 at SRM Institute of Science and Technology, Chennai, India. [**Oral** presentation]

6) **Revati Rani**, N. Kumar, I-Nan Lin; Tribological studies of surface modified ultrananocrystalline diamond thin films under inert and reactive gaseous tribo-atmospheric media, 26th International Symposium on Metastable, Amorphous and Nanostructured Materials **ISMANAM-2019**, 8–12 July, 2019 at Raintree, Annasalai, Chennai, India organized by IIT-Madras. [**Poster** presentation]

IGC article

- **Revati Rani**; High temperature and vacuum tribological properties of ultrananocrystalline diamond thin films, **Young Officer Forum**, **IGC Newsletter**, ISSN 0972-5741, Volume 116 **(April, 2018)** 10−14. [**Invited** article]

Other Journal publications (not included in thesis):

1) K.K. Mishra, **Revati Rani**, N. Kumar, T.R. Ravindran, K.J. Sankaran, I-Nan Lin; High pressure Raman spectroscopic studies on ultrananocrystalline diamond thin films: Anharmonicity and thermal properties of grain boundary, **Diamond Relat. Mater.** 80 **(2017)** 45–53.

2) K. Panda, **Revati Rani**, N. Kumar, K.J. Sankaran, J.Y. Park, K. Ganesan, I-Nan Lin; Dynamic friction behavior of ultrananocrystalline diamond films: A depth-resolved chemical phase analysis, **Ceram. Int.** 45 **(2019)** 23418–23422.

3) D.D. Kumar, **Revati Rani**, N. Kumar, K. Panda, A.M.K. Kirubaharan, P. Kuppusami, R. Baskaran; Tribochemistry of TaN, TiAlN and TaAlN coatings under ambient atmosphere and high-vacuum sliding conditions, **Appl Surf. Sci.** 499 **(2020)** 143989–143999.

Revati Rani

(Revati Rani)
Ph.D Candidate

ACKNOWLEDGEMENTS

I am heartily pleased to acknowledge all those individuals who have made this doctoral thesis work possible with their support, suggestions and encouragements.

First and foremost, I sincerely thank to Dr. M. Kamruddin, my research supervisor for his guidance, significant suggestions and consistent support towards me. I also express my sincere gratitude to Dr. Niranjan Kumar (former research supervisor) who introduced me with the tribology field. He has been a consistent source of learning for me throughout this research work.

I am grateful to Prof. I-Nan Lin's group from Tamkang University, Taiwan for providing me UNCD samples and experimental help. I am very much thankful to Dr. K.J. Sankaran from Hasselt University, Belgium; Dr. K. Panda from IBS, Republic of Korea; Dr. K. Ganesan and Dr. R. Pandian from MSG, IGCAR for providing timely experimental support and fruitful technical discussions.

I sincerely thank to Dr. N.V. Chandra Shekar, my Doctoral Committee Chairman; Dr. T.R. Ravindran, Dr. B. Sundaravel and Dr. Shaju K Albert, DC Members for time to time valuable suggestions to improve the quality of this research work.

I express my sincere gratitude to Dr. R. Rajaraman, Dean Physical Sciences for his timely suggestions and encouragement.

I thankfully acknowledge Dr. A.K. Bhaduri, Director, IGCAR; Dr. Shaju K Albert and Dr. G. Amarendra (former), Director, MSG & MMG; Dr. S. Dhara and Dr. A.K. Tyagi (former), Head, SND for providing their support to pursue this research work.

I express my sincere gratitude to Dr. Tom Mathews and Dr. S. Dash (former), Head, TFCS for always being very kind and supportive towards me.

On personal front, I would like to acknowledge my family members for their love and care towards me. My mother also being my best friend always stood by me in every situation.

I am thankful to my training school batchmate friends. I cherished each and every moment that we spent together.

Last but not the least, I wish to bow down to my beloved Guru for giving me the most precious gift in my life which otherwise I could never even imagine.

Revati Rani

(Revati Rani)

CONTENTS

Page No.

ABSTRACT i

LIST OF FIGURES iii

LIST OF ABBREVIATIONS viii

CHAPTER 1 INTRODUCTION

1.1. The need of smart advanced materials for tribology application 1

1.2. Carbon based materials for tribology applications 1

1.3. Phase diagram of carbon based materials 2

1.4. Crystal structure of diamond 3

1.5. Growth processes of nano/ultranano crystalline diamond films 4

1.6. The applications of UNCD thin films 7

1.7. The parameters affecting the tribological properties of nanostructured diamond films 8

1.8. Tribological contact mechanisms in nanostructured diamond films 9

1.9. Motivation for present thesis work 13

1.10. References 15

CHAPTER 2 EXPERIMENTAL METHODS

2.1. Introduction 23

2.2. Film deposition 23

2.3. Characterization techniques 25

- 2.3.1. High-Resolution transmission electron microscope and Electron energy loss spectroscopy 25
- 2.3.2. Field emission scanning electron microscope and Energy dispersive X-ray spectroscopy 25
- 2.3.3. Atomic force microscopy 26
- 2.3.4. Raman spectroscopy 27
- 2.3.5. X-Ray photoelectron spectroscopy 28
- 2.3.6. Surface profilometer 29
- 2.3.7. Tribology tests 29

2.4. References 32

CHAPTER 3 THE EFFECT OF LOCAL PHASE COMPOSITION ON THE TRIBOLOGICAL PROPERTIES OF UNCD FILMS

3.1. Introduction 33

3.2. Experimental 34

3.3. Results and discussion 34

3.3.1. The morphological analysis of UNCD films 34

3.3.2. The microstructural analysis of UNCD films 35

3.3.3. The friction and wear analysis of UNCD films 38

3.3.3.1. Friction behavior 38

3.3.3.2. Wear behavior 39

3.3.4. The topographical analysis of wear tracks 40

3.3.4.1. 2D and 3D AFM topographical images 40

3.3.4.2. Topographical dynamics of secondary phase nanoparticles in $UNCD_N$ films 43

3.3.5. The chemical analysis of wear track in $UNCD_N$ films 44

3.3.5.1. EDX mapping of wear track 44

3.3.5.2. High-resolution XPS analysis of wear track 45

3.4. Tribology mechanism 47

3.5. Conclusions 47

3.6. References 48

CHAPTER 4 THE EFFECT OF GASEOUS TESTING ENVIRONMENT ON THE TRIBOLOGICAL PROPERTIES OF UNCD FILMS AND ADDRESSING THE RUN-IN REGIME ISSUE

4.1. Introduction 51

4.2. Experimental 52

4.3. Results and discussion 52

4.3.1. The depth-resolved surface chemical analysis of films 52

4.3.2. The depth-resolved surface topographic analysis of films 55

4.3.3. The depth-resolved structural phase analysis of films 56

4.3.4. The gas dependent friction and wear behavior of UNCD Films 57

4.3.5. The chemical analysis of alumina ball scar 59
  4.3.5.1. EDX analysis 59
  4.3.5.2. XPS analysis 60
4.3.6. The tribological mechanisms 63
  4.3.6.1. Ambient tribo-atmospheric condition 63
  4.3.6.2. N_2 tribo-atmospheric conditions 63
  4.3.6.3. Ar tribo-atmospheric condition 64
  4.3.6.4. CH_4 tribo-atmospheric condition 64
4.4. Conclusions 65
4.5. References 66

CHAPTER 5 HIGH TEMPERATURE AND HIGH VACUUM TRIBOLOGICAL PROPERTIES OF UNCD FILMS

5.1. Introduction 71
5.2. Experimental 72
5.3. Results and discussion 72
  5.3.1. Morphological, microstructural and chemical analysis of UNCD films 72
  5.3.2. Friction and wear properties of UNCD films 74
  5.3.3. The morphological and elemental compositional analysis of sliding interface 75
  5.3.4. The chemical phase structural analysis of sliding interface 78
  5.3.5. The local chemical bonding nature of sliding interface 80
  5.3.6. The tribological mechanism 82
5.4. Conclusions 83
5.5. References 84

CHAPTER 6 THE ROLE OF INTRINSIC HYDROGEN ON THE TRIBOLOGICAL PROPERTIES OF UNCD FILMS IN HIGH VACUUM TRIBO-CONDITIONS

6.1. Introduction 87
6.2. Experimental 88
6.3. Results and discussion 88

6.3.1. The topographical and chemical analysis of UNCD films 88
6.3.2. The morphological and microstructural analysis of UNCD films 90
6.3.3. Friction and wear properties of UNCD films 94
6.3.4. Tribo-induced deformation behavior of UNCD films 94
6.3.5. The chemical phase structural analysis of sliding interface 96
6.3.5.1. The dynamics of transferlayer formation with sliding process 98
6.3.6. The elemental analysis of sliding interface 100
6.3.7. The tribology mechanism 100
6.4. Conclusions 102
6.5. References 104
CHAPTER 7 SUMMARY AND FUTURE SCOPE
7.1. Summary of the thesis 107
7.2. Future scope 108

Homi Bhabha National Institute

SYNOPSIS OF Ph.D. THESIS

1. **Name of the Student:** REVATI RANI
2. **Name of the Constituent Institution:** IGCAR-Kalpakkam
3. **Enrolment No. :** PHYS02201604002
4. **Title of the Thesis:** Tribological properties of ultrananocrystalline diamond films at high temperature and controlled atmosphere
5. **Board of Studies:** Physical Sciences

SYNOPSIS

For efficient functioning of any tribological contact in mechanical devices, the mitigation of friction force and wear loss is the primary need and for achieving this, the systematic understanding of the governing tribo-mechanisms is important. The tribological properties of materials depend on their intrinsic parameters e.g. chemical phase composition, morphology and microstructure which basically includes the orientation of the crystalline phase, hardness, elastic modulus, fracture toughness, grain size, grain boundary phase composition, surface roughness and surface inertness etc. The crystalline diamond films find attractive place for tribology applications due to their unique microstructure and chemical properties. Diamond possesses inertness, high thermal conductivity, extremely high hardness and high elastic modulus properties which are desirable for tribological applications. Based upon the grain size, the diamond films can be further classified into micro and nano/ultranano crystalline diamond films. Primary reason for relatively high friction and wear in microcrystalline diamond films compared to other diamond forms is mainly large grain size, high roughness and high energy of the specific orientation of the crystalline plane. Many research reports state that the tribological properties of diamond films are found to improve with the decrease in their grain size. Diamond thin films with the grain size of the order of few nanometers (<10 nm) are known as ultrananocrystalline diamond (UNCD) films. The UNCD grains are surrounded by relatively wider disordered crystal area (thickness ~ few Å) known as grain boundaries. Many of the earlier reports state that the grain boundaries of UNCD films play an important role for all of its outstanding properties e.g. field emission, thermal and tribological properties etc. The core atoms of grain are sp^3 bonded ordered carbon atoms whereas the grain boundaries constitute transpolyacetylene (*t-PA*) segments, short range sp^2 and sp^1 hybridized disordered carbon atoms. The UNCD films can be deposited on suitable substrate using microwave plasma enhanced chemical vapor deposition (MPECVD) system employing either CH_4/Ar or CH_4/N_2 plasma media at relatively low substrate temperature of 400-700^{o}C compared to hot filament chemical vapor deposition (HFCVD) system. These films are of current interest because of their potential applications in nanoscale systems due to improved field emission, better optoelectronic behavior and robust tribological properties, e.g. exceptionally ultralow friction coefficient and high wear resistance properties. These films also find wide range of application in areas such as cutting tools, mechanical assembly components, bio-devices such as joint prosthesis, micro/nano electromechanical systems (MEMS/NEMS) and many more.

The friction and wear behavior of UNCD films is sensitive to intrinsic parameters like microstructure, morphology and chemical phase composition mainly graphite and amorphous carbon (*a-C*) occupying the grain boundaries of sp^3 hybridized diamond nanocrystals. In the literature, the ultralow friction value and high wear resistance of UNCD films are generally explained by *a-C* and graphitic phase present in the grain boundary. Furthermore, the tribological properties of UNCD films show strong dependence on extrinsic parameters like temperature, humidity, specific gaseous environment and vacuum tribo-conditions etc. Many research reports suggest that the main governing tribo-mechanisms in carbon-based materials are either passivation or graphitization. But, these mechanisms are still not yet fully understood and need to be validated using experimental means. It is observed that the friction coefficient of UNCD films deposited in N_2/CH_4 plasma media gradually decreases to ultralow value while sliding against ZrO_2 ball in ambient tribo-condition. Some reports propose that the graphitic tribolayer is formed in the wear track during sliding process. But there is not much experimental evidence supporting for the same. Furthermore, run-in behavior is always a big concern for effective tribological performance of any mechanical device. The comprehensive gas dependent tribological study of UNCD films in both chemically inert and reactive gaseous media is also less reported in literature. This study specifically finds important place for tribological application areas where tribo-contacts are exposed to specific gaseous environment. The ultralow friction value is observed in UNCD films in N_2 gaseous ambience which is believed to be due to formation of nitrogen terminated contact interface. But there is no experimental proof validating the same till date. Many reports suggest that UNCD films are good candidate for high temperature tribological application areas as well. It is quite hard to have the comprehensive understanding of governing mechanism of friction and wear behavior in these films in high vacuum and high temperature tribo-conditions. Besides this, there are many other factors like tribo-chemical transformation at contact interface which is sensitive to contact stress, test temperature and environment etc. further complicate the understanding of tribo-mechanisms. The passivation of dangling bonds and conversion of sp^3 into sp^2/*a-C* mainly depends on temperature and tribo-environmental conditions. Moreover, UNCD films show high friction value under high vacuum tribo-conditions which is supposed to be due to the lack of external passivation mechanism.

Thus, the present thesis work examines some of the issues pertaining to the comprehensive tribological mechanistic understanding of the UNCD films. The tribolayer characteristic in UNCD films is analyzed employing various experimental tools e.g. AFM, FESEM, EDX and XPS etc. Novel technique of low energy Ar^+ ion sputtering process is proposed to address the run-in issue in UNCD films. Furthermore, comprehensive surface chemical analysis of tribo-interfaces is carried out in these films to reveal the governing tribological mechanisms in distinct inert and reactive gaseous atmospheres. The suitable tribo-mechanism for improved superlubrication behavior of UNCD films in high temperature and high vacuum tribo-conditions is also investigated by carrying out the extensive surface characterization of the sliding interfaces. The tribo-mechanism of low friction value for hydrogenated UNCD films in high vacuum tribo-conditions is extensively studied. The comprehensive thesis work is arranged in seven chapters. The outline of each chapter is presented below.

Chapter 1: Introduction

This chapter provides a brief introduction to the topics, e.g. the need of smart advanced materials for tribology applications, potential carbon-based materials for tribology applications, introduction to diamond films, uniqueness of UNCD films over other diamond forms, synthesis methods of UNCD films, deposition parameters optimization process etc. Brief introduction to UNCD films covering their microstructure, morphology, tribological properties and potential applications is also provided. The parameters either intrinsic or extrinsic affecting the tribological properties of diamond films is discussed briefly. The tribological contact mechanisms at various scales ranging from micro to nano scales are discussed. This chapter briefly provides literature review of the earlier works carried out in the tribology area of the UNCD films. The general comparison of tribological properties among various carbon-based films is also provided. The motivation behind the present thesis work towards the understanding of governing tribological mechanisms in modified and improved UNCD films to address the wide range of tribo-application areas is discussed. The outline of the entire thesis work is presented at the end of this chapter.

Chapter 2: Experimental Details

In this chapter, the experimental procedures involved in the synthesis and characterization of UNCD films are briefly explained. The details of MPECVD system employed for the synthesis of UNCD films and optimization process of various deposition parameters i.e. precursor gases composition, temperature, chamber pressure etc. is provided. The pretreatment seeding methods prior to film deposition process employed for enhanced film growth quality are also discussed in brief. Various experimental characterization techniques like FESEM, EDX, AFM, XPS, and micro-Raman spectroscopy etc. employed for the comprehensive microstructural, morphological and chemical analysis of UNCD films are discussed in brief. The detailed experimental setup used for tribological measurement of UNCD films is also presented. Wear profile measurement technique is also briefly discussed.

Chapter 3: The effect of grain boundary phase composition on the tribological properties of UNCD films

The effective role of grain boundary phase composition on the tribological properties of UNCD films is not yet fully understood. Two distinct UNCD films are deposited on Si substrate by varying the deposition parameters i.e. employing either CH_4/Ar plasma or CH_4/N_2 plasma media in MPECVD system. As a result, both UNCD films differ in terms of their grain boundary phase composition. The detailed microstructural, morphological and chemical structural characterization of these films is carried out. Two distinctly different trends of tribo-behaviors are observed in these two set of UNCD films. Interestingly, UNCD films deposited in CH_4/N_2 plasma media shows saturated ultralow friction value after short run-in regime. Special emphasis is given to understand the observed tribo-behavior in these UNCD films employing experimental characterization tools like AFM, EDX and XPS etc. to analyze the morphological and chemical changes inside the wear track during tribo-testing. The in-situ electrical contact resistance (ECR) measurement is also carried out during tribology test. All these results are inter-correlated to understand the underlying friction and wear mechanism in UNCD films. It is understood from the extensive experimental characterization that graphitic tribofilm is formed in wear track during the sliding process which provides ultralow friction value to UNCD films.

Chapter 4: The effect of gaseous testing environment on the tribological properties of UNCD films and addressing run-in regime issue

In the scientific literature, the run-in regime is understood as a result of the chemically adsorbed oxygen and oxy-functional contamination present at UNCD film surface. In this chapter, novel technique of low energy Ar^+ ion sputtering process is employed to address the run-in issue in UNCD films. Detailed morphological and chemical characterization of Ar^+ ion sputtered surface modified UNCD films is carried out. The comprehensive tribological behavior of these modified UNCD films is studied in inert and reactive gaseous environments i.e. ambient humid atmosphere, nitrogen (N_2), argon (Ar) and methane (CH_4) gas environments. It is observed that the run-in regime shortens with the increasing sputtered depth of UNCD films. Furthermore, wear resistance property is also found to improve in surface modified UNCD films. Extensive tribochemical analysis of tribo-interface is carried out employing EDX mapping and XPS characterization to understand the underlying tribo-mechanism of modified UNCD films in all distinct gaseous atmospheres. It is observed that the carbonaceous transferfilm is formed on ball counterbody in all tribo-cases. It is understood that the passivation mechanism by ambient species, dissociated N_2 and H_2 gas molecules which provide repulsive sliding interface is effective tribo-mechanism in ambient, N_2 and CH_4 gaseous media, respectively. Furthermore, weak physical adsorption of Ar gas atoms governs the observed tribo-response of UNCD films in Ar gaseous atmosphere.

Chapter 5: High temperature and high vacuum tribological properties of UNCD films

The UNCD films are promising candidates for high temperature tribological application areas. Thus, in this chapter, the detailed tribological analysis of UNCD films is carried out under high temperature and high vacuum tribo-conditions. The optimized deposition parameters are employed in MPECVD system to grow UNCD films. Detailed morphological, microstructural and chemical structural characterization of UNCD films is carried out. The comprehensive tribological tests of UNCD films are studied in ambient, high vacuum and high temperature high vacuum (HTHV) tribo-conditions. These UNCD films show surprisingly superlow friction value and ultrahigh wear resistance properties in HTHV tribo-atmosphere. The friction and wear behavior is investigated in all tribo-environments based on the distinct chemical structure of carbonaceous transferfilm formed at sliding counterbody employing FESEM, EDX, XPS and micro-Raman spectroscopy techniques. The shear-induced amorphization/graphitization and passivation mechanisms are validated for observed tribo-response of these UNCD films.

Chapter 6: The role of intrinsic hydrogen on the tribological properties of UNCD films in high vacuum tribo-conditions

It is studied in the previous chapter 5 that UNCD films show relatively high friction value and high wear in high vacuum tribo-conditions. Thus, in this chapter, novel method is employed to mitigate this adverse tribo-response of these films in high vacuum tribo-conditions. Novel hydrogenated UNCD films are deposited on Ti alloy substrate by tuning the deposition parameters in MPECVD system. To investigate the role of intrinsic hydrogen in UNCD films, two distinct sets of UNCD films are considered by varying the hydrogen concentration in deposition plasma media during growth process for comprehensive tribo-evaluation. Detailed morphological, microstructural and chemical structural characterization of these two distinct set of UNCD films is carried out. Interestingly, UNCD films having high hydrogen concentration show low friction and wear value compared to UNCD films having low hydrogen concentration in high vacuum tribo-conditions upto certain number of sliding cycles. Detailed tribo-chemical analysis of tribo-interfaces is carried out to understand the underlying tribo-mechanism in these UNCD films. The intrinsic hydrogen passivation mechanism is established in hydrogenated UNCD films at high vacuum tribo-conditions. Once intrinsic hydrogen supply is cut-off due to continuous sliding process, friction value goes to the high value. This study possibly opens up the doors for future inter-atmospheric space applications of UNCD films where these films are exposed to both ambient and high vacuum atmosphere.

Chapter 7: Summary and future scope

This chapter briefly summarizes the important research findings of the entire thesis work and also indicates about the future scope for this research work.

Journal publications out of PhD thesis work

1) ***Revati Rani***, K.J. Sankaran, K. Panda, N. Kumar, K. Ganesan, S. Chakravarty, I-Nan Lin "Tribofilm formation in ultrananocrystalline diamond film" ***Diamond Relat. Mater.*** 78 (**2017**) 12–23.
2) ***Revati Rani,*** K. Panda, N. Kumar, K.A. Titovich, K.V. Ivanovich, S.A. Vyacheslavovich, I-Nan Lin "Tribological properties of ultrananocrystalline diamond films: mechanochemical transformation of sliding interfaces" ***Sci. Rep.*** 8 **(2018)** 283−298.
3) ***Revati Rani,*** K. Panda, N. Kumar, K.J. Sankaran, R. Pandian, M. Ficek, R. Bogdanowicz, K. Haenen, I-Nan Lin "Triboenvironment dependent chemical modification of sliding interfaces in ultrananocrystalline diamond nanowall film: correlation with friction and wear" ***J. Phys. Chem. C*** 122 **(2018)** 945−956.
4) ***Revati Rani,*** K. Panda, N. Kumar, K.J. Sankaran, K. Ganesan, I-Nan Lin "Tribological properties of ultrananocrystalline diamond films in inert and reactive tribo-atmospheres: XPS depth-resolved chemical analysis" ***J. Phys. Chem. C*** 122 **(2018)** 8602−8613**.**

Other Journal publications not included in thesis

1) K.K. Mishra, ***Revati Rani***, N. Kumar, T.R. Ravindran, K.J. Sankaran, I-Nan Lin "High pressure Raman spectroscopic studies on ultrananocrystalline diamond thin films: Anharmonicity and thermal properties of grain boundary" ***Diamond Relat. Mater.*** 80 **(2017)** 45–53.
2) K. Panda, ***Revati Rani***, N. Kumar, K.J. Sankaran, J.Y. Park, K. Ganesan, I-Nan Lin "Dynamic friction behavior of ultrananocrystalline diamond films: A depth-resolved chemical phase analysis" ***Ceram. Int.*** **(2019)** https://doi.org/10.1016/j.ceramint.2019.08.045

Conference papers/presentations

1) ***Revati Rani***, N. Kumar, I-Nan Lin "Tribological properties of ultrananocrystalline diamond nanowire thin film: Influence of sliding counterbodies" International Conference on Thin Films ***ICTF-2017***, 13–17 Nov, 2017 at NPL-CSIR, New Delhi, India. [**Oral** presentation] https://arxiv.org/abs/1806.10765
2) ***Revati Rani***, N. Kumar, I-Nan Lin **"**Ultrananocrystalline diamond film: Tribological studies against metal and ceramic balls**"** 9th International Conference on Industrial Tribology ***ICIT-2017***, 6–9 Dec, 2017 at Vedic Village Spa Resort, Kolkata, India. [**Oral** presentation] https://arxiv.org/abs/1806.10302
3) ***Revati Rani***, N. Kumar, I-Nan Lin "Ultrahigh wear resistance of ultrananocrystalline diamond nanowall thin film" International Nanotribology Forum: Nanoscale Effects in Macrotribology ***INF NanoGoa-2018***, 8–12 Jan, 2018 at Dona Sylvia Beach Resort, Goa, India. [**Poster** presentation & awarded **full scholarship** for conference participation]
4) ***Revati Rani***, N. Kumar, I-Nan Lin "Tribological properties of ultrananocrystalline diamond thin films: Role of intrinsic hydrogen" International Conference on Nano

Science and Technology ***ICONSAT-2018***, 21–23 March, 2018 at IISc, Bengaluru, India organised by CeNS, Bengaluru. [**Poster** presentation]

5) ***Revati Rani***, N. Kumar, I-Nan Lin "Smart ultrananocrystalline diamond thin films for tribological applications" 5th International Conference on Nanoscience and Nanotechnology ***ICONN-2019***, 28–30 January, 2019 at SRM Institute of Science and Technology, Chennai, India. [**Oral** presentation]
6) ***Revati Rani***, N. Kumar, I-Nan Lin "Tribological studies of surface modified ultrananocrystalline diamond thin films under inert and reactive gaseous tribo-atmospheric media" 26th International Symposium on Metastable, Amorphous and Nanostructured Materials ***ISMANAM-2019***, 08–12 July 2019 at Raintree, Annasalai, Chennai, India organized by IIT-Madras. [**Poster** presentation]

IGC report/article

- Invited article "High temperature and vacuum tribological properties of ultrananocrystalline diamond thin films" under the category of "***Young Officer Forum***" ***IGC Newsletter***, ISSN 0972-5741, Volume 116 April, 2018.

Revati Rani

Signature of Student:

Date: 26 Sep. 2019

Doctoral Committee:

S. No.	Name	Designation	Signature	Date
1.	Dr. N. V. Chandra Shekar	Chairman	N.V. Chandra	26/9/19
2.	Dr. M. Kamruddin	Guide/ Convener		26/9/19
3.	Dr. T. R. Ravindran	Member	TR Ravindran	26/9/2019
4.	Dr. B. Sundaravel	Member	B Sundaravel	26/9/2019
5.	Dr. Shaju K Albert	Member		26/9/19

Homi Bhabha National Institute
(A university established under Section 3 of the UGC Act. 1956)
Indira Gandhi Centre for Atomic Research
Kalpakkam – 603 102 Tamil Nadu, India

PRE-SYNOPSIS SEMINAR

Date: 16th Sep, 2019

A Ph.D work titled **"Tribological properties of ultrananocrystalline diamond films at high temperature and controlled atmosphere"** has been carried out by **Ms. Revati Rani**, SO/D (**Enrolment No: PHYS 02 2016 04 002**), TFCS/SND/ANG/MSG. In accordance with the regulations of the Homi Bhabha National Institute (HBNI), the pre-synopsis seminar leading towards the submission of her Ph.D thesis will be held on,

Date : **26/09/2019 (Thursday)**
Time : **11.00 hrs**
Venue : **CMPL Seminar Hall**

Members of the centre and other specialists in the areas related to the subject of the thesis are invited to interact with the candidate, if they so desire, during the public Pre-Synopsis seminar.

All are invited to participate.

(M. Kamruddin)
Guide & Convener, Doctoral Committee

Copy to:

Director, IGCAR
Dean, Acedemic, HBNI, IGCAR
Chairman, Convener & Members, Physical Sciences, HBNI, IGCAR
IGCSC Members, IGCAR
BARC Training School, IGCAR
All notice boards, IGCAR

ABSTRACT

For efficient functioning of tribological contacts in any mechanical device, the mitigation of friction force and wear loss is the primary need. To achieve this, the systematic understanding of the governing tribo-mechanisms is important. Diamond possesses inertness, high thermal conductivity, extreme high hardness and high elastic modulus which are desirable for tribological applications. Diamond thin films with grain size in the range of few nanometers (<10 nm) are known as ultrananocrystalline diamond (UNCD) films. These films show improved field emission, better optoelectronic behavior and robust tribological properties i.e. ultralow friction coefficient and high wear resistance and thus, are suitable for a wide range of potential applications in cutting tools, mechanical assembly components, bio-devices like joint prosthesis and micro/nano-electromechanical systems etc. The friction and wear behavior of UNCD films are sensitive to their microstructure, morphology and local phase composition. The ultralow friction value and high wear resistance properties of UNCD films are generally correlated with *a-C* and graphitic phase present in the grain boundary. Furthermore, the tribological properties of UNCD films also show strong dependence on tribo-test conditions like humidity, specific gaseous environment, temperature and vacuum conditions etc. Thus, the present thesis work examines some of the issues pertaining to the improvement of the tribological properties of UNCD films and also the establishment of the governing tribological mechanisms under wide range of tribo-test conditions e.g. ambient, gaseous, high temperature and high vacuum.

The comprehensive study of effect of local phase composition on the tribological behavior of UNCD films and governing tribo-mechanisms is carried out. Two sets of UNCD films are deposited on Si substrate by employing either CH_4/Ar or CH_4/N_2 plasma media in microwave plasma enhanced chemical vapor deposition system. Two distinctly different trends of tribo-behaviors are observed in these UNCD films. The films deposited in CH_4/N_2 plasma media show saturated ultralow friction value after short run-in regime. While UNCD films deposited in CH_4/Ar plasma media show saturated friction value after long run-in. Based upon the tribo-chemical analysis of sliding interface, the graphitic tribofilm formation mechanism is established which provides steady ultralow friction and high wear resistance properties to UNCD films.

A novel technique of low energy Ar^+-ion sputtering process (1 keV) is employed to modify the UNCD film surface to address the run-in issue. The detailed gas dependent study of

tribological mechanism of Ar^+-ion sputtered UNCD films is carried out in inert and reactive gaseous environments of ambient humid atmosphere, nitrogen (N_2), argon (Ar) and methane (CH_4) gaseous media. It is observed that the run-in regime shortens with the increasing Ar^+-ion sputtered depth in UNCD films. The wear resistance property is also found to improve in surface modified UNCD films. Extensive tribo-chemical analysis of sliding interface is carried out to understand the underlying tribo-mechanism in modified UNCD films for all distinct gaseous atmospheres. The carbonaceous transferfilm is formed on ball counterbody in all tribo-cases. It is proposed that the passivation by dissociated N_2 and H_2 gas molecules which provide the repulsive sliding interface is effective tribo-mechanism in N_2 and CH_4 gaseous media, respectively. Furthermore, weak physical adsorption of Ar gas atoms governs the observed tribo-response of UNCD films in Ar atmosphere. High friction in ambient atmospheric condition is associated with the oxidation of the sliding interfaces.

The UNCD films are potential future materials for high temperature and high vacuum (HTHV) tribological applications. Thus, specific optimized deposition parameters are employed for the growth of UNCD films having nanowall like morphology to improve the HTHV tribological properties. These films show surprisingly superlow friction value and ultrahigh wear resistance properties in HTHV conditions. But these films show relatively high friction and wear in high vacuum tribo-conditions. Based upon the extensive tribo-chemical analysis of sliding interface, the shear-induced amorphization/graphitization and passivation mechanisms are established for observed tribo-response of UNCD films under distinct set of tribo-conditions.

Novel UNCD films are deposited on Ti alloy substrate by employing different hydrogen concentration in deposition plasma media for improvement in the tribological properties of these films in high vacuum conditions and understanding of underlying tribo-mechanisms. Interestingly, UNCD films having high hydrogen concentration show low friction and wear value up to certain number of sliding cycles in high vacuum tribo-conditions compared to UNCD films having low hydrogen concentration. The intrinsic hydrogen passivation mechanism is proposed for observed low friction value in high vacuum tribo-conditions for hydrogenated UNCD films. Once intrinsic hydrogen supply is exhausted due to continuous sliding process, then friction rises to the high value. All tribo-mechanisms are established in UNCD films by carrying out the extensive sliding interface characterization employing experimental tools like AFM, FESEM, EDX, XPS, Raman spectroscopy etc.

LIST OF FIGURES

Figure No.	Figure Description	Page No
Fig. 1.1.	Phase diagram of carbon based materials	2
Fig. 1.2.	Crystal structure of diamond lattice	3
Fig. 1.3.	Schematic of wide range applications of UNCD thin films	8
Fig. 1.4.	Tribological contact mechanisms: (a) macromechanical, (b) material transfer, (c) micromechanical, (d) tribochemical and (e) nanomechanical contact	10
Fig. 2.1.	Schematic of microwave plasma enhanced chemical vapour deposition system	24
Fig. 2.2.	(a) Photograph of HTHV micro-tribometer coupled with Raman spectrometer, (b) photograph of standard micro-tribometer and (c) schematic diagram of ball-on-disc geometry standard micro-tribometer	30
Fig. 3.1.	Morphology of (a) UNCD$_{Ar}$ and (b) UNCD$_{N}$ films with cross-sectional images shown in the insets	35
Fig. 3.2.	Microstructural analysis of (a_i) UNCD$_{Ar}$ and (b_i) UNCD$_{N}$ films, (a) BF and (b) c-DF TEM images of UNCD films with their corresponding SAED patterns shown in insets, (c) HRTEM structure image corresponding to designated region A in panel (a) for both cases	36
Fig. 3.3.	(a) core-loss and (b) plasmon-loss EELS spectra for UNCD films	37
Fig. 3.4.	Friction coefficient and ECR trend in (a) UNCD$_{Ar}$ and (b) UNCD$_{N}$ films	38
Fig. 3.5.	Wear analysis of UNCD$_{Ar}$ and UNCD$_{N}$ films at (a) 500 m and (b) 5 m sliding distances, left side: 2D wear profile of wear tracks, right side: optical images of wear tracks and ball scars in the sliding combination of UNCD$_{Ar}$/ZrO_2 and UNCD$_{N}$/ZrO_2	39
Fig. 3.6.	AFM analysis of UNCD$_{Ar}$ films: (a_i & a_{ii}) surface topography of film and topography of wear track formed at different sliding distances: (b_i & b_{ii}) 100 m and (c_i & c_{ii}) 500 m, sliding direction common for all	41

images

Fig. 3.7. AFM analysis of $UNCD_N$ films: (a_i & a_{ii}) surface topography of film and topography of wear track formed at different sliding distances: (b_i & b_{ii}) 100 m and (c_i & c_{ii}) 500 m, grooves shown by arrow marks, sliding direction common for all images 42

Fig. 3.8. 3D topography of nanodomains formed in the wear track of $UNCD_N$ films at sliding distance of 500 m: scan a to h corresponds to nano domains under respective forces: 10, 20, 40, 60, 80, 100, 120 & 140 nN 44

Fig. 3.9. EDX spectra of wear track in $UNCD_N$ films: (a) Backscattered electron (BSE) image selected for EDX mapping and (a_i) High-resolution image inside wear track, (b) C-K edge, (c) O-K edge, (d) Si-K edge, (e) Zr-L edge and (f) superimposed images of all elements, atomic percentage (at.%) is also shown 45

Fig. 3.10. (a) Survey XPS spectra of (a_i) $UNCD_N$ film surface and (a_{ii} & a_{iii}) at two different spots as shown in the micrograph inside the wear track, HR C1s XPS of (b) film surface and (c) inside wear track 46

Fig. 4.1. Depth-resolved XPS survey spectra: (a_1) as-deposited UNCD film surface and (a_2–a_7) for sputtered film surface of depths 6, 12, 18, 24, 30 and 36 nm 53

Fig. 4.2. Depth-resolved high-resolution C1s spectra: (a_1) as-deposited UNCD film surface and (a_2–a_7) for sputtered film surface of depths 6, 12, 18, 24, 30 and 36 nm, (b) (A/B): sp^2/sp^3 and A/(B+C+D) ratio: $sp^2/(sp^3$+oxygen complexes) and (c) binding energy shift of components A and B at film surface (a_1) and sputtered depth of film surface (a_2-a_7) 54

Fig. 4.3. 3D topography of films: (a) as-deposited, (b) F_{Ar}_15 and (c) F_{Ar}_30 films, (d) average roughness (R_a) and RMS roughness (R_q) of d_1: as-deposited, d_2: F_{Ar}_15 and d_3: F_{Ar}_30 films 55

Fig. 4.4. (a) Raman spectra of films and (b) peak position of v_1, v_2, v_3, D and G bands and I(D)/I(G) ratio: (a_1) as-deposited, (a_2) F_{Ar}_15 and (a_3) F_{Ar}_30 films 56

Fig. 4.5. Friction coefficient vs sliding cycles (1k = 1000 cycles) of (a) as-Deposited, (b) F_{Ar}_15 and (c) F_{Ar}_30 films and (d) friction coefficient with standard deviation of (d_1) as-deposited, (d_2) F_{Ar}_15 and (d_3) F_{Ar}_15 films in different tribo-atmospheric conditions: Amt, N_2, Ar, and CH_4 media 57

Fig. 4.6. (a) Optical image of wear tracks and ball scars, (b) wear dimensions of sliding interfaces in bar graph: (a_1, b_1) as-deposited, (a_2, b_2) F_{Ar}_15 and (a_3, b_3) F_{Ar}_30 films in different tribo-atmospheric conditions: Amt, N_2, Ar, and CH_4 media 58

Fig. 4.7. In the left panel: EDX elemental mapping of the alumina ball scar while sliding against F_{Ar}_30 films, In the right panel: EDX spectra of the whole area mapping of ball scar developed in (a) ambient, (b) N_2, (c) Ar and (d) CH_4 media 60

Fig. 4.8. Optical image of alumina ball scar in (a_1) Amt, (b_1) N_2, (c_1) Ar and (d_1) CH_4 atmosphere, and corresponding high-resolution XPS spectra: (a_2−d_2) C1s spectra, (a_3−d_3) O1s spectra, (b_4) N1s spectra and (c_4) Ar2p spectra, (e_1) (A/B): sp^2/sp^3 and A/(B+C+D): $sp^2/(sp^3+C{-}O/C{-}OH+C{=}O)$ ratio and (e_2) binding energy shift of sp^2 (A) and sp^3 (B) components: (a_2−d_2 in x-axis) in (e_1) and (e_2) correspond to (a_2) Amt, (b_2) N_2, (c_2) Ar and (d_2) CH_4 tribo-atmosphere 61

Fig. 5.1. (a) SEM image of UNCD film surface and (b) HRTEM image of typical nanowall feature of film surface, (c & d) Raman spectra and (e & f) XPS: (c & e) UNCD film surface at RT and (d & f) UNCD film surface exposed to temperature of ~ 623 K 73

Fig. 5.2**.** (a) Friction coefficient vs sliding cycles of UNCD films: (a_1) ambient, (a_2) HV and (a_3) HTHV tribo-conditions, two-dimensional wear track profile in (b) ambient, (c) HV and (d) HTHV tribo-conditions, SEM images of the corresponding wear tracks are embedded for each condition 74

Fig. 5.3. (a) SEM image of wear track and EDX locations a_1-a_3 with (b) corresponding EDX spectra b_1-b_3 of each locations, (c) SEM image of ball scar and selected locations c_1-c_3 with (d) corresponding EDX spectra 76

d_1-d_3 of each location; in ambient condition

Fig. 5.4. (a) SEM image of wear track and EDX location in red rectangle with (b) corresponding EDX spectra of whole image selected in red rectangle, (c) SEM image of ball scar and (d) corresponding EDX spectra; in HV condition 77

Fig. 5.5. (a) SEM image of wear track and EDX locations a_1-a_2 with (b) corresponding EDX spectra b_1-b_2 of each locations, (c) SEM image of ball scar and selected locations c_1-c_2 with (d) corresponding EDX spectra d_1-d_2 of each location; in HTHV condition 77

Fig. 5.6. Raman spectra: (a & b) ambient, (c & d) HV and (e & f) HTHV, (a, c & e) inside the wear track of UNCD films and (b, d & f) corresponding alumina ball scars, optical images of wear tracks and corresponding alumina ball scars are also embedded for each tribo-condition 78

Fig. 5.7. D, G and I(D)/I(G) ratio of wear track in three different tribo-conditions, first half and second half panel in x-axis describes peak shift of D and G bands and I(D)/I(G) ratio, respectively; in each wear track more than 20 Raman spectra are obtained and error bar is also given 80

Fig. 5.8. XPS spectra: (a & b) ambient, (c & d) HV and (e & f) HTHV, (a, c & e) survey XPS and (b,d &f) corresponding C1s HR-XPS spectra of alumina ball scars 81

Fig. 6.1. (a_i, a_{ii}) Surface topography, (b_i, b_{ii}) Raman spectra) and (c_i, c_{ii}) SIMS depth profile of: (a_i, b_i, c_i) UNCD(6%H_2) and (a_{ii}, b_{ii}, c_{ii}) UNCD(0%H_2) films 89

Fig. 6.2. Surface morphology of (a) UNCD(6%H_2) films and (b) UNCD(0%H_2) films 90

Fig. 6.3. (a_i, b_i) BF(TEM) micrograph and (a_{ii}, b_{ii}) c-DF micrograph: (a_i, a_{ii}) UNCD(6%H_2) and (b_i,b_{ii}) UNCD(0%H_2) films with SAED shown in inset 91

Fig. 6.4. HRTEM image of (a) UNCD(6%H_2) and (b) UNCD(0%H_2) films, FT_0 92

image in ‘a’ and ‘b’ shows the Fourier transformed diffractogram corresponding to entire structure image in ‘a’ and ‘b’, whereas FT_1 to FT_4 are FT images corresponding to areas 1 to 4, respectively

Fig. 6.5. (a) Carbon edge core-loss EELS and (b) plasmon-loss EELS of (I) UNCD(6%H_2) and (II) UNCD(0%H_2) films, respectively 93

Fig. 6.6. Friction coefficient of (a) UNCD(6%H_2) and (b) UNCD(0%H_2) films in ambient and high vacuum (3×10^{-6} mbar) tribology conditions 94

Fig. 6.7. Wear track morphology of (a) UNCD(6%H_2) and (b) UNCD(0%H_2) films; tribology condition: ambient 95

Fig. 6.8. Wear track morphology of (a) UNCD(6%H_2) and (b) UNCD(0%H_2) films; tribology condition: high vacuum (3×10^{-6} mbar) 95

Fig. 6.9. Raman spectra at various locations of: (a_i, b_i) wear track and (a_{ii}, b_{ii}) ball scar in the sliding combination of: (a_i, a_{ii}) UNCD(6%H_2)/Al_2O_3) and (b_i, b_{ii}) UNCD(0%H_2)/ Al_2O_3; tribology condition: ambient 96

Fig. 6.10. Raman spectra at various locations of: (a_i, b_i) wear track and (a_{ii}, b_{ii}) Ball scar in the sliding combination of: (a_i, a_{ii}) UNCD(6%H_2)/Al_2O_3 and (b_i, b_{ii}) UNCD(0%H_2)/Al_2O_3; tribology condition: high vacuum (3×10^{-6} mbar) 97

Fig. 6.11. Raman spectra at various locations of: (a_i-a_{iii}) wear track and (b_i-b_{iii}) ball scar in the sliding combination of UNCD(6%H_2)/Al_2O_3 at sliding cycles of: (a_i, b_i) 2×10^3, (a_{ii}, b_{ii}) 5×10^3 and (a_{iii}, b_{iii}) 1×10^4; tribology condition: high vacuum (3×10^{-6} mbar) 99

Fig. 6.12. (a_i, a_{ii}) Backscattered diffraction (BSD) image, (b_i, b_{ii}) EDX Elemental mapping image of square area indicated in panel (a_i, a_{ii}) and (c_i, c_{ii}) EDX spectra of alumina ball scar sliding against UNCD(0%) films; (a_i, b_i, c_i) for ambient and (a_{ii}, b_{ii}, c_{ii}) for high vacuum tribology conditions 100

Chapter 1

Introduction

This chapter briefly describes about the need of smart materials suitable for tribological applications. Carbon based materials and specifically diamond thin films are discussed briefly. Literature review of the earlier works carried out in the tribology area of distinct form of nanostructured diamond films i.e. ultrananocrystalline diamond films is presented. Motivation behind the current thesis work is explained in brief.

1.1. The need of smart advanced materials for tribology applications

One of the most significant aspect of the tribological study of any contacting mechanical system is to reduce/control the friction and wear losses and also to enhance the tribo-performance by using the smart materials. Moreover, low friction and wear free motion of any mechanical device is the primary requirement for enhanced energy efficiency and longer lifetime. The high friction and wear loss affect the tribo-performance of any mechanical device at scales ranging from macro to nano scale [1]. A huge amount of energy is lost in the form of heat during tribological processes. There is a huge demand to develop smart energy efficient materials for tribological applications to address the environmental safety concerns as well. Thus, considerable amount of energy can be saved by designing the materials such that they possess surface inertness, low roughness and high hardness properties to minimise the friction and wear loss [1]. Carbon in both crystalline and amorphous forms is quite suitable for improved tribological response [2-9].

1.2. Carbon based materials for tribological applications

Carbon based materials place an important role in the tribology area for enhanced tribological applications. Carbon with atomic number 6 is a unique element in the periodic table which can exhibit multiple stable hybridization states of sp^1, sp^2 and sp^3. Moreover, carbon can bond strongly with numerous other atoms e.g. nitrogen, oxygen and hydrogen as well. In last few decades, a variety of carbon based thin films are developed which find an attractive place for tribological purposes [2-9]. Diamond thin films are one such important class of carbon based thin films which show superior tribological properties. Diamond film forms nano/ultranano crystalline diamond (NCD/UNCD) films show improved tribological properties i.e. low/ultralow friction coefficient and high wear resistance [7-13]. Moreover, NCD thin films show similar mechanical properties to diamond which is hardest known material [14]. Furthermore, one more interesting form of carbon based thin films is diamond-like carbon (DLC) films. The main compositional variable in these DLC films is the carbon hybridization states specifically sp^2 versus sp^3 bonds and atomic H content [15]. It is reported that a particular form of DLC films known as near frictionless carbon (NFC) show superlow friction and extremely high wear resistant properties [15].

1.3. Phase diagram of carbon based materials

The phase diagram of carbon based materials is shown in Fig. 1.1 [16]. With the advent of new deposition systems in last few decades, the diamond films growth process is feasible at relatively relaxed conditions of temperature and pressure compared to conventional methods.

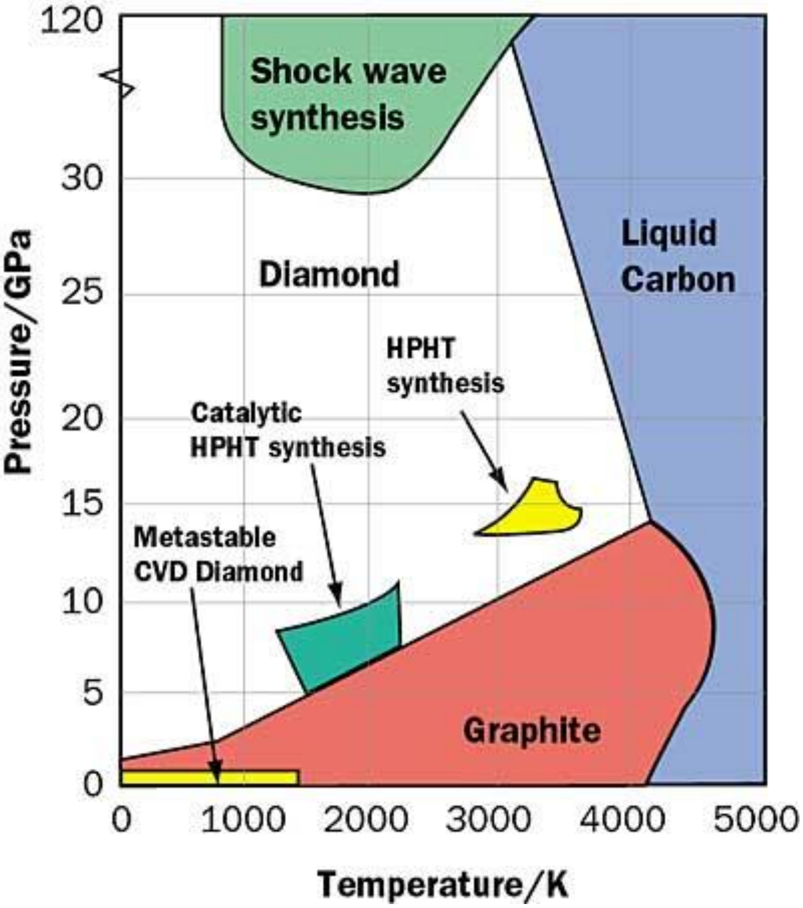

Fig. 1.1. *Phase diagram of carbon based materials [from Ref (16)]*

Chemical vapor deposition (CVD) is an extensively used deposition technique for the synthesis of diamond thin films. The metastable nature of diamond makes its growth process difficult. It is clearly shown in the Fig. 1.1 that the CVD diamond growth regime is surrounded by the graphitic one. The nucleation of both diamond and graphite crystals is favorable for given set of deposition parameters. At normal temperature and pressure conditions, the activation energy of graphite is just few eV higher than diamond which results in the formation of diamond. But once the diamond crystal is formed, the only way it can be converted into graphite is by completely destroying the diamond lattice.

1.4. Crystal structure of diamond

Diamond is having a face centered cubic (FCC) crystal lattice structure having a unique arrangement of carbon atoms. The diamond structure is constituted of total eight corner atoms, six face centered atoms and four other atoms from adjacent interpenetrating lattices offset by one quarter of the body diagonal as shown in the Fig. 1.2 [17]. Each carbon atoms is bonded to four nearest carbon atoms in a covalent fashion which provides it a strong sp^3 character. The distinct chemical bonding arrangement of diamond provides it numerous surprising material properties e.g. high hardness, high thermal conductivity, low friction and high wear resistance etc. The diamond possesses a lattice constant (a_0) of 3.567 Å, bond length of 1.54 Å and atomic density of 1.76×10^{23} cm^{-3}.

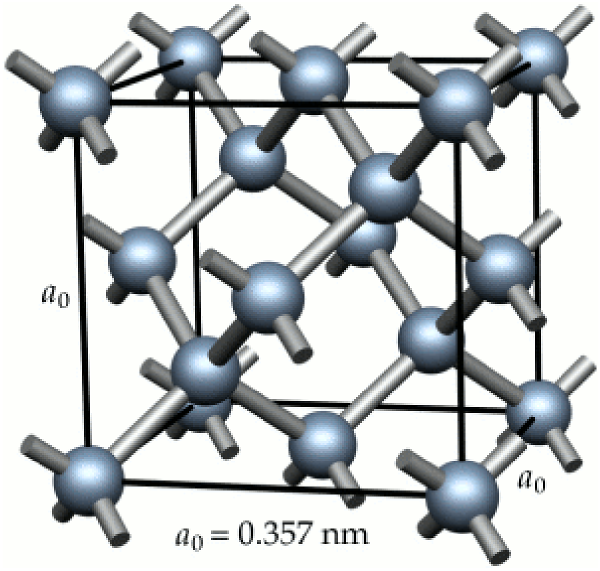

Fig. 1.2. *Crystal structure of diamond lattice [from Ref (17)]*

1.5. Growth processes of nano/ultranano crystalline diamond films

Diamond thin films can be grown on any suitable substrate using CVD techniques e.g. either hot filament CVD (HFCVD) or microwave plasma CVD (MPCVD) systems by employing hydrogen-rich chemistry [H_2(balance)/CH_4(0.1–4%)] [18,19]. The CVD systems can easily produce synthetic diamonds by creating the conditions necessary for the carbon atoms in a gaseous phase to settle on a substrate in the crystalline form. The synthetic deposition process of diamonds has gained a lot of attention in the materials research community as it allows exploring many of the new applications which were considered too expensive before. However, deposition of diamond films on nondiamond substrate requires surface pretreatment or seeding procedures employing chemical, physical or mechanical means to enhance the nucleation process. If the initial nucleation density is well below $10^{10}/cm^2$, the microcrystalline diamond (MCD) films are formed with thickness in the few micrometers range 0.1–5 μm [19]. Moreover, these MCD films possess a columnar like grain structure. The large grains of size ~1–5 μm further coarsen with the increasing thickness of these films and therefore, root mean square (RMS) roughness value is generally ~10% of the entire film thickness. Furthermore, if the initial nucleation densities are very high ($>10^{12}/cm^2$), then relatively smooth and high quality NCD films are grown with the thickness range of 0.03–5 µm. Due to very high nucleation density, the grain size and surface roughness of NCD films do not change considerably for a film thickness up to few microns and these films still exhibit columnar structure [14]. The NCD films can be grown employing 0.1–1% CH_4 gas in H_2 plasma media at relatively low substrate temperatures of ~720°C [14]. The NCD films have a much smaller grain size ~20–200 nm compared to MCD and RMS roughness value lies in the few nanometers range i.e. 10–30 nm. Moreover, if CH_4 gas fraction is further increased to 4%, very fine grained and smooth NCD films are grown. But these films possess slightly high fraction of nondiamond carbon i.e. sp^2 bonds and noncrystalline configurations. But once the diamond nuclei are formed from the seeding process, the growth is usually homoepitaxial (including twinning and defect configuration) on the seeds along with some nondiamond carbon incorporated in the grain boundaries.

In CVD process of diamond, the main growth species is CH_3 radicals [19]. The atomic hydrogen is necessary to drive the hydrogen abstraction reactions in the growth plasma media. Thus, the CH_3 adsorption site is prepared by abstracting a hydrogen atom from the hydrogen-terminated diamond surface and then from the adsorbed CH_3 and nearby surface sites, thereby allowing the carbon atoms to be incorporated into diamond lattice site. In addition to this, the atomic hydrogen also preferentially etches the undesirable graphitic and amorphous carbon phases which grow simultaneously along with the diamond phase. Though the atomic hydrogen also etches the diamond phase but at a relatively significant lower rate.

There is also one more relatively new form of diamond thin films named as UNCD films which can be grown employing an Ar-rich/CH_4 plasma media [Ar (99%)/CH_4(1%)] in MPCVD system. The carbon dimers (C_2) are formed either from the collision-induced methane fragmentation in the Ar plasma media or by the thermal conversion process via following reactions:

$$2CH_4 \rightarrow C_2H_2 + 3H_2$$

$$C_2H_2 \rightarrow C_2 + H_2$$

Though the Ar-rich/CH_4 plasma produces a complex mixture of carbon i.e. C_2 dimers and hydrocarbon species including CH_3C_2H, C_2H_2 and other hydrocarbons; the C_2 dimers play a significant role in the UNCD nucleation and growth process [20]. Some theoretical calculations in the literature report that the C_2 dimers have low activation energy (~6 kcal/mol) for insertion into the film growing interface and thus, establishing the unique growth characteristics of UNCD films. Though the C_2 population is high in the plasma, the population near the surface is low and thus, other hydrocarbon radicals e.g. CH_3, C_2H etc. also significantly participate in the growth process [20,21]. This model still could not elucidate the low-temperature growth characteristics of UNCD films with a modest growth rate. The unique characteristics of the UNCD film growth process is such that the plasma contains significantly small fraction of hydrogen (~1.5%) which is mainly from the thermal decomposition of methane to acetylene in the plasma. The plasma media employed for UNCD film growth process is generally 1% CH_4/99% Ar for 2.45 GHz and 915 MHz MPECVD systems. The UNCD nucleation and growth process results in a nanostructure comprised of equiaxed grains of size ~3–5 nm and atomically abrupt ~0.4 nm wide grain boundaries. Moreover, the UNCD films grown employing nitrogen rich gas plasma consists of 7–10 nm grain size and 1–2 nm wide grain boundaries [22,23].

The mechanical and thermal properties of nanostructured diamond films mainly depend on the growth parameters, nucleation pretreatment methods and surface chemistry. The Young’s modulus and hardness values of UNCD and NCD films are reported to approach the single crystal diamond which is several times higher than Si/SiO_2. The Poisson’s ratio is reported to be

0.057±0.038 for HFCVD grown UNCD films and 0.12±0.04 for MPCVD grown NCD films [11,14] which is close to that of single crystal diamond. Furthermore, two seeding methods employed prior to growth process are compared. One involves the mechanical polishing of the silicon substrate using micron sized diamond powder whereas other employs the ultrasonic agitation of the silicon substrate in an alcohol solution containing nanodiamond powder [24]. In both the cases, Weibull statistics is followed indicating that the pre-existing flaws govern the brittle failure of these films. For nucleation process by mechanical polishing, the fracture strength ranges from 1.74–2.26 GPa whereas with ultrasonic seeding process, it lies in the range of 4.08–5.03 GPa. The difference in these values arises due to the variation in the size of the largest defect present in the given volume of material. Much denser and smoother UNCD films are obtained using ultrasonic seeding process and thus, minimizing the risk of defect prone regions at the underside of the film. Interestingly, the fracture strength normally scale up with the specimen volume and not the surface area [24] indicating that the flaws occurring at the film substrate interface leads to defective structure throughout the bulk of the film. This feature specifically highlights the critical roles of seeding and nucleation process. Similar behavior is observed in the case of NCD films where the effect of seeding density on the Young's modulus and thermal diffusivity is reported earlier [14]. The Young's modulus of NCD films grown with low nucleation densities (10^{10}/cm^2) was approximately half of the films grown with much high nucleation density ($\geq 10^{12}$/cm^2). For diamond films grown with high nucleation density, the Young's modulus approaches approximately the value for single crystal diamond or high quality CVD grown polycrystalline diamond films (1120 GPa). The higher nucleation density during the growth process leads to rapid film coalescence and thus, lowers the volume of voids and non-diamond carbon forms at the nucleation site (film/substrate interface) which influences the Young's modulus and fracture toughness of these films and also provides surprisingly high thermal diffusivity [14].

The role of surface chemistry including the amorphous carbon participation at the nucleation site during the growth process of NCD/UNCD films along with different pretreatment methods was further studied using surface sensitive spectroscopy tools e.g. photoelectron emission microscopy coupled with near edge X-ray absorption fine structure spectroscopy (PEEM-NEXAFS), Auger electron spectroscopy (AES) and X-ray photoelectron spectroscopy (XPS) [7,9,12,13]. These experiments enable the characterization of the chemistry and bonding configuration of UNCD and NCD film surfaces which influences the adhesion and friction properties of these diamond films. Since the underside of these films can be the part of tribological interface for a given micro/nano-electromechanical systems (MEMS/NEMS) device geometry and thus, this understanding becomes significant for better design and fabrication of the diamond based tribological devices [12].

Till today, UNCD films are the only diamond films which can be grown at temperatures as low as 350–400ºC on the wafer scale with complementary metal oxide semiconductor (CMOS) compatibility [22]. The variation in the thickness uniformity of UNCD films on 150 mm and 200 mm diameter silicon wafers is approximately ±5% and ±11%, respectively. Though the UNCD films growth rate is modest (~0.1–0.2 μm/h), the low growth temperature opens up the door way for the development of monolithically integrated UNCD-MEMS/NEMS/CMOS devices by integrating UNCD films with CMOS electronics which has a very limited thermal budget [22,25]. The MEMS/NEMS are an extension of integrated circuit (IC) technology where the electrical and mechanical subsystems are integrated together to convert physical stimuli and events to electrical, mechanical and optical signals and vice versa. Due to their smaller size (a few microns to a few tens of nanometers), a large number of devices can be batch fabricated on a single wafer with enhanced functionality. However, as the size of the device reduces, there are additional issues that happen due to the increased surface-to-volume ratio. Thus, the surface and interface properties become dominant at this micro/nano scale, driving the need to find suitable candidate materials. Diamond satisfies most of the expectations of MEMS/NEMS designers due to its extraordinary physical, chemical, mechanical and electrical properties. Specifically, UNCD/NCD based MEMS/NEMS devices are energy efficient compared to conventional silicon-based devices.

1.6. The applications of UNCD thin films

The UNCD films find a huge range of applications in the tribology area due to their unique microstructure and morphology. The UNCD thin films show superior tribological and field emission properties compared to bulk single crystalline diamond material [13,26]. The UNCD films are in high demand in enormous range of nanoscale systems. These films exhibit bio-medical compatibility [27,28], enhanced field emission properties [26,29], suitability for MEMS/NEMS systems [30], optoelectronic properties [31], reduced band gap [32], enhanced toughness [33] and enhanced tribological properties e.g. ultralow friction coefficient and extremely high wear resistance [13,34] etc. The schematic diagram illustrating broad application areas of UNCD films e.g. artificial retina, UNCD glaucoma valve, UNCD coated dental implant, UNCD coated Ti alloy based artificial hip implant, UNCD coated SiC seal, UNCD coated commercial NG/Cu anode for Li-ion batteries (LIB), Hybrid PZT/UNCD micro-resonator, PZT/UNCD NEMS system switch, UNCD deposited CMOS-chip and UNCD based atomic force microscopy tip etc. is shown in Fig. 1.3 below.

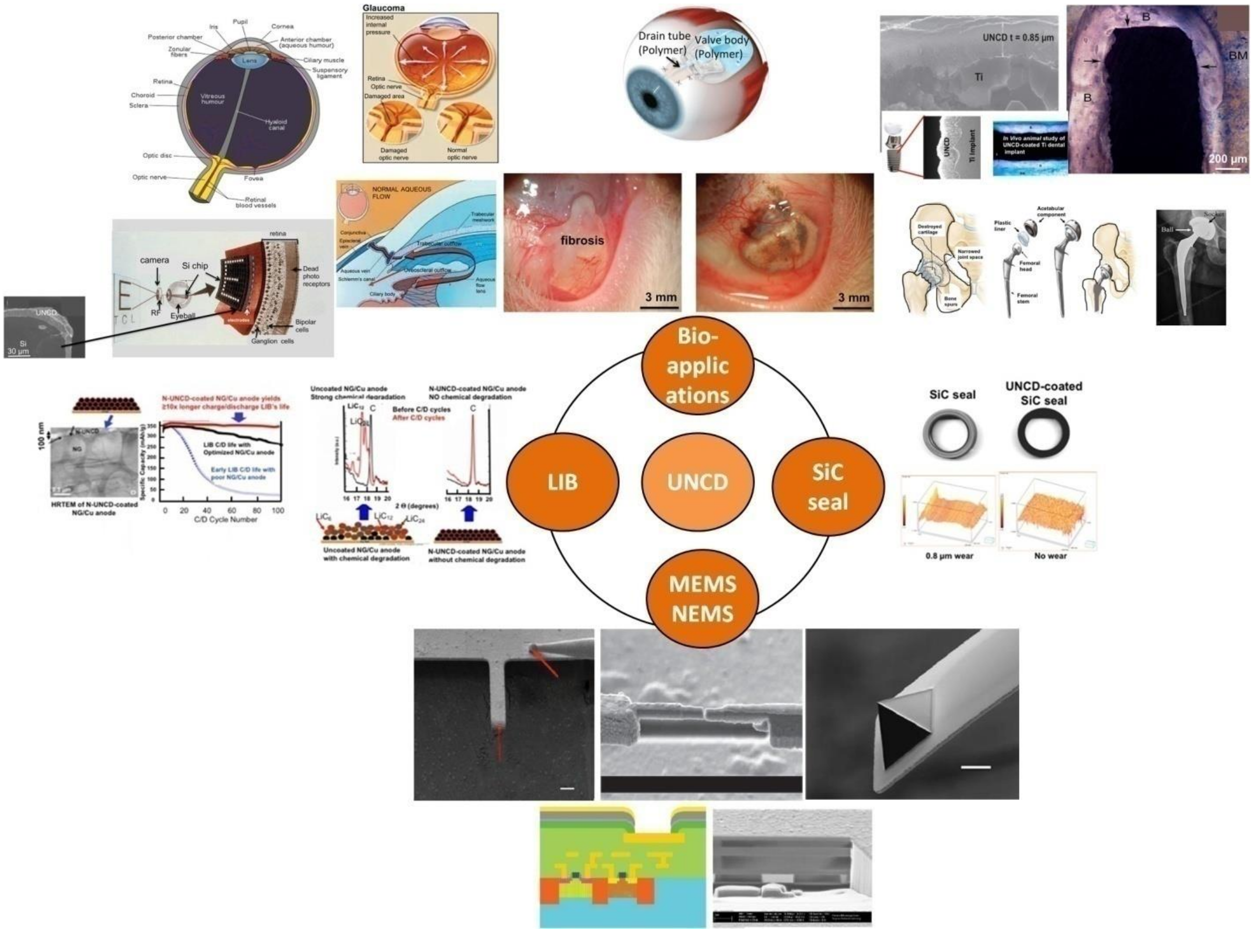

__Fig. 1.3.__ Schematic of wide range applications of UNCD thin films [images are taken from the references provided above]

1.7. The parameters affecting the tribological properties of nanostructured diamond films

The tailoring of the microstructure and phase segregation in nanocrystalline/amorphous carbon-based nanocomposite coatings leads to superior mechanical and tribological properties [35]. The plasma chemistry employed for the growth process controls the grain size and volume fraction of the grain boundary which is occupied by amorphous carbon (*a-C*) and graphitic phase in NCD/UNCD films [36,37]. The grain size, grain orientation, grain boundaries volume fraction, chemical phase composition, microstructure and surface morphology are key parameters which tailor the friction and wear behavior in nanostructured diamond films. The ultralow friction coefficient and superior wear resistance is observed in UNCD nanowire films. These films exhibit nanowire like morphology and each of the nanowire is constituted of many ultranano diamond grains. Post deposition process, these UNCD nanowire films are treated in hydrogen and oxygen plasma media [7,38]. It is reported that UNCD nanowire films consist of UNCD grains surrounded by sp^2 C=C/*a-C* bonded grain boundaries [37,39]. However, the grain boundary volume fraction significantly reduces after H_2/O_2 plasma post treatment [7,38]. In these films, low friction coefficient is understood as a result of the passivation mechanism of carbon dangling bonds and adsorption of atmospheric H_2O molecules [7,13,40-42].

Tribological properties of diamond films are also influenced by the experimental conditions like normal load, sliding speed, physical/chemical nature of the sliding counterbodies, tribo-test temperature and atmosphere [43-45] etc. It is reported that the atmospheric conditions can influence the sliding interfaces chemically, forming both weak and strong chemical bonds resulting in low and high friction behavior, respectively [44,46]. The friction and wear behaviors in UNCD films are not yet completely understood and needs further study for comprehensive understanding of the tribo-properties under wide range of tribological conditions.

1.8. Tribological contact mechanisms in nanostructured diamond films

A complete understanding of the tribological contact process is a difficult task because of the simultaneous occurrence of friction, wear and deformation through various mechanisms at different scales [1]. The tribological changes can take place in various forms e.g. the macro/micro/nano scale mechanical effects, the chemical effects and material transfer, as schematically shown in Fig. 1.4 [1]. The mechanism of the friction and wear behavior that is observed on macro scale is usually understood by the processes occurring at micro scale. Thus, microstructure and morphology of materials place a very important role from tribological understanding point of view. The micro mechanical tribological mechanisms describe the stress and strain generation at asperity-to-asperity level, the crack formation and propagation, material liberation and particle formation. In typical engineering contacts, these phenomena usually happen at micrometer scale and sometimes can go down even to nanometer scale. The chemical reactions taking place at the sliding interfaces during tribo-process can modify the composition and mechanical properties of outermost contact surface layer which has a significant influence on the friction and wear response.

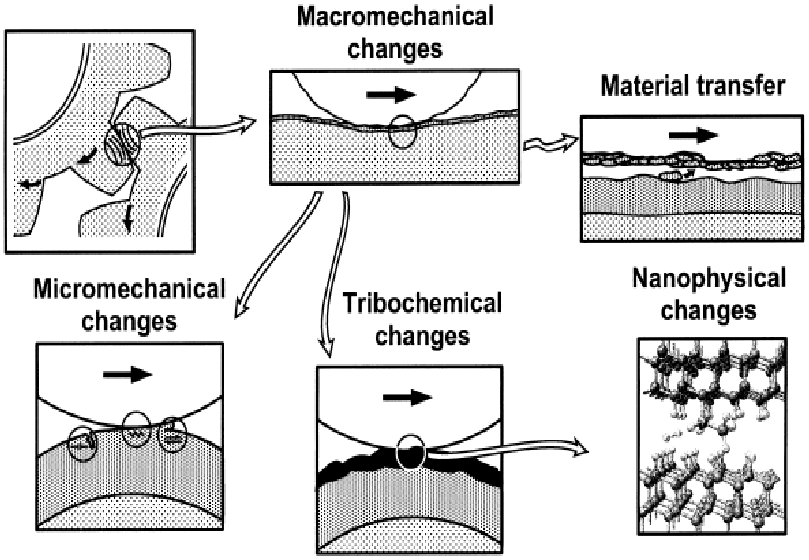

__Fig. 1.4.__ Tribological contact mechanisms: (a) macromechanical, (b) material transfer, (c) micromechanical, (d) tribochemical and (e) nanomechanical contact [from Ref (1)]

The chemical reactions occurring at the sliding surfaces are mainly influenced by the local contact pressures and flash temperatures which can sometimes reach upto 1000°C at spots where asperities collide directly. It is obviously beneficial if the substrate under the hard coating is as hard as possible to improve the load support and to decrease the real area of contact in order to avoid the brittle fracture of the coating by deformation process etc. Diamond being inert, hard and good thermal conductor is definitely a good candidate for tribological applications.

The ultralow friction value of polished diamond and DLC coatings is probably due to their very smooth surface so that interlocking and asperity ploughing effects are minimized and these hard coating reduces the ploughing component of the friction as well [47]. C.S. Abreu has established a self polishing mechanism that occurs when NCD films slide against diamond coated counterbody [48]. The friction value is high that results from the mechanical interlocking of diamond asperities. After run-in, steady state is observed where friction coefficient gradually saturates to ultralow value. It is reported by Tian group that the tribological properties improve with the decrease in the grain size of diamond [49]. The improvement in friction and wear response is correlated with the decrease in the roughness value and the enhancement of *a-C* and graphitic phase in the grain boundary. Moreover, the graphitic phase exhibits low shear resistance property mainly because of layered lattice structure of weakly bonded intra-graphitic planes. The synergistic action of ultranano diamond grains and graphitic phase improve the tribology properties of UNCD films.

The nano tribological properties of UNCD films i.e. nanoscale adhesion and friction were probed using AFM technique equipped with a diamond AFM tip that exactly mimics the single asperity contact of diamond sliding against diamond. The hydrogen plasma treatment is given to UNCD film surface for its H-termination and etching of nondiamond carbon present at film surface. Upon H-termination, the work of adhesion is reduced to 10 mJ/m^2 from 59.2 mJ/m^2 [12]. In contrast, Si-Si contacts exhibit the work of adhesion of 826±186 mJ/m^2 which arises from the hydrophilic interactions between the native oxide surfaces. Nanoscale friction is also found to reduce by more than a factor of two after H-termination process. From tribological point of view, H-terminated NCD surfaces perform similar to H-terminated single crystal diamond which is far better than silicon. The large scale friction measurements for self mated NCD surfaces showed low friction and wear even under relatively low humid tribological conditions which are usually considered unfavorable for diamond tribology [50]. Even at 1.0% relative humidity (RH) level, ultralow friction coefficient of value 0.04 was observed. Surface chemical imaging using PEEM, NEXAFS techniques demonstrated that low friction is indeed resulted by dissociative chemisorptions of water forming oxide- containing chemical groups on the surface. Though higher fraction of sp^2 bonds is formed on film surface, there was no evidence of graphite formation. Studies of silicon nitride and NCD surfaces also showed low friction under high load conditions [50]. These experiments demonstrate the possibility of controlling the nanoscale adhesion and friction properties of diamond films by tuning the surface chemistry.

Moreover, phase transformation at sliding interface further makes understanding of tribological behavior difficult [40]. Furthermore, such transformation is sensitive to the contact stress, test temperature, test environment and chemical affinity of sliding counterbodies etc. [34,40,44,45]. It is observed in many reports that during tribo-testing, diamond and DLC convert to *a-C* and graphite phases which mainly influence the friction and wear behavior in these materials [51-55]. In one of the studies, it is reported that the removal of the surface oxide layer is responsible for the observed high friction run-in regime in DLC films in different atmospheres

[56]. Moreover, chemical transformation of sp^3 into *a-C* phase is also possible in this regime mainly because of the high frictional energy [40,57-60]. Alazizi et al. have reported that carbon based films are useful for tribological applications in gaseous and vapor phase environments [61]. It is also reported by many that the intrinsic hydrogen passivation mechanism is active controlling the friction and wear behavior of hydrogenated DLC and diamond films [40,62,63]. In hydrogen free carbon films, water vapor passivates the sliding interfaces in ambient humid conditions resulting in low friction value [13,42]. DLC and diamond films showed high friction and wear value in inert gas and vacuum conditions due to active participation of the dangling σ bonds at sliding interface [42,64-66]. However, an ultralow friction value was observed in hydrogenated DLC and hydrogenated amorphous carbon (*a-C*:H) films in N_2 and Ar atmospheres [67,68]. Moreover, the friction value of these films was higher in O_2 and ambient conditions. The electrostatic repulsion of nitrogen terminated sliding interfaces is responsible for the reduction in the friction value of *a-C*:H and diamond films [69]. Moreover, the experiments carried out on diamond coatings sliding against ceramic surface in dry N_2 atmosphere showed that micro-graphitization mechanism takes place which results in ultralow friction value of 0.04 [70]. The ultralow friction value of DLC films in CH_4 atmosphere is correlated with the passivation of carbon dangling bonds at the sliding interfaces by hydrogen atoms/molecules which are chemically decomposed product of CH_4 gas [67].

The improvement in high temperature tribological properties of DLC and diamond films is a challenging task because of the phase transformation tendency of carbon structure at high temperature. The DLC films undergo gradual transformation from highly disordered/amorphous state to an increasingly ordered/graphitic state at elevated temperature in ambient atmosphere [71,72]. Though, the hydrogenated DLC films provide low friction up to 300°C for shorter sliding cycles. But these films wear out faster during repeated sliding process [71]. Moreover, friction value of these films tend to increase with increasing test temperature mainly due to the thermal desorption of water and other adsorbed species. The friction value and wear rate of thermally annealed polycrystalline diamond films were found to decrease due to carbonaceous transferfilm formation [73]. The graphitization/amorphization of diamond films has an adverse effect on friction and wear response in high vacuum conditions which is explained by the lack of external passivation mechanism [65,74]. Moreover, at higher temperature, tribological properties of UNCD films were considerably degraded and failure happened mainly due to the oxidation and amorphization/polymerization process at the sliding interface [75].

1.9. Motivation for present thesis work

Though a lot of research work is already done in UNCD tribology area but underlying tribo-mechanisms are not yet fully understood in different tribological conditions. The run-in behavior is always a big concern for effective tribological performance of any mechanical device. The comprehensive gas dependent tribological study of UNCD films in both chemically inert and reactive gaseous media is also less reported in literature. This study specifically finds important place for tribological application areas where tribo-contacts are exposed to specific gaseous environment. The UNCD films can be a future promising candidate for high temperature tribological application areas as well. Thus, it is important to have the comprehensive understanding of the governing mechanisms of friction and wear behavior in these films in high temperature and high vacuum tribo-conditions. Furthermore, UNCD films show high friction value under high vacuum tribo-conditions which is supposed to be due to the lack of external passivation mechanism. There are many factors like tribo-chemical transformation at contact interface which is sensitive to contact stress, test temperature and tribo-test environment etc. which complicate the understanding of governing tribo-mechanisms.

Thus, the current thesis work is devoted to improve the tribological properties of UNCD films under wide range of tribological conditions of distinct gaseous media, high temperature and high vacuum and also to have a comprehensive understanding of the governing tribological mechanisms. The comprehensive study of effect of local phase composition on the tribological behavior of UNCD films and governing tribo-mechanisms is carried out. The graphitic tribofilm formation mechanism for observed ultralow friction behavior in UNCD films is explored. Run-in issue is addressed to some extent employing novel Ar^+-ion sputtering technique. Gas dependent tribological mechanisms in UNCD films are studied comprehensively under inert and reactive gaseous environments. Enhancement in tribological properties of UNCD films in high temperature and high vacuum conditions is studied. The governing tribo-mechanisms for observed superlubrication properties of UNCD films at high temperature and high vacuum conditions are established. Improvement in tribological properties of UNCD films in high vacuum conditions and understanding of underlying tribo-mechanisms is carried out. Novel hydrogenated UNCD films are grown and intrinsic hydrogen passivation mechanisms are established for observed low friction value in high vacuum tribo-conditions. All tribo-mechanisms are studied by carrying out the comprehensive sliding interface characterization employing experimental tools e.g. AFM, FESEM, EDX, XPS, Raman spectroscopy etc. The current thesis work is definitely going to provide better understanding to researchers about governing tribological mechanisms in UNCD films under wide range of tribological conditions.

1.10. References

1) K. Holmberg, A. Matthews, H. Ronkainen, Coatings tribology–Contact mechanisms and surface design, Tribol. Int. 31 (1998) 107–20.
2) O. Auciello, A.V. Sumant, Status review of the science and technology of ultrananocrystalline diamond (UNCD™) films and application to multifunctional devices, Diamond Relat. Mater. 19 (2010) 699–718.
3) Y. Liao, R. Pourzal, M.A. Wimmer, J.J. Jacobs, A. Fischer, L.D. Marks, Graphitic tribological layers in metal-on-metal hip replacements, Science 334 (2011) 1687–90.
4) X. Liu, J. Yang, J. Hao, J. Zheng, Q. Gong, W. Liu, A near-frictionless and extremely elastic hydrogenated amorphous carbon film with self-assembled dual nanostructure, Adv. Mater. 24 (2012) 4614–17.
5) L. Pastewka, S. Moser, P. Gumbsch, M. Moseler, Anisotropic mechanical amorphization drives wear in diamond, Nat. Mater.10 (2011) 34–38.
6) D. Bernoulli, K. Häfliger, K. Thorwarth, G. Thorwarth, R. Hauert, R. Spolenak, Cohesive and adhesive failure of hard and brittle films on ductile metallic substrates: A film thickness size effect analysis of the model system hydrogenated diamond-like carbon (*a-C*:H) on Ti substrates, Acta. Mater. 83 (2015) 29–36.
7) R. Radhika, N. Kumar, K.J. Sankaran, R. Dumpala, S. Dash, M.S.R. Rao, **D. Arivuoli**, A.K. Tyagi, N.H. Tai, I.N. Lin, Extremely high wear resistance and ultralow friction behaviour of oxygen-plasma-treated nanocrystalline diamond films, J. Phys. D: Appl. Phys. 46 (2013) 425304–13.
8) N. Kumar, K. Panda, S. Dash, C. Popov, J.P. Reithmaier, B.K. Panigrahi, A.K. Tyagi, B. Raj, Tribological properties of nanocrystalline diamond films deposited by hot filament chemical vapor deposition, AIP Adv. 2 (2012) 032164–77.
9) A.V. Sumant, D.S. Grierson, J.E. Gerbi, J. Carlisle, O. Auciello, R.W. Carpick, Surface chemistry and bonding configuration of ultrananocrystalline diamond surfaces and their effects on nanotribological properties, Phys. Rev. B 76 (2007) 235429–39.
10) S.Y. Luo, J.K. Kuo, B. Yeh, J.C. Sung, C.W. Dai, T.J. Tsai, The tribology of nanocrystalline diamond, Mater. Chem. Phys. 72 (2001) 133–35.

11) V.P. Adiga, A.V. Sumant, S. Suresh, C. Gudeman, O. Auciello, J.A. Carlisle, R.W. Carpick, Mechanical stiffness and dissipation in ultrananocrystalline diamond microresonators, Phys. Rev. B 79 (2009) 245403–10.

12) A.V. Sumant, D.S. Grierson, J.E. Gerbi, J. Birrell, U.D. Lanke, O. Auciello, J.A. Carlisle, R.W. Carpick, Toward the ultimate tribological interface: Surface chemistry and nanotribology of ultrananocrystalline diamond, Adv. Mater. 17 (2005) 1039–45.

13) A.R. Konicek, D.S. Grierson, P.U.P.A. Gilbert, W.G. Sawyer, A.V. Sumant, R.W. Carpick, Origin of ultralow friction and wear in ultrananocrystalline diamond, Phys. Rev. Lett. 100 (2008) 235502–05.

14) J. Philip, P. Hess, T. Feygelson, J.E. Butler, S. Chattopadhyay, K.H. Chen, L.C. Chen, Elastic, mechanical and thermal properties of nanocrystalline diamond films, J. Appl. Phys. 93 (2003) 2164–71.

15) D.S. Grierson, R.W. Carpick, Nanotribology of carbon-based materials, Nanotoday 2 (2007) 12–21.

16) Electronic reference: http://phycomp.technion.ac.il/~anastasy/thesis/node6.html.

17) Electronic reference: http://m-newton.ex.ac.uk/research/qsystems/people/sque.togo/diamond/structure/.

18) J.E. Butler, H. Windischmann, Developments in CVD-diamond synthesis during the past decade, MRS Bull. 23 (1998) 22–27.

19) E.J. Dawnkaski, D. Srivastava, B.J. Garrison, Time dependent Monte Carlo simulations of H reactions on the diamond {001}(2×1) surface under chemical vapor deposition conditions, J. Chem. Phys. **102** (1995) 9401–11.

20) M. Sternberg, P. Zapol, L.A. Curtiss, Carbon dimers on the diamond (100) surface: Growth and nucleation, Phys. Rev. B 68 (2003) 205330–38.

21) P.W. May, M.N.R. Ashfold, Y.A. Mankelevich, Microcrystalline, nanocrystalline, and ultrananocrystalline diamond chemical vapor deposition: Experiment and modeling of the factors controlling growth rate, nucleation, and crystal size, J. Appl. Phys. 101 (2007) 53115–23.

22) A.V. Sumant, O. Auciello, H.C. Yuan, Z. Ma, R.W. Carpick, D.C. Mancini, Large area low temperature ultrananocrystalline diamond (UNCD) films and integration with CMOS devices for monolithically integrated diamond MEMS/NEMS-CMOS systems, Micro-

and Nanotechnology Sensors, Systems, and Applications, eds. T. George, M.S. Islam, A.K. Dutta (Proceedings of the SPIE-The International Society for Optical Engineering) Proceedings SPIE 7318 (2009) 731817–23.

23) J. Birrell, J.A. Carlisle, O. Auciello, D.M. Gruen, J.M. Gibson, Morphology and electronic structure in nitrogen-doped ultrananocrystalline diamond, Appl. Phys. Lett. 81 (2002) 2235–37.

24) H.D. Espinosa, B. Peng, B.C. Prorok, N. Moldovan, O. Auciello, J.A. Carlisle, D.M. Gruen, D.C. Mancini, Fracture strength of ultrananocrystalline diamond thin films-Identification of Weibull parameters, J. Appl. Phys. 94 (2003) 6076–84.

25) X. Xiao, J. Birrell, J.E. Gerbi, O. Auciello, J.A. Carlisle, Low temperature growth of ultrananocrystalline diamond, J. Appl. Phys. 96 (2004) 2232–39.

26) D. Pradhan, I.N Lin, Grain-size-dependent diamond-nondiamond composite films: Characterization and field-emission properties, ACS Appl. Mater. Interfaces 1 (2009) 1444–50.

27) O. Auciello, P. Gurman, M.B. Guglielmotti, D.G. Olmedo, A. Berra, M.J. Saravia, Biocompatible ultrananocrystalline diamond coatings for implantable medical devices, MRS Bull. 39 (2014) 621–29.

28) O. Auciello, Novel biocompatible ultrananocrystalline diamond coating technology for a new generation of medical implants, devices, and scaffolds for developmental biology, Biomater. Med. Appl. 1:1 (2017) 1–11.

29) K.J. Sankaran, S. Kunuku, K.C. Leou, N.H. Tai, I.N. Lin, Enhancement of the electron field emission properties of ultrananocrystalline diamond films via hydrogen post-treatment, *ACS Appl. Mater. Interface* 6 (2014) 14543–51.

30) A.V. Sumant, O. Auciello, R.W. Carpick, S. Srinivasan, J.E. Butler, Ultrananocrystalline and nanocrystalline diamond thin films for MEMS/NEMS applications, MRS Bull. 35 (2010) 281–88.

31) K.J. Sankaran, S. Kunuku, B. Sundaravel, P.Y. Hsieh, H.C. Chen, K.C. Leou, N.H. Tai, I.N. Lin, Gold nanoparticle–ultrananocrystalline diamond hybrid structured materials for high-performance optoelectronic device applications, Nano 7 (2015) 4377–85.

32) O.A. Williams, M. Nesladek, M. Daenen, S. Michaelson, A. Hoffman, E. Osawa, K. Haenen, R.B. Jackman, Growth, electronic properties and applications of nanodiamond, Diamond Relat. Mater. 17 (2008) 1080–88.

33) H.D. Espinosa, B. Peng, N. Moldovan, T.A. Friedmann, X. Xiao, D.C. Mancini, O. Auciello, J. Carlisle, C.A. Zorman, M. Merhegany, Elasticity, strength, and toughness of single crystal silicon carbide, ultrananocrystalline diamond, and hydrogen-free tetrahedral amorphous carbon, Appl. Phys. Lett. 89 (2006) 073111–13.

34) R. Rani, N. Kumar, A.T. Kozakov, K.A. Googlev, K.J. Sankaran, P.K. Das, S. Dash, A.K. Tyagi, I.N. Lin, Superlubrication properties of ultra-nanocrystalline diamond film sliding against a zirconia ball, RSC Adv. 5 (2015) 100663–73.

35) S. Zhou, L. Wang, Z. Lu, Q. Ding, S.C. Wang, R.J.K. Wood, Q. Xue, Tailoring microstructure and phase segregation for low friction carbon-based nanocomposites coatings, J. Mater. Chem. 22 (2012) 15782–92.

36) K.J. Sankaran, P.T. Joseph, H.C. Chen, N.H. Tai, I.N. Lin, Investigation in the role of hydrogen on the properties of diamond films grown using $Ar/H_2/CH_4$ microwave plasma, Diamond Relat. Mater. 20 (2011) 232–237.

37) Y. Tzeng, S. Yeh, W.C. Fang, Y. Chu, Nitrogen-incorporated ultrananocrystalline diamond and multi-layer-graphene-like hybrid carbon films, Sci. Rep. 4 (2014) 4531–37.

38) K.J. Sankaran, N. Kumar, H.C. Chen, C.L. Dong, A. Bahuguna, S. Dash, A.K. Tyagi, C.Y. Lee, N.H. Tai, I.N. Lin, Near frictionless behavior of hydrogen plasma treated diamond nanowire films, Sci. Adv. Mater. 5 (2013) 1–12.

39) R. Arenal, P. Bruno, D.J. Miller, M. Bleuel, J. Lal, D.M. Gruen, Diamond nanowires and the insulator-metal transition in ultrananocrystalline diamond films, Phys. Rev. B 75 (2007) 195431–41.

40) J.D. Schall, G. Gao, J.A. Harrison, Effects of adhesion and transfer film formation on the tribology of self-mated DLC contacts, J. Phys. Chem. C 114 (2010) 5321–30.

41) G.T. Gao, P.T. Mikulski, J.A. Harrison, Molecular-scale tribology of amorphous carbon coatings: Effects of film thickness, adhesion, and long-range interactions, J. Am. Chem. Soc. 124 (2002) 7202–09.

42) M.I.D.B. Bouchet, G. Zilibotti, C. Matta, M.C. Righi, L. Vandenbulcke, B. Vacher, J.M. Martin, Friction of diamond in the presence of water vapor and hydrogen gas. Coupling gas phase lubrication and first-principles studies, J. Phys. Chem. C 116 (2012) 6966−72.

43) N. Kumar, N. Sharma, S. Dash, C. Popov, W. Kulisch, J.P. Reithmaier, G. Favaro, A.K. Tyagi, B. Raj, Tribological properties of ultrananocrystalline diamond films in various test atmosphere, Tribol. Int. 44 (2011) 2042–49.

44) N. Sharma, N. Kumar, S. Dhara, S. Dash, M. Kamruddin, A.K. Tyagi, B. Raj, Tribological properties of ultrananocrystalline diamond film- Effect of sliding counterbodies, Tribol. Int. 53 (2012) 167–78.

45) R. Radhika, N. Kumar, S. Dash, A.K. Tyagi, I.N. Lin, Anomalous behavior of load dependent friction on ultrananocrystalline diamond film, Adv. Eng. Mater. 16 (2014) 1098–104.

46) R. Radhika, N. Kumar, A.T. Kozakov, K.J. Sankaran, S. Dash, A.K. Tyagi, N.H. Tai, I.N. Lin, Role of transfer layer on tribological properties of nanocrystalline diamond nanowire film sliding against alumina allotropes, Diamond Relat. Mater. 48 (2014) 6–18.

47) M.N. Gardos, Tribology and wear behavior of diamond in synthetic diamond: Emerging CVD science and technology, ed. K. E. Spear and J. P. Dismukes. John Wiley and Sons (1994) 419–502.

48) C.S. Abreu, F.J. Oliveira, M. Belmonte, A.J.S. Fernandes, R.F. Silva, J.R. Gomes, Grain size effect on self-mated CVD diamond dry tribosystems, Wear 259 (2005) 771–78.

49) Q. Tian, B. Yang, H. Zhuang, Y. Guo, C. Wang, Z. Zhai, L. Liu, N. Huang, X. Jiang, Hybrid diamond/graphite films: Morphological evolution, microstructure and tribological properties, Diamond Relat. Mater. 70 (2016) 179–85.

50) A. Erdemir, G.R. Fenske, A.R. Krauss, D.M. Gruen, T. McCauley, R.T. Csencsits, Tribological properties of nanocrystalline diamond films, Surf. Coat. Technol. 120–121 (1999) 565–72.

51) Y. Liu, A. Erdemir, E.I. Meletis, An investigation of the relationship between graphitization and frictional behavior of DLC coatings, Surf. Coat. Technol. 86–87 (1996) 564–568.

52) J. Solis, H. Zhao, C. Wang, J.A. Verduzco, A.S. Bueno, A. Neville, Tribological performance of an H-DLC coating prepared by PECVD, Appl. Surf. Sci. 383 (2016) 222–32.

53) K. Panda, N. Kumar, B.K. Panigrahi, S.R. Polaki, B. Sundaravel, S. Dash, A.K. Tyagi, I.N. Lin, Tribological properties of N^+ ion implanted ultrananocrystalline diamond films, Tribol. Int. 57 (2013) 124–36.

54) A.A. Voevodin, A.W. Phelps, J.S. Zabinski, M.S. Donley, Friction induced phase transformation of pulsed laser deposited diamond-like carbon, Diamond Relat. Mater. 5 (1996) 1264–69.

55) N. Salah, A. Alshahrie, J. Iqbal, P.M.Z. Hasan, M.S. Abdel-wahab, Tribological behavior of diamond-like carbon thin films deposited by the pulse laser technique at different substrate temperatures, Tribol. Int. 103 (2016) 274–80.

56) M.J Marino, E. Hsiao, Y. Chen, O.L. Eryilmaz, A. Erdemir, S.H. Kim, Understanding run-in behavior of diamond-like carbon friction and preventing diamond-like carbon wear in humid air, Langmuir 27 (2011) 12702–08.

57) M.I.D.B. Bouchet, C. Matta, B. Vacher, T.L. Mogne, J.M. Martin, J.V. Lautz, T. Ma, L. Pastewka, J. Otschik, P. Gumbsch, M. Moseler, Energy filtering transmission electron microscopy and atomistic simulations of tribo-induced hybridization change of nanocrystalline diamond coating, Carbon 87 (2015) 317–29.

58) T.B. Ma, L.F. Wang, Y.Z. Hu, X. Li, H. Wang, A shear localization mechanism for lubricity of amorphous carbon materials, Sci. Rep. 4 (2014) 3662–67.

59) S.R. Polaki, N. Kumar, K. Ganesan, K. Madapu, A. Bahuguna, M. Kamruddin, S. Dash, A.K. Tyagi, Tribological behavior of hydrogenated DLC film: Chemical and physical transformation at nano-scale, Wear 338–339 (2015) 105–13.

60) W. Qin, W. Yue, C. Wang, Understanding integrated effects of humidity and interfacial transfer film formation on tribological behaviors of sintered polycrystalline diamond, RSC Adv. 5 (2015) 53484–96.

61) A. Alazizi, A.J. Barthel, N.D. Surdyka, J. Luo, S.H. Kim, Vapors in the ambient–A complication in tribological studies or an engineering solution of tribological problems? Friction 3 (2015) 85–114.

62) S. Dag, S. Ciraci, Atomic scale study of superlow friction between hydrogenated diamond surfaces, Phys. Rev. B 70 (2004) 241401−04.

63) G. Zilibotti, M.C. Righi, Ab initio calculation of the adhesion and ideal shear strength of planar diamond interfaces with different atomic structure and hydrogen coverage, Langmuir 27 (2011) 6862–67.

64) C. Matta, O.L. Eryilmaz, M.I.D.B. Bouchet, A. Erdemir, J.M. Martin, K. Nakayama, On the possible role of triboplasma in friction and wear of diamond-like carbon films in hydrogen-containing environments, J. Phys. D: Appl. Phys. 42 (2009) 075307−14.

65) Z. Feng, Y. Tzeng, J.E. Field, Friction of diamond on diamond in ultra-high vacuum and low-pressure environments, J. Phys. D: Appl. Phys. 25 (1992) 1418–24.

66) K.D. Koshigan, F. Mangolini, J.B. McClimon, B. Vacher, S. Bec, R.W. Carpick, J. Fontaine, Understanding the hydrogen and oxygen gas pressure dependence of the tribological properties of silicon oxide–doped hydrogenated amorphous carbon coatings, Carbon 93 (2015) 851–60.

67) S.R. Polaki, N. Kumar, K. Madapu, K. Ganesan, N.G. Krishna, S.K. Srivastava, S. Abhaya, M. Kamruddin, S. Dash, A.K. Tyagi, Interpretation of friction and wear in DLC film: Role of surface chemistry and test environment, J. Phys. D: Appl. Phys. 49 (2016) 445302–14.

68) J. Shi, Z. Gong, C. Wang, B. Zhang, J. Zhang, Tribological properties of hydrogenated amorphous carbon films in different atmospheres, Diamond Relat. Mater. 77 (2017) 84–91.

69) C. Wang, B. Li, X. Ling, J. Zhang, Superlubricity of hydrogenated carbon films in a nitrogen gas environment: Adsorption and electronic interactions at the sliding interface, RSC Adv. 7 (2017) 3025–34.

70) S.M. Pimenov, A.A. Smolin, E.D. Obraztsova, V.I. Konov, U. Bogli, A. Blatter, M. Maillat, A. Leijala, J. Burger, H.E. Hintermann, E.N. Loubnin, Tribological behaviour of smooth diamond films, Surf. Coat. Technol. 76–77 (1995) 572–578.

71) A. Erdemir, G.R. Fenske, Tribological performance of diamond and diamondlike carbon films at elevated temperatures, Tribol. Trans. 39 (4) (1996) 787–94.

72) W.J. Wu, M.H. Hon, Thermal stability of diamond-like carbon films with added silicon, Surf. Coat. Technol. 111 (1999) 134–40.

73) J. Li, W. Yue, W. Qin, C. Wang, Approach to controllable tribological properties of sintered polycrystalline diamond compact through annealing treatment, Carbon 116 (2017) 103–12.

74) K. Miyoshi, Considerations in vacuum tribology (adhesion, friction, wear, and solid lubrication in vacuum), Tribol. Int. 32 (1999) 605–16.

75) R. Ramadoss, N. Kumar, K.J. Sankaran, P. Das, T.R. Ravindran, S. Dash, A.K. Tyagi, N.H. Tai, I.N. Lin, Temperature dependent tribological studies and phase transformation in ultra-nanocrystalline diamond films, Sci. Adv. Mater. 6 (4) (2014) 751–59.

Chapter 2

Experimental Methods

2.1. Introduction

This chapter presents the experimental procedures followed in the synthesis and characterization of UNCD films. The UNCD films are grown on suitable substrate using microwave plasma enhanced chemical vapor deposition system (MPECVD) employing optimized deposition parameters after pretreatment seeding process. Suitable experimental techniques are used for structural, morphological and chemical characterization of UNCD films. Detailed microstructure and local bonding analysis of these films are carried out using high-resolution transmission electron microscopy (HRTEM) and electron energy loss spectroscopy (EELS), respectively. Friction and wear behavior of UNCD films are studied in detail under various set of tribological conditions using ball-on-disc geometry micro-tribometer. Two dimensional (2D) wear profiles are measured using stylus profilometer working in contact mode. The morphology and elemental composition of UNCD films and wear tracks/ball scars are analyzed using field emission scanning electron microscope (FESEM) and energy dispersive X-ray spectroscopy (EDX), respectively. The surface topography of film and wear tracks is obtained by atomic force microscopy (AFM). The chemical structure of films and wear tracks/ball scars is examined using micro-Raman spectrometer. Detailed surface chemical analysis of film surface and wear tracks/ball scars is carried out using X-ray photoelectron spectroscopy (XPS).

2.2. Film deposition

The UNCD films are grown on mirror polished Si substrates employing MPECVD system (2.45 GHz 600 IPLAS-CYRANNUS) using optimized set of deposition parameters. Before the deposition process, the substrates are ultrasonicated in a methanol solution containing a mixture of nano-diamond (~5 nm) and titanium (325 nm) powders for 45 minutes to facilitate the nucleation process. The CH_4 and Ar/N_2 are employed as precursor gases for UNCD deposition process. The equiaxed diamond grains are formed while employing Ar plasma whereas needle-like morphology of UNCD films is obtained in nitrogen plasma media [1]. The difference in ionization potential of inert gases (Ar and nitrogen) significantly influences the nucleation and growth process of UNCD films. The ionization potential basically determines the effective pressure of reactive gases and substrate temperature required for growth process to take place. In general, inert gas choice, deposition chamber pressure and temperature conditions tailor the morphology, microstructure and chemical composition of the UNCD films. All deposition process parameters e.g. plasma gas composition, microwave power, chamber pressure and substrate temperature etc. are optimized before actual deposition process is carried out. The schematic of MPECVD system is shown in Fig. 2.1 [2]. Details of complete set of deposition parameters used for specific tribological study of UNCD films are provided in the respective chapters.

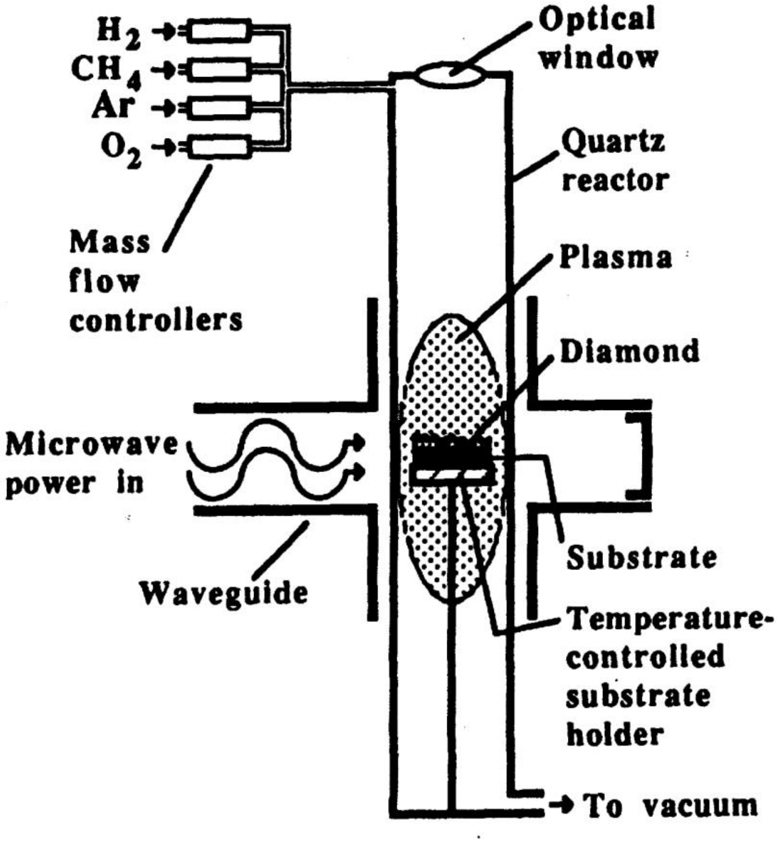

Fig. 2.1. *Schematic of microwave plasma enhanced chemical vapour deposition system [from Ref (2)]*

2.3. Characterization techniques

2.3.1. High-resolution transmission electron microscope and Electron energy loss spectroscopy

Detailed microstructures and local bonding of UNCD films are studied using HRTEM (TEM; JEOL 2100) and EELS (Getan, Enfina), respectively. In principle, an electron beam from the electron gun, accelerated at few hundreds of kV is transmitted through an ultrathin section of a microscopic object and image is magnified by the electromagnetic fields. The resolution of an electron microscope is limited to about 1-2 Å. The high-resolution imaging mode of the microscope allows one to observe planer, line defects, grain boundaries and interfaces etc. with atomic scale resolution. The bright field/dark field imaging modes of the microscope are combined with electron diffraction pattern to provide invaluable information about crystal phases and defects etc. which are present in a material.

To avoid the surface contamination, bulk segment of film is considered for detailed microstructural analysis. The TEM and EELS samples are prepared by mechanical grinding (or dimpling) followed by Ar-ion milling of UNCD films. Thus, the thin foil used for TEM analysis is basically from the close vicinity of the UNCD film surface. The Bright Field (BF) TEM microstructures of UNCD films along with the selected area electron diffraction (SAED) pattern are studied for detailed microstructural analysis of these films. The SAED pattern of UNCD films show sharp diffraction rings corresponding to (111), (220) and (311) planes of the diamond lattice confirming that these films are polycrystalline in nature. The lattice plane spacing of (311), (220) and (111) planes are found to be 0.11, 0.12 and 0.21 nm, respectively, which confirm the crystalline diamond structure [3]. The diffused ring in the center of SAED pattern indicates the presence of *a-C*/sp^2 bonded phase. The diamond and *a-C* phases are further confirmed by Fourier Transform (FT) images.

2.3.2. Field emission scanning electron microscope and Energy dispersive X-ray spectroscopy

Morphologies of UNCD films are obtained using FESEM (Zeiss Supra 55). The thickness of UNCD samples are measured using cross-sectional SEM image of freshly cleaved edge of Si/UNCD system. In FESEM, a field emission cathode of the electron gun provides narrower probing beams at low as well as high electron energy with less spread and thus, resulting in improved spatial resolution and minimized sample charging and damage. In principle, the specimen is exposed to a narrow electron beam from an electron gun. The electron beam is accelerated through a high voltage (e.g. ~20 kV) and passes through a system of aperture and electromagnetic lenses to produce a fine beam of electrons which rapidly scans the surface of the specimen and thus, generating secondary electrons, backscattered electrons and characteristic X-rays. These signals are collected by suitable detectors. The secondary electron imaging shows the morphology of surface features a few nm across. The Z contrast features seen in the backscattered electron (BSE) image can be analyzed for elemental mapping using EDX and to identify the elemental composition of materials imaged in SEM for all elements with an atomic number greater than boron. The energy of each X-ray photon is characteristic of the element which produced it. The EDX spectroscopy allows one to identify the particular elements present in the sample and their relative proportions. The FESEM technique combined with EDX is very much useful for understanding the tribological mechanism in UNCD films. Post tribology, the wear track/ball scar dimensions and their deformation behavior are studied using FESEM technique. Moreover, elemental mapping using EDX on ball scars reveal the distinct nature of transferlayer formed as a result of tribological sliding process.

2.3.3. Atomic force microscopy

The AFM (NT-MDT) is employed to analyze surface topography and roughness of UNCD films and wear tracks. The UNCD films generally exhibit very smooth surface with roughness of the order of only few nanometers (nm) [1]. The basic principle of AFM is that a sharp probe is maintained in close contact with the sample surface by a feedback mechanism. As the probe scans the surface, the vertical movement of the probe to stay at the same probe-sample distance is taken to be the sample topography. The most commonly used probes are micro-fabricated silicon (Si) or silicon-nitride (Si_3N_4) cantilevers with sharp tips. Typically, the probe radius varies between 5 to 20 nm. The bending of the cantilever normal to the sample surface is usually monitored by an optical lever. The movement of the probe over the surface is controlled by a scanner. The scanner is normally made from a piezoelectric material which can move the probe very precisely across x, y and z axes. The signal from the four quadrant photo detector passes through a feedback circuit and into the z movement part of the scanner to maintain the probe-sample distance at a set value. As the cantilever acts as a spring, a fixed cantilever deflection means a fixed sample-probe force is maintained. The amount by which the scanner has to move in z-axis to maintain the cantilever deflection is considered to the sample topography. In this thesis work, the tribolayer formation characteristic in UNCD films is studied in detail using the AFM technique.

2.3.4. Raman spectroscopy

Raman spectroscopy is one of the most widely used techniques to characterize the carbon based materials. The detailed chemical structural characterization of UNCD films and wear tracks/ball scars are analyzed employing micro-Raman spectrometer (Andor SR-500i-C-R, λ=532 nm). Moreover, transferlayer formation characteristic in these films is studied in detail using Raman spectroscopy to understand the governing tribological mechanisms. Raman spectroscopic measurements are carried out to record the chemical structure of UNCD films and wear tracks/ball scars. Raman spectroscopy involves molecular and crystal lattice vibrations and therefore, it is sensitive to composition, bonding, phase and crystalline structure of the sample material. Raman spectroscopy comprises a family of spectral measurements made on molecular media based on inelastic scattering of electromagnetic radiation. During the process, the energy is exchanged between the photon and the molecule such that the scattered photon is either of higher or lower energy than the incident photon. The difference in energy is made up by the change in the rotational and vibrational energies of the molecule and provides information on its energy levels. These scattered photons are collected by the detector where electrical signals are triggered and leading to appearance of Raman spectrum.

Using Raman spectroscopy, UNCD films are characterized by their grain boundary phase. The characteristic peaks of UNCD films are located at 1138, 1195 and 1468 cm^{-1} and are assigned as non-degenerate A_g mode [4]. These bands arise from the resonance Raman scattering processes involving π state of sp^2 bonded carbon atoms associated with *t-PA* segments in the grain boundaries and are termed as v_1, v_2 and v_3 modes [5]. These *t-PA* mode vibrations consist of the combination of C=C and C-H wagging atomic vibrations in *t-PA* segment [5,6]. The v_1-band is associated with the C-H in-plane bending mode [4] while the v_3-band corresponds to the C=C symmetric stretching [6] vibration. The broad and weak v_2-band centered at 1195 cm^{-1} corresponds to the C-H stretching vibration [5]. The G-band located at 1559 cm^{-1} arises from first order Raman scattering process; this is a doubly degenerate E_{2g} mode involving sp^2 bonded in-plane C-atom vibration of grain boundaries while D-band located at 1365 cm^{-1} is associated with a second order Raman scattering process involving a zone boundary A_{1g} phonon and defects in the sp^2 phase [7]. Therefore, D- and G-bands have an origin in sp^2 phase in the grain boundary. The predominant hybridized sp^2 carbon in the grain boundary (D and G bands) has a high scattering cross-section in visible wavelength regime while the sensitivity of scattering cross-section decreases significantly for sp^3 bonded diamond phase (grain) [8]. Therefore, the presently recorded Raman spectrum excited using a visible laser line is dominated by the contribution from sp^2 carbon rich grain boundaries. On the other hand, a weak D^*-band at 1336 cm^{-1} corresponds to sp^3 nanodiamond phase [5]. The full width at half maximum (FWHM) of this band is 52 cm^{-1}, much larger than that observed in bulk diamond (FWHM=1.2 cm^{-1}) [9]. This broadening in Raman band is related to the phonon confinement effect due to nano size of the diamond grains.

2.3.5. X-Ray photoelectron spectroscopy

The detailed surface chemical analysis of UNCD films and wear tracks/ball scars are carried out by XPS (Sigma probe-Thermo VG Scientific) equipped with hemispherical analyzer and micro-focused monochromatic X-ray source with spatial resolution of 50 µm. The XPS is carried out using Al Kα radiation (E = 1486.6 eV) with an energy resolution of 0.47 eV. This enables one to explore chemical characteristic not only on the surface but also inside the wear track/ball scar. In XPS, the sample is illuminated with soft (~1.5 kV) X-ray radiation in ultrahigh vacuum (10^{-10} Torr). The photoelectric effect caused by the X-rays leads to the production of photoelectrons, the energy spectrum of which is readily obtained. The energy spectrum permits us to determine the chemical composition of the sample. The kinetic energy of the emitted photoelectrons E_k is measured. Knowing the photon energy hv, one can plot the binding energies E_B of the photoelectrons on a spectrum using the Einstein equation: $E_K = hv- E_B$. As the binding energies of the electron orbitals in atoms are known, the positions of the peaks allow one to identify the elements present on the sample surface. A measurement of the relative areas of the photoelectron peaks allows the composition of the sample to be determined quantitatively. Because the photoelectrons are attenuated by passage through the sample material itself, the information is limited to a surface, with a sampling depth of the order of 5-10 nm. Chemical bonding will frequently have the effect on the binding energy of the electron orbital and give rise to an observable chemical shift in the kinetic energy of the photoelectrons. These binding energies can be used to extract information of the chemical nature (such as chemical oxidation state) from the sample surface. In one specific study in this thesis work, low energy Ar^+-ion beam (E = 1 keV) coupled with XPS chamber in ultrahigh vacuum (~10^{-10} mbar) condition is used for the surface modification of UNCD films to address run-in behavior and also for carrying out detailed gas dependent tribological analysis of these films. For comprehensive chemical analysis of the film surface, depth-resolved XPS analysis is carried out simultaneously after each sputtering cycle of 5, 10, 15, 20, 25 and 30 min. For this purpose, the wide range and high-resolution XPS spectra of C1s and O1s are recorded. XPS technique also helps to characterize transferlayer/tribolayer formation in wear tracks/ball scars to understand the tribological mechanisms in UNCD films.

2.3.6. Surface profilometer

Two dimensional (2D) contact profilometer is used for the measurement of wear track dimensions to assess wear loss. A stylus-based surface profiler measures the physical surface of the sample. The profilometer takes measurements electromechanically by moving the sample beneath a diamond-tipped stylus. The high-precision stage moves a sample beneath the stylus according to a user programmed scan length, speed and stylus force. The Dektak 6M profiler contains the mechanical and optical components for sample placement, sample viewing and scanning/measurement. The radius of the standard diamond stylus is 12.5 µm. The stylus is mechanically coupled to the core of an LVDT (Linear variable differential transformer). As the stage moves the sample, the stylus rides over the sample surface. Surface variations cause the stylus to be translated vertically. Electrical signals corresponding to stylus movement are produced as the core position of the LVDT changes. The LVDT scales an AC reference signal proportional to the position change, which in turn is conditioned and converted to a digital format through a high precision, integrating, analog-to-digital converter. The digitized signals from printing a single scan are stored in computer memory for display, manipulation, measurement and printing.

2.3.7. Tribology tests

Tribometer measures the magnitude of friction as the two surfaces slide against each other in given set of tribological conditions. For tribology measurement, a flat or a spherical probe is placed on the test sample and loaded with a precisely known weight. Several possible contact geometries include pin-on-disc, ball-on-disc and flat-on-disc etc. The resulting frictional forces acting between the probe and sample are measured. In this present thesis work, the friction behavior of UNCD films is measured by a ball-on-disc geometry standard micro-tribometer operating in a linear reciprocating mode. Furthermore, high temperature and high vacuum tribological tests of UNCD films are carried out using ball-on-disc geometry high temperature and high vacuum tribometer (HTHVT, Anton Paar, Switzerland)) working in circular motion mode. The images of HTHV tribometer coupled with micro-Raman spectrometer and standard tribometer used for the tribological measurements of UNCD films and the schematic of ball-on-disc geometry standard micro-tribometer are shown in Fig. 2.2.

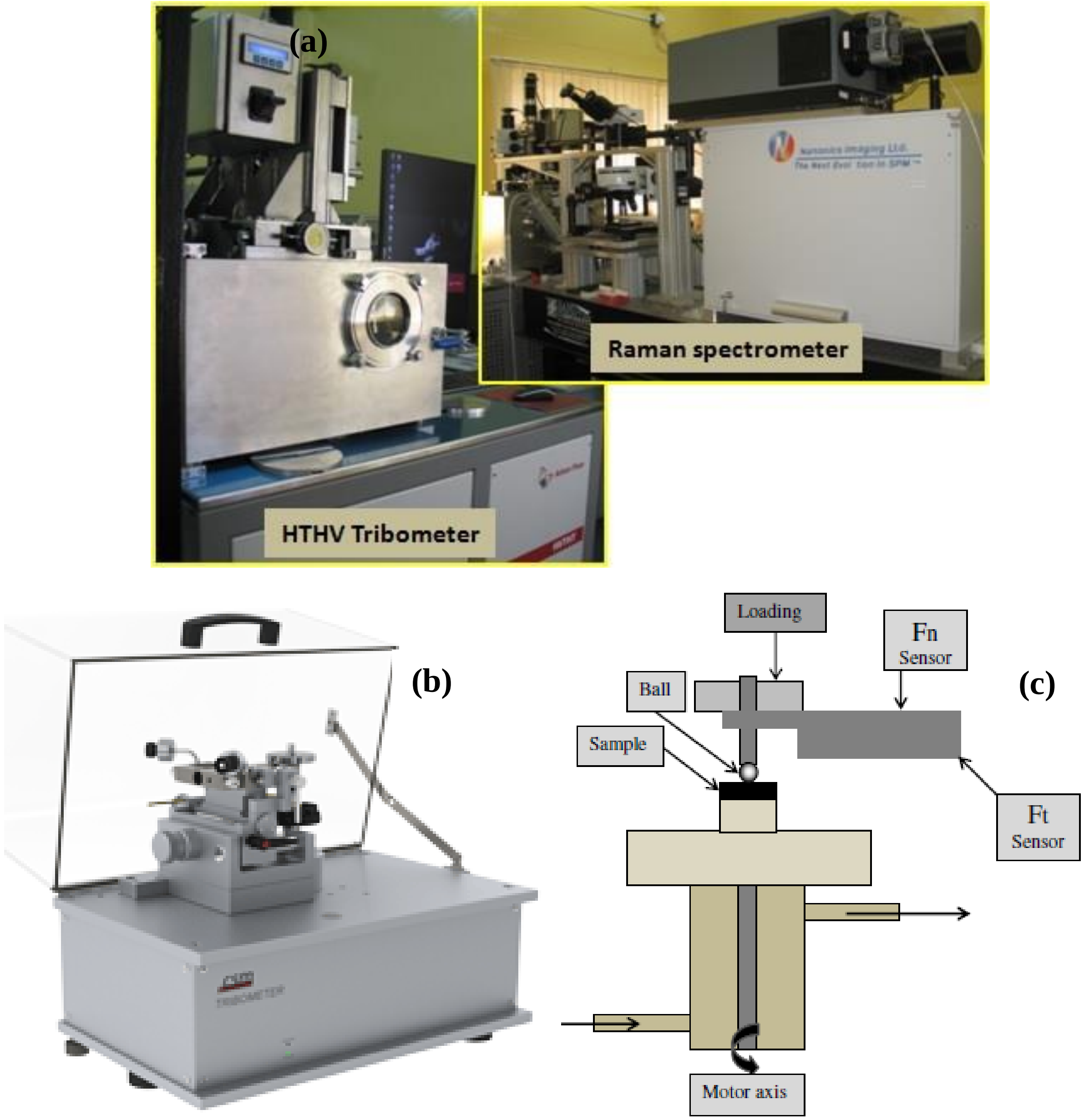

Fig. 2.2. *(a) Photograph of HTHV micro-tribometer coupled with micro-Raman spectrometer, (b) photograph of standard micro-tribometer and (c) schematic diagram of ball-on-disc geometry standard micro-tribometer*

The ball is mounted on a stiff lever, designed as a frictional force transducer. The friction coefficient is calculated during the tribo-test by measuring the deflection of the elastic arm by LVDT sensor. The coefficient of friction is measured as the ratio of tangential force to normal force i.e. $\mu = F/N$.

In this thesis work, the detailed tribology behavior of UNCD films is explored. Inert Zirconia (ZrO_2, 6mm dia.) and Alumina (Al_2O_3, 6mm dia.) balls are selected as counterbody against UNCD film samples for tribological testing. The comprehensive tribological behavior of UNCD films is studied in ambient atmosphere, inert and reactive gaseous media, high temperature and high vacuum tribological conditions. The main emphasis is given to improve the tribological properties of UNCD films and also to understand the governing tribological mechanism in these films under different set of tribological test conditions. The details of tribo-test parameters used for the specific tribological study will be discussed in the respective chapters.

2.4. References

1) R. Rani, N. Kumar, A.T. Kozakov, K.A. Googlev, K.J. Sankaran, P.K. Das, S. Dash, A.K. Tyagi, I.N. Lin, Superlubrication properties of ultra-nanocrystalline diamond film sliding against a zirconia ball, RSC Adv. 5 (2015) 100663–73.
2) Electronic reference: http://www.tvu.com/PC60diamWeb.html.
3) K.J. Sankaran, J. Kurian, H.C. Chen, C.L. Dong, C.Y. Lee, N.H. Tai, I N. Lin, Origin of a needle-like granular structure for ultrananocrystalline diamond films grown in N_2/CH_4 plasma, J. Phys. D: Appl. Phys. 45 (2012) 365303–11.
4) M. Rybachuka, J.M. Bell, Electronic states of trans-polyacetylene, poly (p-phenylene vinylene) and sp-hybridised carbon species in amorphous hydrogenated carbon probed by resonant Raman scattering, Carbon 47 (2009) 2481–90.
5) A.C. Ferrari, J. Robertson, Origin of the 1150 cm^{-1} Raman mode in nanocrystalline diamond, Phys. Rev. B 63 (2001) 121405–08.
6) T. López-Rı´os, É. Sandré, S. Leclercq, É. Sauvain, Polyacetylene in diamond films evidenced by surface enhanced Raman scattering, Phys. Rev. Lett. 76 (1996) 4935–38.
7) K.K. Mishra, S. Ghosh, T.R. Ravindran, S. Amirthapandian, M. Kamruddin, Thermal conductivity and pressure-dependent Raman studies of vertical graphene nanosheets, J. Phys. Chem. C 120 (2016) 25092–100.
8) A.C. Ferrari, J. Robertson, Raman spectroscopy of amorphous, nanostructured, diamondlike carbon, and nanodiamond, Philos. Trans. R. Soc. A 362 (2004) 2477–512.
9) H. Kuzmany, R. Pfeiffer, N. Salk, B. Gunther, The mystery of the 1140 cm^{-1} Raman lines in nanocrystalline diamond films, Carbon 42 (2004) 911–17.

Chapter 3

The Effect of Local Phase Composition on the Tribological Properties of UNCD Films

3.1. Introduction

Friction and wear behavior of any material can be controlled effectively only when we understand the governing tribological mechanisms in detail. The microstructural parameters e.g. the grain size, orientation of the crystalline phase, grain boundary phase composition, roughness, hardness and elastic modulus etc. influence the tribological properties of carbon based materials [1-6]. Moreover, grain and grain boundary phase characteristics are important factors to understand the friction and wear behavior in nano/ultrananocrystalline diamond films [4,7]. The tribological properties of diamond are shown to improve with the decrease in their grain size which is supposed to be due to increase in amorphous carbon (*a-C*) and graphite phase in the grain boundary [6]. The chemical phase transformation in tribo-contact interface further makes the understanding of tribo-mechanisms a bit complex subject. It is reported in the literature that friction and wear of diamond and DLC films decrease when graphitic tribolayer is formed in the sliding interface [8-14]. But there is not much experimental reports available in literature to support the same for UNCD films. Moreover, some studies suggest that the passivation mechanism governs the ultralow friction value observed in UNCD films [15,16].

In this chapter, the comprehensive understanding of the governing mechanisms behind the role of local phase composition on the friction and wear behavior of UNCD films is developed. Two different sets of UNCD films are grown on silicon (100) substrates using MPECVD system to have comparative tribological study with respect to local phase composition. In-situ electrical contact resistance (ECR) measurements are also carried out to analyze the electrical resistivity of the sliding interface which can provide some insight about the tribofilm formation process. Furthermore, the dynamics of topographical evolution of secondary phase i.e. tribofilm in wear track during tribological process and its chemical characterization is also studied in detail. The underlying mechanism for observed tribological properties is established in these UNCD films.

3.2. Experimental

One set of UNCD films designated as $UNCD_{Ar}$ is grown on silicon (100) substrate using CH_4(1%)/Ar(rest) plasma media, microwave power of 1200 W, pressure of 120 Torr and substrate temperature of 450°C using MPECVD system. While deposition parameters used for the growth of other set of UNCD films designated as $UNCD_N$ are CH_4(6%)/N_2(rest) plasma media, microwave power of 1200 W, pressure of 50 Torr and a substrate temperature of 700°C [5]. The morphologies and chemical structures of films are studied using FESEM and Raman spectroscopy, respectively. The microstructure and local bonding configuration of these films is analyzed using HRTEM and EELS, respectively.

The tribological properties of these UNCD films is studied using ball-on-disc geometry micro-tribometer working in a linear reciprocating mode and coupled with ECR measuring device under ambient (dry and unlubricated) conditions. For these measurements; the normal load, sliding speed and stroke length are chosen as 2 N, 4 cm/s and 4 mm, respectively. The chemically stable ZrO_2 ball with 6 mm diameter and average roughness (R_a) 45 nm is selected as sliding counterbody mainly to avoid oxidation/corrosion wear [17]. The hardness and elastic modulus of ZrO_2 balls is 12 GPa and 200 GPa, respectively. Two dimensional wear profiles are measured by stylus profilometer. The surface topography of films and wear tracks are analyzed by AFM. Moreover, detailed chemical analysis of UNCD films and wear tracks are carried out using EDX, Raman spectroscopy and XPS techniques.

3.3. Results and discussion

3.3.1. The morphological analysis of UNCD films

The FESEM micrographs of UNCD films are shown in Figs. 3.1a,b. The densely packed nanostructural characteristics are observed in both films. The $UNCD_{Ar}$ films consist of uniformly distributed equiaxed fine spherical features while in $UNCD_N$ films, needle like elongated sharp features of ~50−200 nm in length and few nanometers in diameter are seen. The different set of plasma conditions employed for the deposition of UNCD films modifies the morphology of these films [5]. Both films are of similar thickness ~400-500 nm as evident from the FESEM cross-sectional image as shown in the inset of Figs. 3.1a,b.

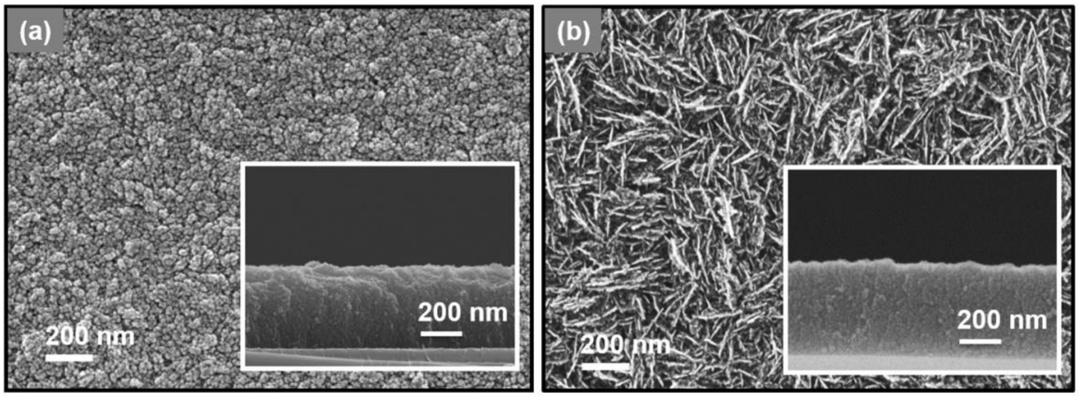

Fig. 3.1. *Morphology of (a) UNCD$_{Ar}$ and (b) UNCD$_N$ films with cross-sectional images shown in the insets*

3.3.2. The microstructural analysis of UNCD films

The detailed microstructural analysis of both sets of UNCD films is carried out using TEM and is presented in Fig. 3.2. The bright field (BF) TEM micrograph image with SAED pattern as shown in the inset of Fig. 3.2a$_i$,a confirms that UNCD$_{Ar}$ films are primarily constituted of diamond nanocrystals. Moreover, diffused central ring indicates the presence of the sp^2-bonded carbon (graphitic or *a-C* phase). So, diamond nanocrystals are embedded in sp^2 carbon or amorphous carbon. The distribution of phase constituents is clearly understood by composed dark field (c-DF) image which is superposition of several dark field images corresponding to different portions of SAED pattern (Fig. 3.2a$_i$,b). The inset 'I' in Fig. 3.2a$_i$,c reveals that diamond grains are ~5 nm in size. Moreover, HRTEM micrograph shown in Fig. 3.2a$_i$,c reveals the structure image of designated area 'A' in Fig. 3.2a$_i$,a. The Fourier transformed diffractogram of the whole structure image (FT$_0$) shows the presence of spotted diffraction pattern and diffused central ring. The corresponding FT$_1$ and FT$_2$ images of designated areas '1' and '2' confirm the presence of diamond and *a-C* phases in UNCD$_{Ar}$ films, respectively.

Similarly, the detailed microstructural analysis for UNCD$_N$ films is shown in Fig. 3.2b$_i$. BFTEM image shown in Fig. 3.2b$_i$,a indicates the randomly oriented nanowire like feature of 50−200 nm in length and few nanometers in diameter. The SAED pattern implies that these nanowires are comprised of diamond structure. Prominent diffused central ring signify the existence of large fraction of graphitic phase in these films. The microstructural report on UNCD$_N$ films states that graphitic phase is formed during the growth process while employing CH_4/N_2 plasma media [18]. The c-DF image shown in Fig. 3.2b$_i$,b indicates that each of the needle-like diamond grains is surrounded by graphitic phase. The FT pattern (FT_0) shown in the inset of Fig. 3.2b_i,c reveals the presence of diamond and graphite phases. The FT_1 and FT_2 image corresponding to area '1' and '2' confirms the presence of diamond and graphitic structures, respectively. These results collectively indicate that $UNCD_N$ films possess diamond nanowires which are encapsulated by the sheath of graphitic phase.

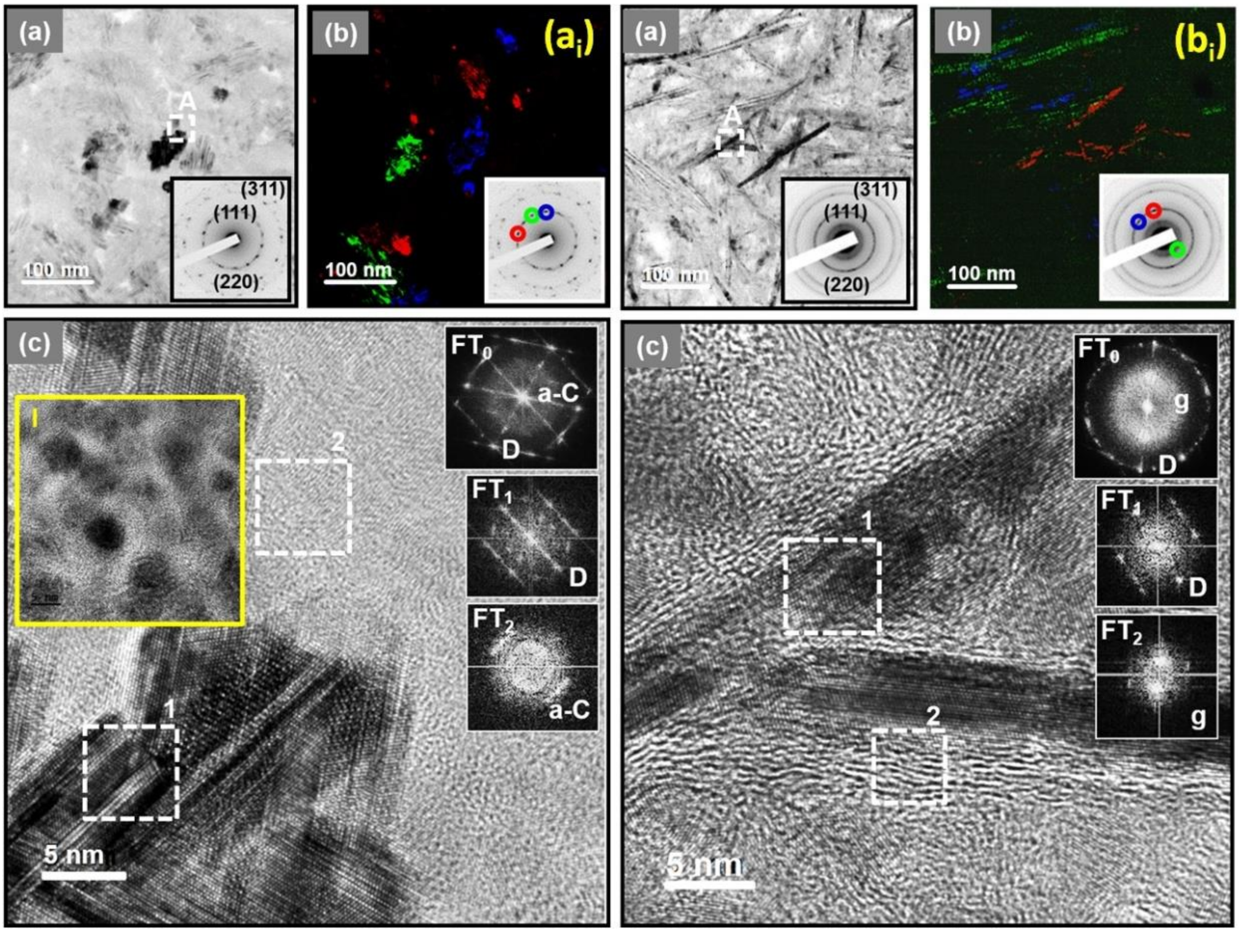

Fig. 3.2. *Microstructural analysis of (a_i) $UNCD_{Ar}$ and (b_i) $UNCD_N$ films, (a) BF and (b) c-DF TEM images of UNCD films with their corresponding SAED patterns shown in insets, (c) HRTEM structure image corresponding to designated region A in panel (a) for both cases*

To confirm further about the nature of sp^2-bonded carbon phase in UNCD films i.e. amorphous or crystalline, the EELS spectra [19] corresponding to BFTEM micrographs of Fig. 3.2a_i,a and Fig. 3.2b_i,a are examined (Fig. 3.3). EELS is a unique technique to characterize the local bonding nature in UNCD films [19-20]. Curve I and II in Fig. 3.3a correspond to core-loss EELS spectrum of $UNCD_{Ar}$ and $UNCD_N$ films, respectively. An abrupt rise in σ*-band (near 290 eV) and a deep valley near 302 eV is observed in $UNCD_{Ar}$ films correspond to typical EELS spectrum of diamond [20,21]. Moreover, a small π*-band at 284.5 eV indicates the presence of some sp^2-bonded carbon in $UNCD_{Ar}$ films. Interestingly, distinct high intensity of π*-band in Curve II indicating the larger proportion of sp^2-bonded carbon phase in $UNCD_N$ films.

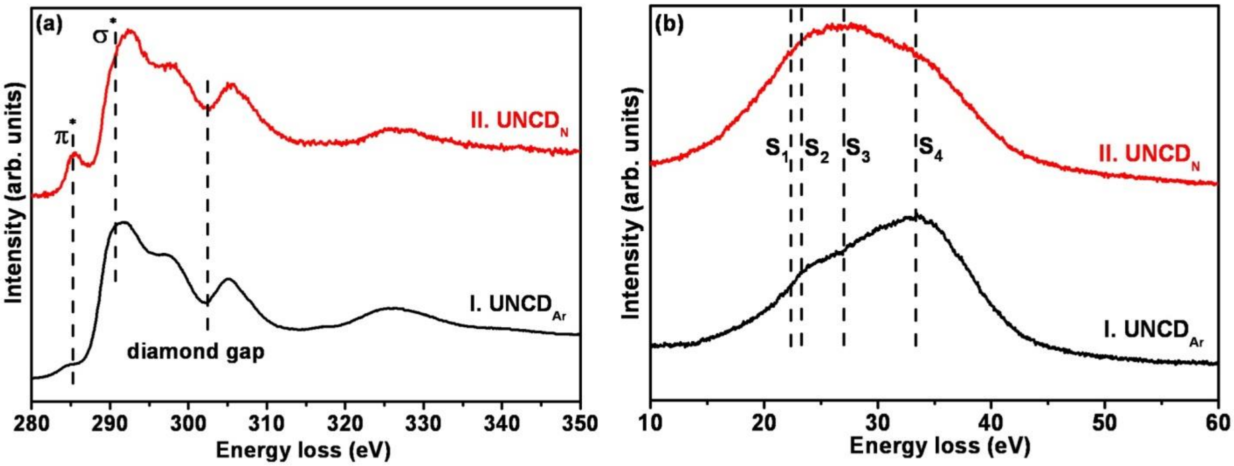

Fig. 3.3. *(a) core-loss and (b) plasmon-loss EELS spectra of UNCD films*

Furthermore, the plasmon-loss EELS spectrum is examined to differentiate the crystalline sp^2-bonded carbon (i.e. graphite) from *a-C* phase in these UNCD films. The graphitic phase shows a prominent peak at position s_3 (27 eV) while *a-C* shows at s_1 (22 eV) [20,21] as indicated in Fig. 3.3b. The crystalline sp^3-bonded carbon (i.e. diamond) shows a peak at s_4 (33 eV) corresponding to bulk plasmon loss and a shoulder at s_2 (23 eV) corresponding to surface plasmon loss. The $UNCD_{Ar}$ films (curve I, Fig. 3.3b) shows s_2 and s_4 peaks, indicating that these films constitute predominately diamond [21] with small fraction of sp^2-bonded carbon. However, for $UNCD_N$ films (curve II, Fig. 3.3b), the plasmon-loss spectrum is dominated by s_3-band (~27 eV) and s_2- and s_4-bands are of much lower intensity, indicating that sp^2-bonded carbon (π*-band) implied by core-loss EELS is nanographitic phase rather than *a-C*.

The Raman spectroscopy analysis also confirms that $UNCD_N$ film consists of higher graphitic phase fraction compared to $UNCD_{Ar}$ films [22]. Moreover, Hardness and elastic modulus values in $UNCD_N$ films are 14.8 and 165 GPa, respectively, compared to 23 and 215 GPa in $UNCD_{Ar}$ films which is supposed to be due to relatively high graphitic phases in $UNCD_N$ films [5].

3.3.3. The friction and wear analysis of UNCD films

3.3.3.1. Friction behavior

The tribological tests coupled with in-situ ECR measurements are carried out for both UNCD films while sliding against ZrO_2 ball counterbody in ambient (dry and unlubricated) conditions. The friction trend against sliding distance is shown in Fig. 3.4 for both sets of UNCD films. The tribological tests are carried out for long sliding distance of 500 m to study the saturated friction coefficient value.

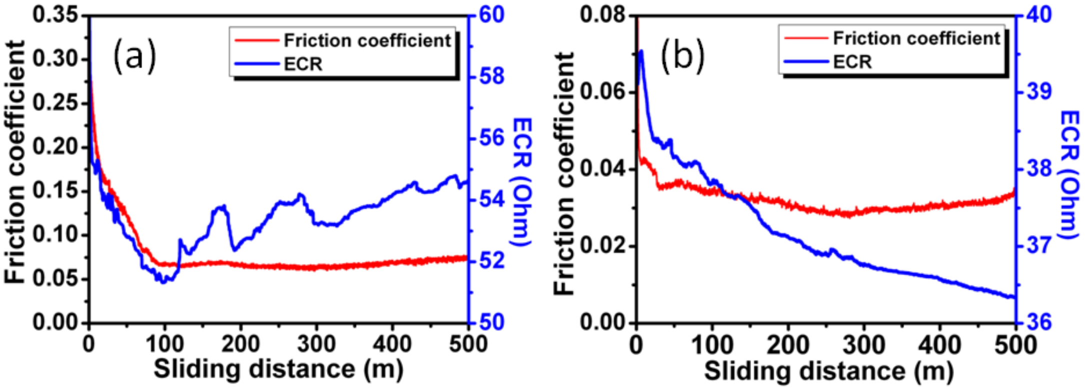

Fig. 3.4. *Friction coefficient and ECR trend in (a) $UNCD_{Ar}$ and (b) $UNCD_N$ films*

The observed trend of friction value is different in both films. For $UNCD_{Ar}$ films, the friction coefficient is large ~0.27 at the initial stage of sliding process and gradually saturates to ultralow value ~0.08 after long run-in period of ~100 m (Fig. 3.4a). While for $UNCD_N$ films, it rapidly saturates to ultralow value ~0.04 with negligibly small run-in regime (Fig. 3.4b). These tribological results are found to be reproducible as well. In Fig. 3.4(a), ECR drops initially along with friction for $UNCD_{Ar}$ films, but then it rises again almost to the original value while friction remains constant. In Fig. 3.4(b), ECR keeps dropping throughout the whole sliding process for $UNCD_N$ films while friction drops initially and then remains almost constant. The decrease in ECR value is significantly observed in $UNCD_N$ films. The distinct trend of friction value in these films depends on several factors e.g. chemical composition, sp^2/sp^3 phase fraction, surface roughness and mechanical properties of films etc. However, surface roughness value of $UNCD_{Ar}$ and $UNCD_N$ films are similar i.e. 9.4 and 13 nm, respectively [5]. Therefore, the surface roughness parameter alone is not a governing factor for observed distinct friction trend in these films. Thus, it is supposed that different local phase composition in these films probably tailors the observed friction behavior in UNCD films.

3.3.3.2. Wear behavior

The detailed wear analysis in both sets of UNCD films is presented in Fig. 3.5. Wear loss from $UNCD_{Ar}$ films is negligibly small (only few nm in depth) even after covering sliding distance of 500 m as depicted in 2D wear profile and optical image (Fig. 3.5a). Thus, $UNCD_{Ar}$ films exhibit good wear resistant property even after covering 500 m of sliding distance. However, large scar size on ZrO_2 ball counterbody is observed. In contrast, negligible loss from ZrO_2 ball and considerable wear dimension (~100 nm in depth) from $UNCD_N$ films is seen. To have better understanding of wear dynamics in both UNCD films, wear analysis is carried out at the beginning of sliding process as well i.e. 5 m of sliding distance (Fig. 3.5b).

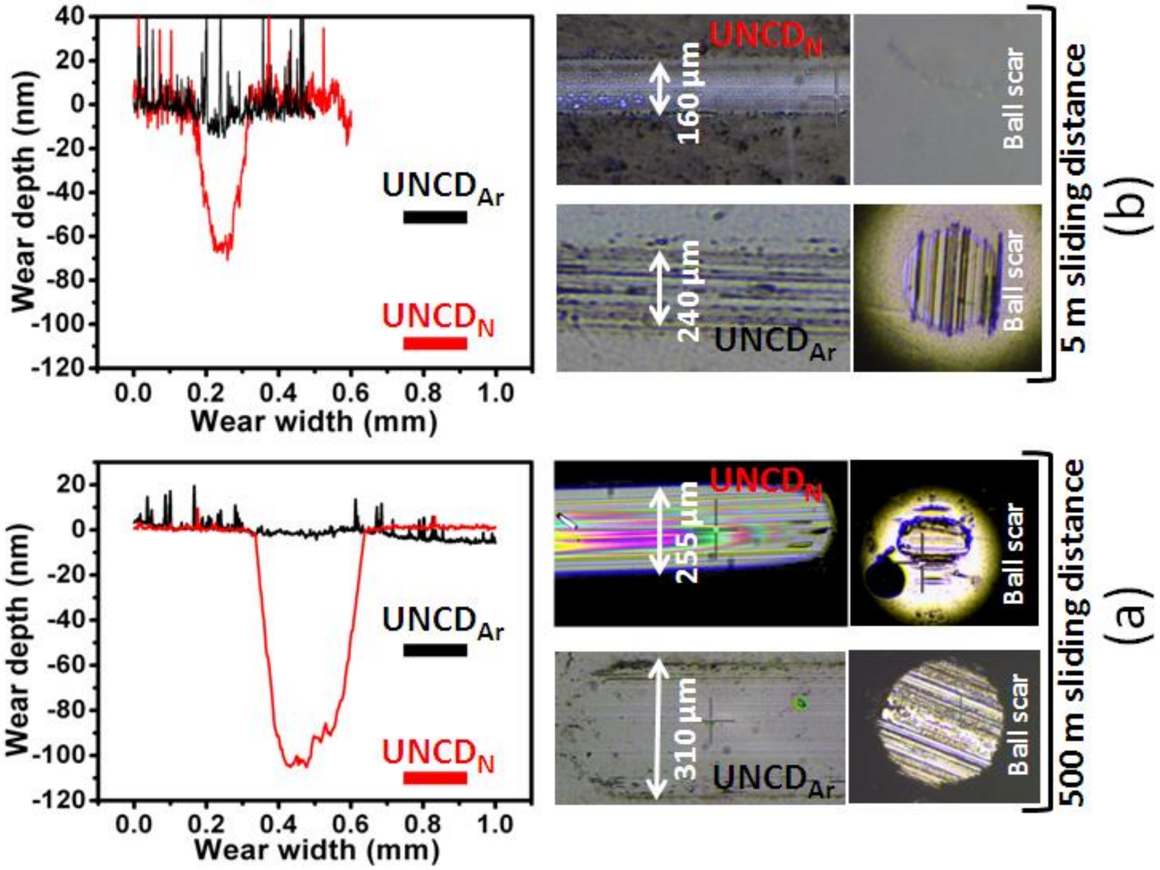

Fig. 3.5. *Wear analysis of* $UNCD_{Ar}$ *and* $UNCD_N$ *films at (a) 500 m and (b) 5 m sliding distances, left side: 2D wear profile of wear tracks, right side: optical images of wear tracks and ball scars in the sliding combination of* $UNCD_{Ar}/ZrO_2$ *and* $UNCD_N/ZrO_2$

Similar wear trend is observed in UNCD$_{Ar}$ films throughout the whole sliding process i.e. at the beginning (5 m) and at the end (500 m) of sliding process. Even at 5 m sliding distance, the wear of ball counterbody is noticeably high. This kind of wear behavior is possibly due to hard UNCD$_{Ar}$ film sliding against soft zirconia ball and small amount of graphitic/*a-C* phases. In contrast, for UNCD$_N$ films, even at 5 m sliding distance, considerable wear from film (~70 nm in depth) is observed while ball does not wear out. This distinct behavior is probably due to large amount of soft phases i.e. graphite and *a-C* encasing the needle-like diamond grains which are ripped off during the sliding process.

3.3.4. The topographical analysis of wear tracks

3.3.4.1. 2D and 3D AFM topographical images

To understand the distinct tribological behavior of both UNCD films, the sliding distance dependent 2D and 3D topographical analysis of wear track is carried out using AFM technique (Fig. 3.6). Granular shaped and densely packed diamond nanoparticles are present at UNCD$_{Ar}$ film surface as clearly shown in 2D and 3D topographical images (Figs. 3.6a$_i$,a$_{ii}$). The 2D and 3D topographies of wear tracks at sliding distance of 100 m (i.e. end of run-in regime) and 500 m (i.e. end of sliding process) are presented in Figs. 3.6b$_i$,b$_{ii}$ and c$_i$,c$_{ii}$, respectively. At sliding distance of 100 m, the UNCD film surface shows signature of onset of plastic deformation process. Moreover, severe plastic deformation is observed in the wear track at sliding distance of 500 m where ultranano feature of diamond particles disappeared and elongated secondary phase is formed which is distributed all over the wear track. The morphology of these secondary particles is completely different from UNCD$_{Ar}$ film surface.

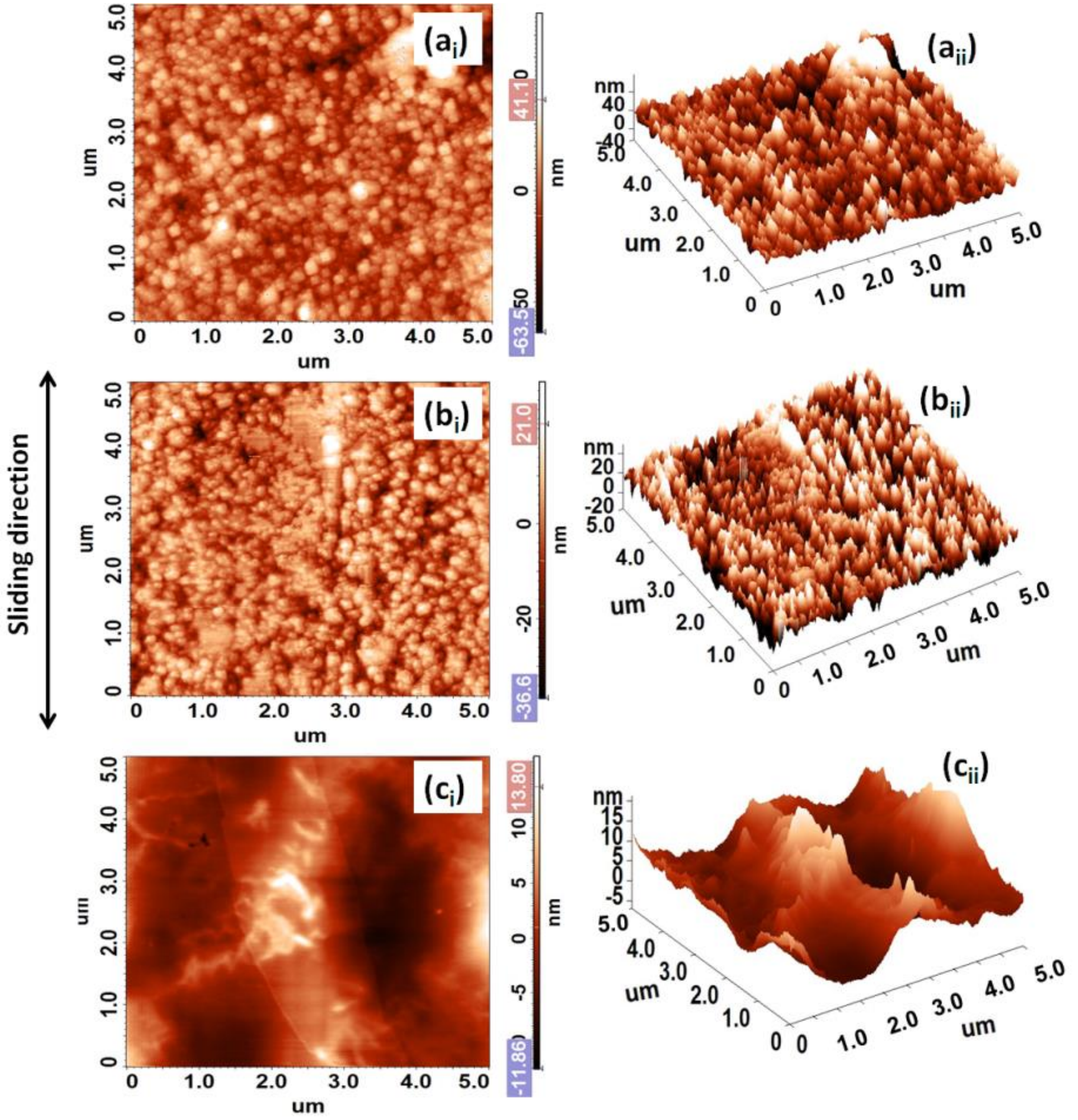

Fig. 3.6. *AFM analysis of UNCD$_{Ar}$ films: (a$_i$ & a$_{ii}$) surface topography of film, and topography of wear track formed at different sliding distances: (b$_i$ & b$_{ii}$) 100 m and (c$_i$ & c$_{ii}$) 500 m, sliding direction common for all images*

Similarly for UNCD$_N$ films, the 2D & 3D topographical images are shown in Figs. 3.7a$_i$,a$_{ii}$. At sliding distance of 100 m, big diamond particles transform into secondary phase fine particles due to plastic deformation process under continuous tribological stress condition (Figs. 3.7b$_i$,b$_{ii}$).

Moreover, due to these fine particles which act as third body, grooves appear in the wear track under non-homogeneous contact stress distribution as indicated by arrow marks in Fig. 3.7b$_i$ and also clearly shown in 3D image (Fig. 3.7b$_{ii}$).

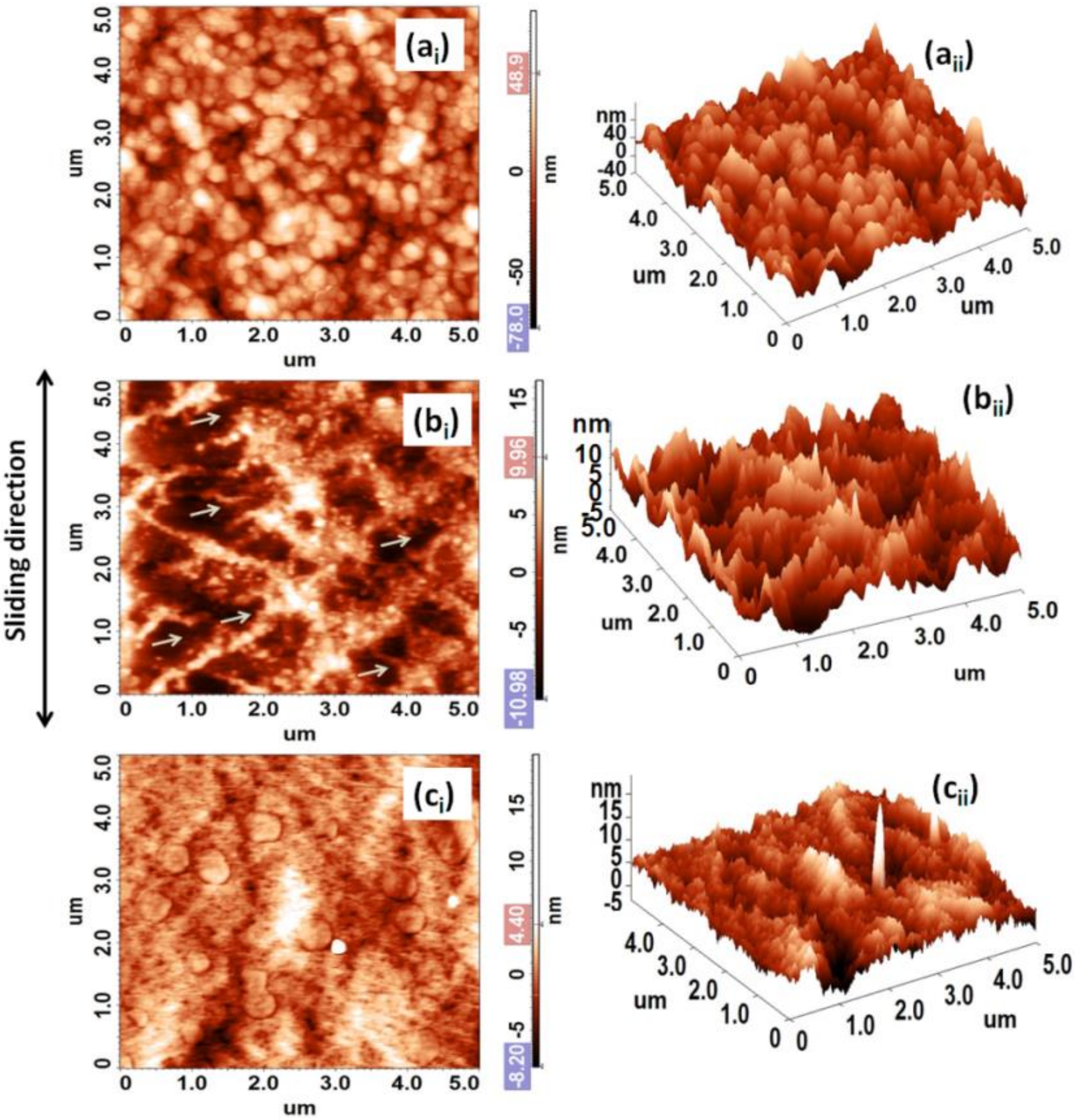

Fig. 3.7. *AFM analysis of UNCD$_N$ films: (a_i & a_{ii}) surface topography of film and topography of wear track formed at different sliding distances: (b_i & b_{ii}) 100 m and (c_i & c_{ii}) 500 m, grooves shown by arrow marks, sliding direction common for all images*

The plastic deformation and wear process of these $UNCD_N$ films is relatively easy compared to $UNCD_{Ar}$ films due to high fraction of graphitic phase encasing the needle-like diamond grains. The friction coefficient drops to saturated low value once surface contamination is removed and nanodomain secondary particles are formed. At sliding distance of 500 m, spherical nanodomains are observed which are grown to size of 200-300 nm (Figs. 3.7c_i,c_{ii}). In the beginning of plastic deformation process, the size of these secondary particles is very small (Figs. 3.7b_i,b_{ii}), indicating high surface energy and one possible way to reduce its energy is by growing into bigger one. The cohesive energy barrier for nucleation process is also small due to small size particles which possess high surface energy [23,24]. Moreover, the mobility of these nanodomains under continuous tribo-stress conditions favors them to nucleate with other nanosize domains to form bigger particles (Figs. 3.7c_i,c_{ii}). From topographical analysis, it is confirmed that some tribolayer is formed inside wear track under continuous sliding process.

Furthermore, in both UNCD films, the virgin film surface gets smoothened during tribological tests due to continuous plastic deformation process which acts as polishing media. This is clearly shown in 3D images of Fig. 3.6 and Fig. 3.7. The average roughness value (R_a) of wear tracks at sliding distance of 100 m and 500 m is reduced to 4.9 nm and 3.3 nm, respectively, for $UNCD_{Ar}$ films and 3.3 nm and 1.4 nm, respectively, for $UNCD_N$ films which are considerably less compared to that of virgin films.

3.3.4.2. Topographical dynamics of secondary phase nanoparticles in $UNCD_N$ films

High-resolution AFM images inside wear track of $UNCD_N$ films at the end of sliding process are analyzed to understand the topographical dynamics of these secondary phase nanoparticles under progressive loading conditions of 10, 20, 40, 60, 80, 100, 120 and 140 nN (Figs. 3.8a-h). At lowest force condition (i.e. 10 nN), these secondary particles possess lateral dimension of ~200-300 nm and thickness of ~2-3 nm (Fig. 3.8a). With increasing force magnitude, the extent of deformation increases along with slight changes in thickness value (Figs. 3.8b-h). Moreover, these particles are completely deformed at higher loading condition as shown in Figs. 3.8g,h. The topography of these nanodomains appears quite similar to two dimensional (2D) graphitic platelets. As $UNCD_N$ films contain more graphite phase encasing the needle-like diamond grains and thus, the deformation of this phase may lead further nucleation of 2D secondary graphitic phase under tribo-stressed conditions during continuous sliding process.

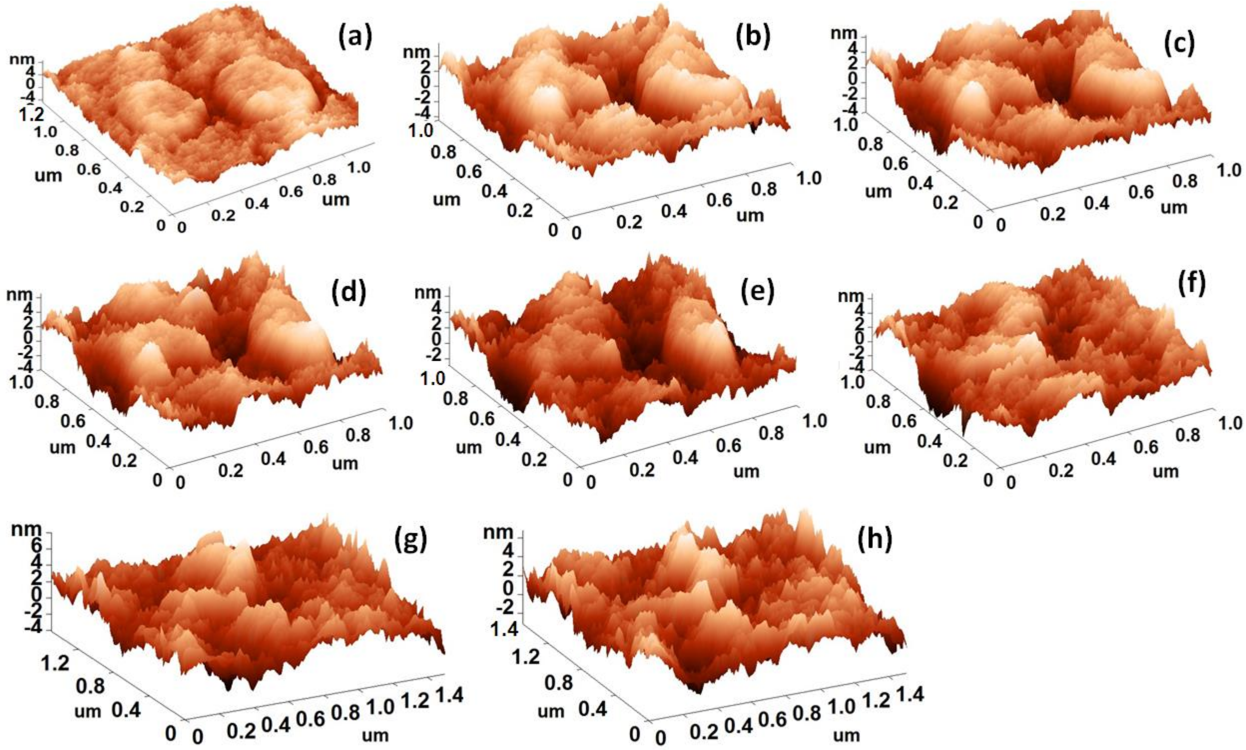

Fig. 3.8. *3D topography of nanodomains formed in the wear track of UNCD*$_N$ *films at sliding distance of 500 m: scan a to h corresponds to nanodomains under respective forces: 10, 20, 40, 60, 80, 100, 120 & 140 Nn*

3.3.5. The chemical analysis of wear track in UNCD$_N$ films

3.3.5.1. EDX mapping of wear track

To understand the chemical nature of tribofilm formed inside wear track of UNCD$_N$ films, the elemental composition of secondary phase nanoparticles is analyzed using EDX elemental mapping technique (Fig. 3.9). The EDX spectra are recorded at various locations inside the wear track and the spectral characteristic is found to be similar. The elemental composition analysis clearly suggests that particles inside the wear track are mainly constituted of carbon (97 atomic percent, at.%) (Fig. 3.9a). The morphology of these secondary particles is also shown in high-resolution backscattered electron (BSE) image (Fig. 3.9a$_i$). Furthermore, O, Si and Zr elemental composition is negligibly small i.e. only 1 at.% as shown in Figs. 3.9b-e. The very weak intensity of Zr clearly confirms the absence of Zr/ZrO$_2$ adhesive layer formation inside the wear track. The superimposed image of all elements is shown in Fig. 3.9f. Thus, from this analysis, it is clear that chemical nature of tribofilm formed inside wear track is carbonaceous.

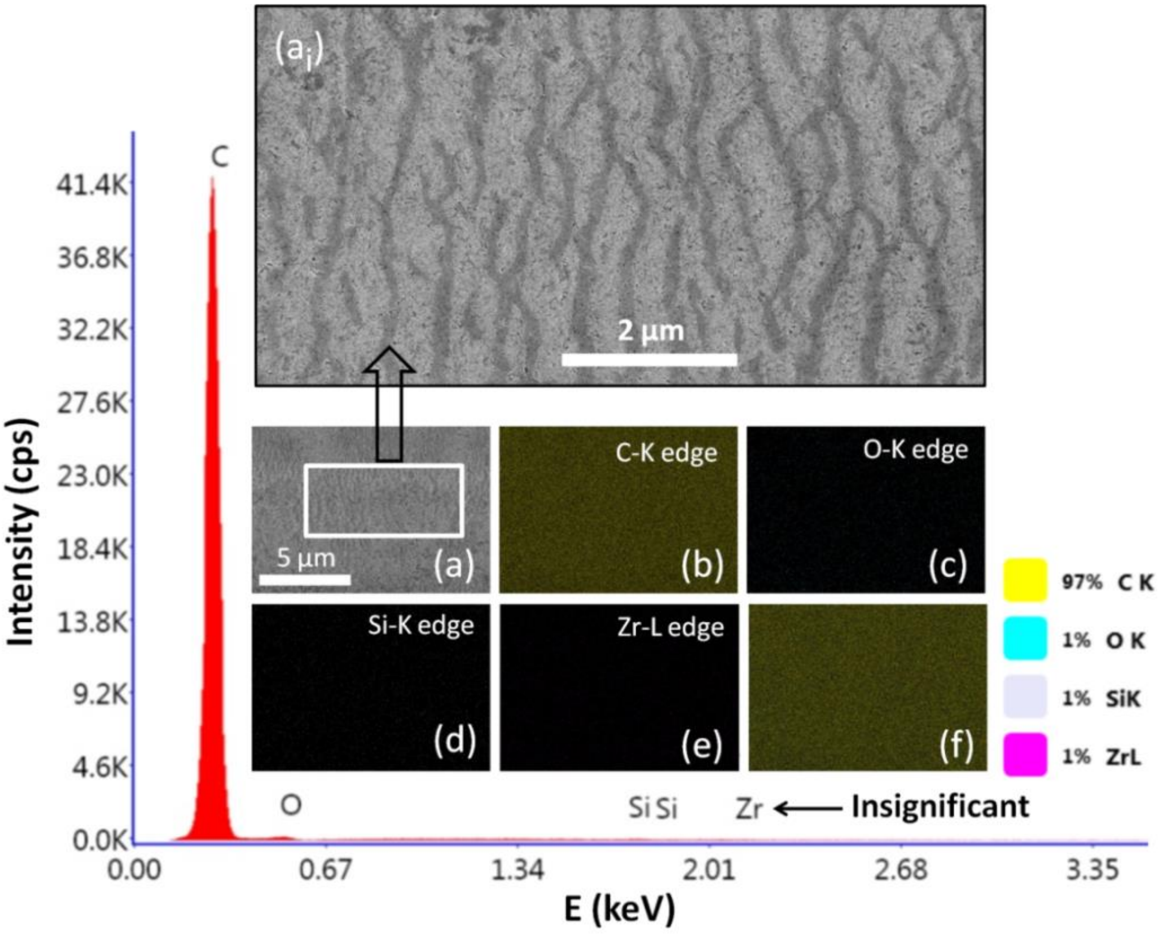

Fig. 3.9. *EDX spectra of wear track in UNCD$_N$ films: (a) Backscattered electron (BSE) image selected for EDX mapping and (a$_i$) High-resolution image inside wear track, (b) C-K edge, (c) O-K edge, (d) Si-K edge, (e) Zr-L edge and (f) superimposed images of all elements, atomic percentage (at.%) is also shown*

3.3.5.2. High-resolution XPS analysis of wear track

The high-resolution XPS analysis is carried out inside wear track of UNCD$_N$ films to know more about the chemical bonding nature of tribofilm. The XPS of UNCD$_N$ film surface is shown in Fig. 3.10a$_i$ for reference purpose. The survey spectra at film surface shows strong peak of carbon (C1s) and oxygen (O1s) at 285.5 and 533.1 eV, respectively (Fig. 3.10a$_i$). Moreover, XPS is taken at two different locations inside the wear track (Figs. 3.10a$_{ii}$-a$_{iii}$). In wear track also, strong bands of C1s and O1s are observed and a very small peak of Zr3d is also present at 182.8 eV [25]. The at.% of C, O and Zr elements is 76.43, 22.29 and 1.28, respectively. The Zr/C+O ratio is ~0.01 which clearly rules out the Zr/ZrO$_2$ adhesive transferlayer formation inside the wear track. This study indicates that the tribofilm is mainly constituted of carbon/oxidized-carbon components.

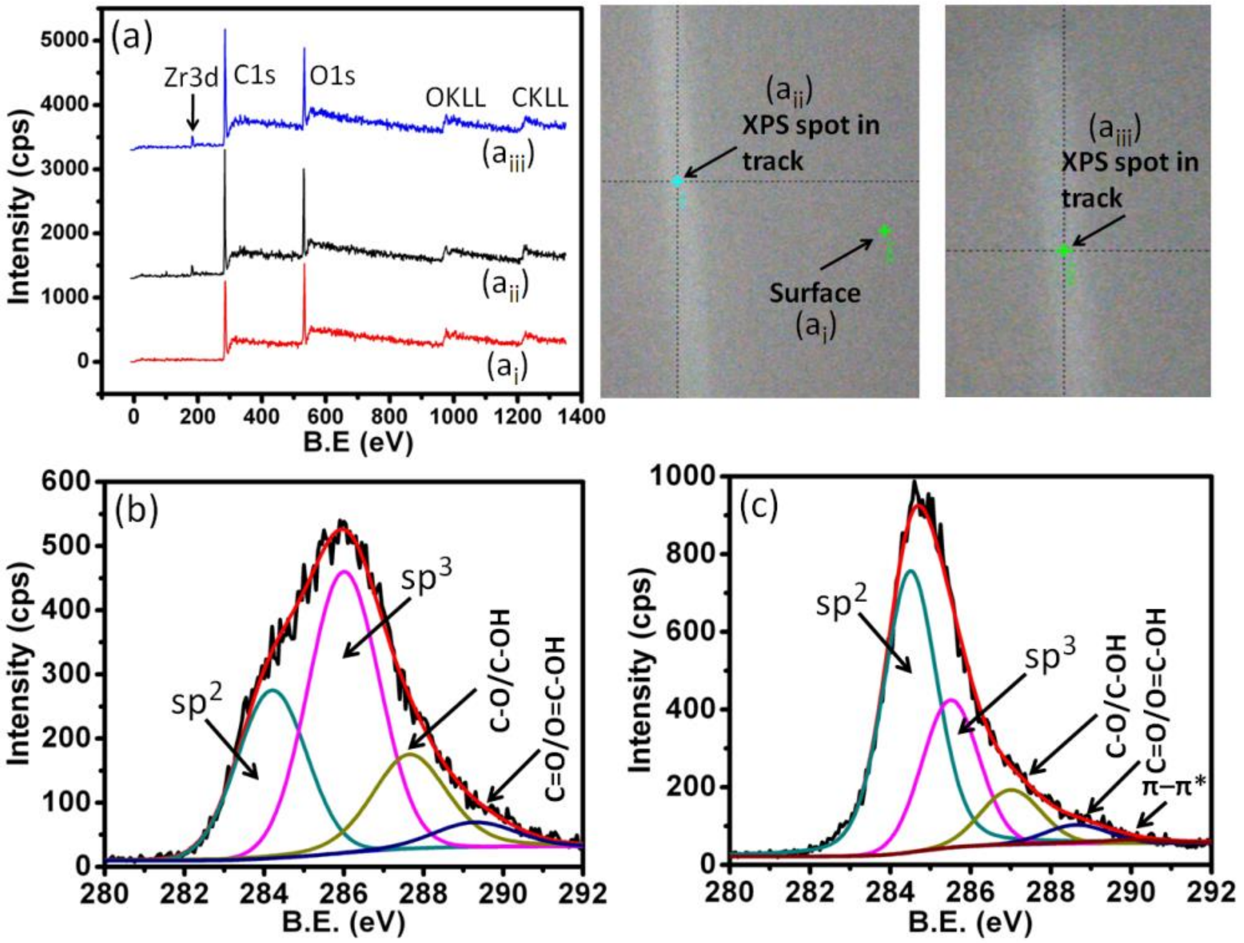

Fig. 3.10. *(a) Survey XPS spectra of (a_i) UNCD$_N$ film surface and (a_{ii} & a_{iii}) at two different spots as shown in the micrograph inside the wear track, HR C1s XPS of (b) film surface and (c) inside wear track*

The deconvoluted XPS spectra of UNCD$_N$ film surface and wear track are shown in Figs. 3.10b,c, respectively. The deconvoluted bands located at 284.2 and 286 eV at film surface correspond to sp^2 and sp^3 carbon network, respectively [26,27]. The Shirley fitting procedure is followed for XPS spectra deconvolution [28]. In wear track, sp^3 peaks are shifted to lower binding energy side i.e. 285.5 eV which is indicative of high sp^2 phase fraction [29,30]. Moreover, small peak of π–π* shake-up signal at 290.0 eV is characteristic of sp^2 hybridized carbon [31] which arises due to interaction of excited (emitted) photoelectrons with the electrons of graphite structure. The sp^2/sp^3 ratio is increased to 2.01 inside wear track compared to 0.58 on the film surface which is due to tribochemical transformation of sp^3 UNCD into graphite phases. This clearly confirms that carbonaceous tribofilm is mainly composed of graphite phase [30]. Detailed Raman measurements inside wear track of these films also corroborated with these results [22].

3.4. Tribology mechanism

The chemical affinity of ZrO_2 ball is weak towards diamond films which restricts adhesive tribolayer formation process. The friction and wear of diamond films is high for counterbody having high chemical affinity which can form adhesive tribolayer [32]. The ECR value of $UNCD_N$ films is high in the beginning of tribo-test which gradually decreases with sliding distance (Fig. 3.4b). This suggests the formation of conductive graphitized tribolayer and simultaneous decrease in friction value also. The nucleation of nanographitic phase during tribo-test is clearly evident from AFM, EDX and XPS analysis of wear track which explains short run-in regime and low stable friction coefficient value in $UNCD_N$ films. However, decrease in ECR value in $UNCD_{Ar}$ films is not much significant (Fig. 3.4a) which suggests that the nucleation of nanographitic phase in the wear track is limited for these films. Furthermore, the limited graphitic phase in $UNCD_{Ar}$ films makes these films highly wear resistant (Fig. 3.5).

3.5. Conclusions

Two sets of UNCD films are grown on Si substrate employing distinct CH_4 or N_2 plasma media in MPECVD system in order to study the effect of local phase composition on the tribological properties of UNCD films. Two different friction and wear behavior are observed in both sets of UNCD films. For $UNCD_{Ar}$ films, longer run-in is observed and the value of friction coefficient is also high in this regime. The microscopic observation of wear track shows the plastic deformation of film surface with sliding distance. The secondary phase constituted of graphitic nanodomains nucleated inside wear track of $UNCD_N$ films due to tribochemical reaction during continuous sliding process is clearly evident by in-situ ECR measurement, AFM and spectroscopic techniques. Thus, short run-in regime, low stable friction coefficient value observed in $UNCD_N$ films is governed by graphitic tribofilm formation mechanism.

3.6. References

1) K. Miyoshi, R.L.C. Wu, A. Garscadden, P.N. Barnes, H.E. Jackson, Friction and wear of plasma-deposited diamond films, J. Appl. Phys. 74 (1993) 4446–54.
2) G. Gao, R.J. Cannara, R.W. Carpick, J.A. Harrison, Atomic-scale friction on diamond: A comparison of different sliding directions on (001) and (111) surfaces using MD and AFM, Langmuir 23 (2007) 5394–405.
3) A.R. Konicek, D.S. Grierson, A.V. Sumant, T.A. Friedmann, J.P. Sullivan, P.U.P.A. Gilbert, W.G. Sawyer, R.W. Carpick, Influence of surface passivation on the friction and wear behavior of ultrananocrystalline diamond and tetrahedral amorphous carbon thin films, Phys. Rev. B 85 (2012) 15448–60.
4) R. Radhika, N. Kumar, K.J. Sankaran, R. Dumpala, S. Dash, M.S.R. Rao, D. Arivuoli, A.K. Tyagi, N.H. Tai, I.N. Lin, Extremely high wear resistance and ultralow friction behaviour of oxygen-plasma-treated nanocrystalline diamond films, J. Phys. D. Appl. Phys. 46 (2013) 425304–13.
5) R. Rani, N. Kumar, A.T. Kozakov, K.A. Googlev, K.J. Sankaran, P.K. Das, S. Dash, A.K. Tyagi, I.N. Lin, Superlubrication properties of ultra-nanocrystalline diamond film sliding against a zirconia ball, RSC Adv. 5 (2015) 100663–73.
6) Q. Tian, B. Yang, H. Zhuang, Y. Guo, C. Wang, Z. Zhai, L. Liu, N. Huang, X. Jiang, Hybrid diamond/graphite films: Morphological evolution, microstructure and tribological properties, Diam. Relat. Mater. 70 (2016) 179–85.
7) K.J. Sankaran, N. Kumar, S. Dash, H.C. Chen, A.K. Tyagi, N.H. Tai, I.N. Lin, Significance of grain and grain boundary characteristics of ultrananocrystalline diamond films and tribological properties, Surf. Coat. Technol. 232 (2013) 75–87.
8) S.R. Polaki, N. Kumar, K. Ganesan, K. Madapu, A. Bahuguna, M. Kamruddin, S. Dash, A.K. Tyagi, Tribological behavior of hydrogenated DLC film: Chemical and physical transformations at nano-scale, Wear 338–339 (2015) 105–13.
9) Y. Liu, A. Erdemir, E.I. Meletis, An investigation of the relationship between graphitization and frictional behavior of DLC coatings, Surf. Coat. Technol. 86–87 (1996) 564–68.

10) K. Panda, N. Kumar, B.K. Panigrahi, S.R. Polaki, B. Sundaravel, S. Dash, A.K. Tyagi, I.N. Lin, Tribological properties of N^+ ion implanted ultrananocrystalline diamond films, Tribol. Int. 57 (2013) 124–36.

11) A.A. Voevodin, A.W. Phelps, J.S. Zabinski, M.S. Donley, Friction induced phase transformation of pulsed laser deposited diamond-like carbon, Diam. Relat. Mater. 5 (1996) 1264–69.

12) N. Salah, A. Alshahrie, J. Iqbal, P.M.Z. Hasan, M.S. Abdel-wahab, Tribological behavior of diamond-like carbon thin films deposited by the pulse laser technique at different substrate temperatures, Tribol. Int. 103 (2016) 274–80.

13) B.K. Yen, B.E. Schwickert, M.F. Toney, Origin of low-friction behavior in graphite investigated by surface x-ray diffraction, Appl. Phys. Lett. 84 (2004) 4702–04.

14) M. Dienwiebel, G.S. Verhoeven, N. Pradeep, J.W.M. Frenken, J.A. Heimberg, H.W. Zandbergen, Superlubricity of graphite, Phys. Rev. Lett. 92 (2004) 126101–04.

15) A.R. Konicek, D.S. Grierson, P.U.P.A. Gilbert, W.G. Sawyer, A.V. Sumant, R.W. Carpick, Origin of ultralow friction and wear in ultrananocrystalline diamond, Phys. Rev. Lett. 100 (2008) 1–4.

16) G. Zilibotti, S. Corni, M.C. Righi, Load-induced confinement activates diamond lubrication by water, Phys. Rev. Lett. 111 (2013) 146101–05.

17) W. Zhang, G. Ji, A. Bu, B. Zhang, Corrosion and tribological behavior of ZrO_2 films prepared on stainless steel surface by the sol–gel method, *ACS Appl. Mater. Interfaces* 7 (2015) 28264–72.

18) K.J. Sankaran, J. Kurian, H.C. Chen, C.L. Dong, C.Y. Lee, N.H. Tai, I.N. Lin, Origin of a needle-like granular structure for ultrananocrystalline diamond films grown in a N_2/CH_4 plasma, J. Phys. D. Appl. Phys. 45 (2012) 365303–11.

19) A. Dato, V. Radmilovic, Z. Lee, J. Philips and M. Frenklach, Substrate-free gas-phase synthesis of graphene sheets, Nano Lett. 8 (2008) 2012–16.

20) P. Kovarik, E.B.D. Bourdon, R.H. Prince, Electron-energy-loss characterization of laser-deposited a-C, a-C:H, and diamond films, Phys. Rev. B 48 (1993) 12123–29.

21) S. Prawer, J.L. Peng, J.O. Orwa, J.C. McCallum, D.N. Jamieson, L.A. Bursill, Size dependence of structural stability in nanocrystalline diamond, Phys. Rev. B 62 (2000) 16360–63.

22) R. Rani, K. J. Sankaran, K. Panda, N. Kumar, K. Ganesan, S. Chakravarty and I-Nan Lin, Tribofilm formation in ultrananocrystalline diamond film, Diam. Relat. Mater. 78 (2017) 12–23.

23) Q. Jiang, J.C. Li, B.Q. Chi, Size-dependent cohesive energy of nanocrystals, Chem. Phys. Lett. 366 (2002) 551–54.

24) W.H. Qi, M.P. Wang, W.Y. Hu, Calculation of the cohesive energy of metallic nanoparticles by the Lennard-Jones potential, Mater. Lett. 58 (2004) 1745–49.

25) M. Zhang, Y. Mao, J. Guo, W. Zhou, M. Chao, N. Zhang, M. Yang, X. Kong, X. Kong, E. Liang, A novel negative thermal expansion material of $Zr_{0.70}V_{1.33}Mo_{0.67}O_{6.73}$, RSC Adv. 7 (2017) 3934–40.

26) P. Merel, M. Tabbal, M. Chaker, S. Moisa, J. Margot, Direct evaluation of the sp^3 content in diamond-like-carbon films by XPS, Appl. Surf. Sci. 136 (1998) 105–10.

27) N. Kumar, R. Radhika, A.T. Kozakov, K.J. Sankaran, S. Dash, A.K. Tyagi, N.H. Tai, I-Nan Lin, Humidity-dependent friction mechanism in an ultrananocrystalline diamond film, J. Phys. D: Appl. Phys. 46 (2013) 275501–08.

28) D.A. Shirley, High-resolution X-Ray photoemission spectrum of the valance bands of gold, Phys. Rev. B 5 (1972) 4709–14.

29) A. Fujimoto, Y. Yamada, M. Koinuma, S. Sato, Origins of sp^3 C peaks in C1s X-ray photoelectron spectra of carbon materials, Anal. Chem. 88 (2016) 6110−14.

30) A.C. Popescu, G.E. Stan, L. Duta, C. Nita, C. Popescu, V.A. Surdu, M.A. Husanu, B. Bita, R. Ghisleni, C. Himcinschi, V. Craciun, The role of ambient gas and pressure on the structuring of hard diamond-like carbon films synthesized by pulsed laser deposition, Materials 8 (2015) 3284–305.

31) R.H. Bradley, K. Cassity, R. Andrews, M. Meier, S. Osbeck, A. Andreu, C. Johnston, A. Crossley, Surface studies of hydroxylated multi-wall carbon nanotube, Appl. Surf. Sci. 258 (2012) 4835–43.

32) N. Sharma, N. Kumar, S. Dhara, S. Dash, A. Bahuguna, M. Kamruddin, A.K. Tyagi, B. Raj, Tribological properties of ultra nanocrystalline diamond film-effect of sliding counterbodies, Tribol. Int. 53 (2012) 167–78.

Chapter 4

The Effect of Gaseous Testing Environment on the Tribological Properties of UNCD Films and Addressing the Run-in Regime Issue

4.1. Introduction

The diamond thin films are used extensively for huge range of mechanical, biological and tribological applications [1-3]. The UNCD films showed ultralow friction coefficient and negligible wear [4,5] as studied in the previous chapter. However, the run-in regime is sustained for long duration of sliding process which is supposed to be due to surface contamination and adsorption of atmospheric species at film surface [6-8]. In few cases, run-in period is reported to be due to initially high film surface roughness only [9-11]. The run-in regime is reported to shorten with the increase in sp^2-bonded graphitic phase fraction in NCD/UNCD films [5,12]. The run-in tribological behavior of DLC and diamond films depend on humidity [12-15] and gaseous environmental conditions also [16,17]. It is reported that the removal of surface oxide layer is responsible for the observed run-in regime in DLC films. Furthermore, the nature of run-in regime is also distinct for different gaseous conditions [6]. So far, the tribological analysis of crystalline diamond films is less reported in different gaseous tribological conditions compared to DLC films. The low friction value studied in UNCD films in ambient/humid atmospheric conditions is reported to be due to effective passivation of dangling bonds by decomposed water molecule species [14,15,18,19]. The ultralow friction value is reported in hydrogenated carbon films in N_2 and Ar gaseous atmosphere conditions [16,20]. Adsorption of N_2 molecules at sliding interface provides electrostatically repulsive nitrogen-terminated sliding interface which is supposed to be responsible for ultralow friction value in these films [21]. But there is no experimental proof available in the literature yet to validate this hypothesis. Moreover, ultralow friction of DLC films in CH_4 atmosphere is associated with the passivation of dangling carbon bonds by hydrogen atoms/molecules, the decomposition product of CH_4 at sliding interface [16].

Thus, in this chapter, to address the run-in regime issue, chemically adsorbed oxygen/oxy-functional contaminations are removed from UNCD film surface using novel low-energy (1 keV)

Ar^+-ion sputtering process. The UNCD films are sputtered to the depths of 6, 12, 18, 24, 30 and 36 nm. The run-in regime and tribological properties of these surface modified UNCD films are studied comprehensively in distinct gaseous conditions of both inert and reactive. The friction and wear mechanisms are established in these films under different tribo-atmospheric conditions based upon experimentally observed results.

4.2. Experimental

The UNCD films are deposited on mirror-polished silicon (100) substrates using MPECVD system employing optimized deposition parameters of CH_4(4%)/Ar(rest) plasma media, microwave power of 1200 W, pressure 150 Torr and substrate temperature 550° C. In-situ depth-resolved surface chemical analysis of UNCD films is carried out after each sputtering cycle of 5, 10, 15, 20, 25 and 30 min using XPS. The surface topography and chemical structure of these films is analyzed using AFM and micro-Raman spectroscopy, respectively.

The detailed tribological analysis of UNCD films is carried out in ambient atmosphere, N_2, Ar and CH_4 gaseous media while sliding against alumina Al_2O_3 ball (6 mm diameter, R_a ~ 45 nm) using ball-on-disc geometry micro-tribometer, operating in linear reciprocating mode. Tribology test parameters; normal load, sliding speed and linear track length are kept fixed as 0.5 N, 3 cm/sec and 4 mm, respectively, for all tribo-tests. Residual RH in tribometer chamber is 5 ± 2% for N_2, Ar and CH_4 gaseous conditions and 63 ± 2% for ambient atmosphere (Amt). The as-deposited and Ar^+-ion sputtered films for 15 and 30 min designated as F_{Ar}_15 and F_{Ar}_30, respectively, are selected for detailed tribology study. Optical microscope is used for 2D wear analysis of these UNCD films and alumina balls. Moreover, chemical nature of transferfilm formed on alumina ball scar is analyzed using EDX and XPS techniques.

4.3. Results and discussion

4.3.1. The depth-resolved surface chemical analysis of films

The comprehensive depth-resolved surface chemical analysis of UNCD films is carried out using XPS. These films are sputtered to 6, 12, 18, 24, 30 and 36 nm of depths vertically corresponding to sputter time of 5, 10, 15, 20, 25 and 30 min, respectively and XPS spectra are recorded after each sputtering cycle. The survey XPS spectra are shown in Fig. 4.1 which represents the decrease in O1s/C1s peak intensity ratio with increasing sputtering depth. This clearly indicates that more oxygen is adsorbed at film surface either physically or chemically compared to the inner depth of the film surface. This oxygen contamination probably comes either from atmosphere or during film deposition process. Apart from these carbon and oxygen peaks, less intense Si2p and Si2s peaks are also observed in these spectra which are related to silicon substrate.

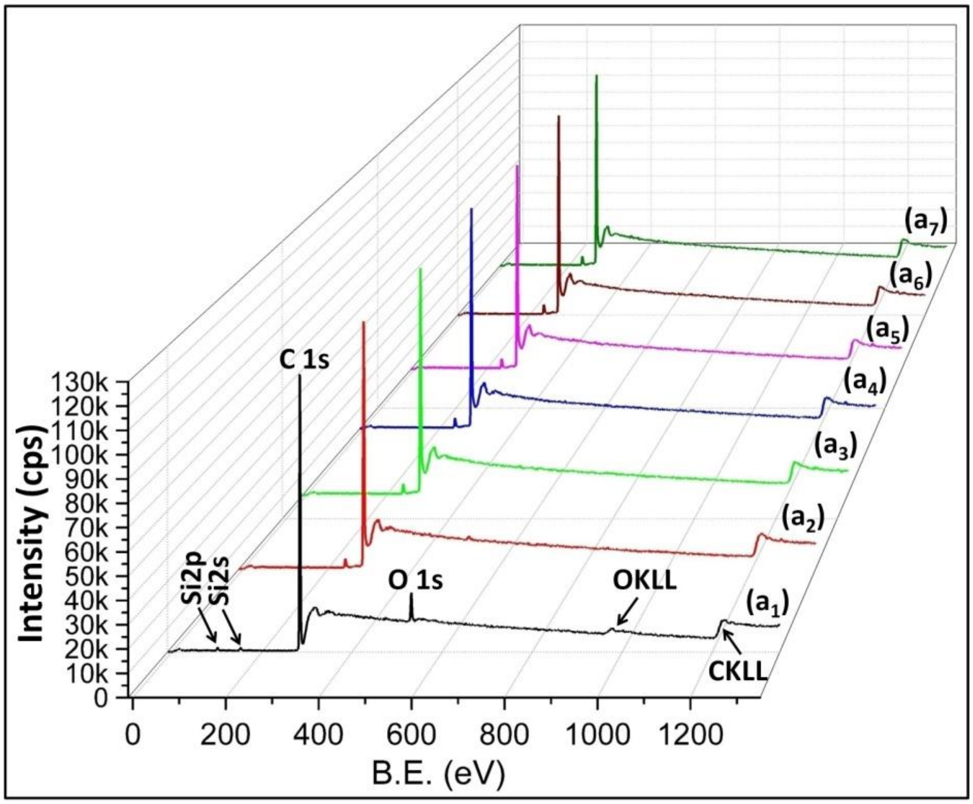

Fig. 4.1. *Depth-resolved XPS survey spectra: (a_1) as-deposited UNCD film surface and (a_2−a_7) for sputtered film surface of depths 6, 12, 18, 24, 30 and 36 nm*

Furthermore, the depth-resolved high-resolution XPS analysis of UNCD films is also carried out to have better understanding about bonding characteristics of carbon phase (Fig. 4.2a_1-a_7). The C1s spectra are deconvoluted into four individual components A, B, C and D by following Shirley method [22] where these components correspond to sp^2, sp^3 hybridized carbon phase, carboxylic (C−O/C−OH) and carbonyl (C=O) functional groups, respectively [14,23,24]. Furthermore, high-resolution depth-resolved XPS analysis of O1s photoelectrons is also carried out which clearly indicate the removal of oxygen entities from sputtered film surfaces [25]. It is clearly evident from these XPS results that sp^2/sp^3 phase fraction ratio is high for as-deposited film surface compared to Ar^+-ion sputtered films i.e. sp^2 carbon phase with oxygen functional groups is dominating at as-deposited film surface (Fig. 4.2b). Also, the possibility of Ar^+-ion sputtering induced sp^2 to sp^3 carbon phase transformation is ruled out because significant changes in sp^2 carbon phase fraction is not observed in sputtered film surfaces for inner depths.

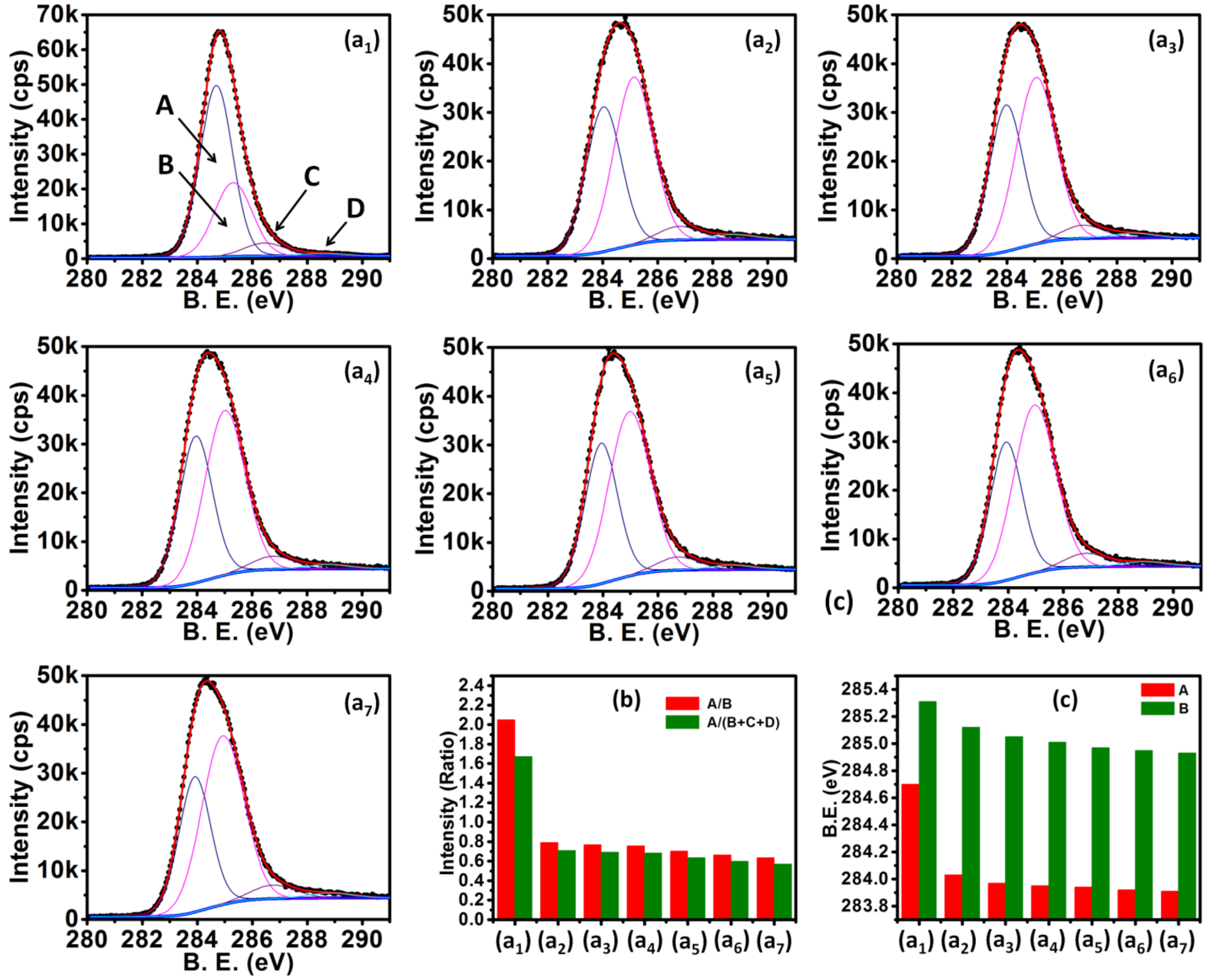

Fig. 4.2. *Depth-resolved high-resolution C1s spectra:* (a_1) *as-deposited UNCD film surface and* (a_2-a_7) *for sputtered film surface of depths 6, 12, 18, 24, 30 and 36 nm, (b) (A/B):* sp^2/sp^3 *and A/(B+C+D) ratio:* $sp^2/(sp^3+\text{oxygen complexes})$ *and (c) binding energy shift of components A and B at film surface* (a_1) *and sputtered depth of film surface* $(a_2\text{-}a_7)$

Moreover, the binding energies for both sp^2 and sp^3 hybridized states is found to decrease with sputtered depth of film surface (Fig. 4.2c) which is supposed to be due to relieving of electronic charge-screening effect of sp^2 and sp^3 states by oxygen atoms once these chemically adsorbed oxygen and oxygen-functional groups are removed by Ar^+-ion sputtering process [24]. So, the sputtered film surface is relatively chemically clean which contains more sp^3 carbon phase and fewer amounts of oxygen and oxy-functional groups compared to as-deposited film surface.

Hereafter, as-deposited UNCD films, Ar^+-ion sputtered films for 15 and 30 min i.e. F_{Ar}_15 and F_{Ar}_30, respectively, will be considered for further detailed tribological analysis.

4.3.2. The depth-resolved surface topographic analysis of films

The depth-resolved surface topographic analysis of UNCD films is carried out using AFM technique. The 3D topographical feature of Ar^+-ion sputtered UNCD films is quite similar to as-deposited films as shown in Figs. 4.3a-c. The average roughness values (R_a) in as-deposited, F_{Ar}_15 and F_{Ar}_30 films are 19 ± 3, 22 ± 2 and 21 ± 4 nm, respectively. While the root mean square roughness values (R_q) in as-deposited, F_{Ar}_15 and F_{Ar}_30 films is 24 ± 4, 28 ± 3 and 27 ± 5 nm, respectively (Fig. 4.3d). The slight variation in the roughness values observed in these films is supposed to be due to Ar^+-ion sputtering induced surface etching and decontamination of film surface as discussed above in XPS section.

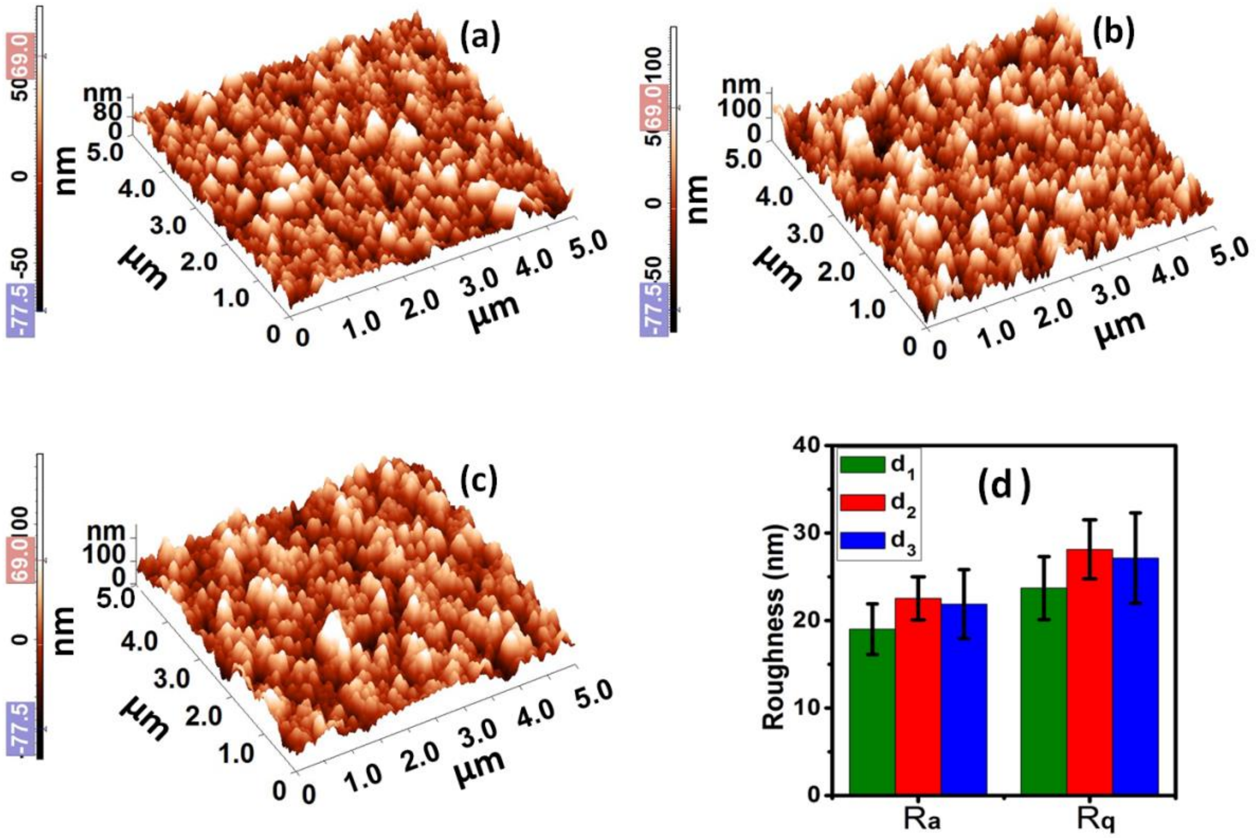

Fig. 4.3. *3D topography of films: (a) as-deposited, (b) F_{Ar}_15 and (c) F_{Ar}_30 films, (d) average roughness (R_a) and RMS roughness (R_q) of d_1: as-deposited, d_2: F_{Ar}_15 and d_3: F_{Ar}_30 films*

4.3.3. The depth-resolved structural phase analysis of films

The depth-resolved structural phase analysis of UNCD films i.e. as-deposited, F_{Ar}_15 and F_{Ar}_30 films is carried out using micro-Raman spectroscopy as shown in Fig. 4.4a. The characteristic Raman spectral signature of UNCD is clearly evident in all these films [26].

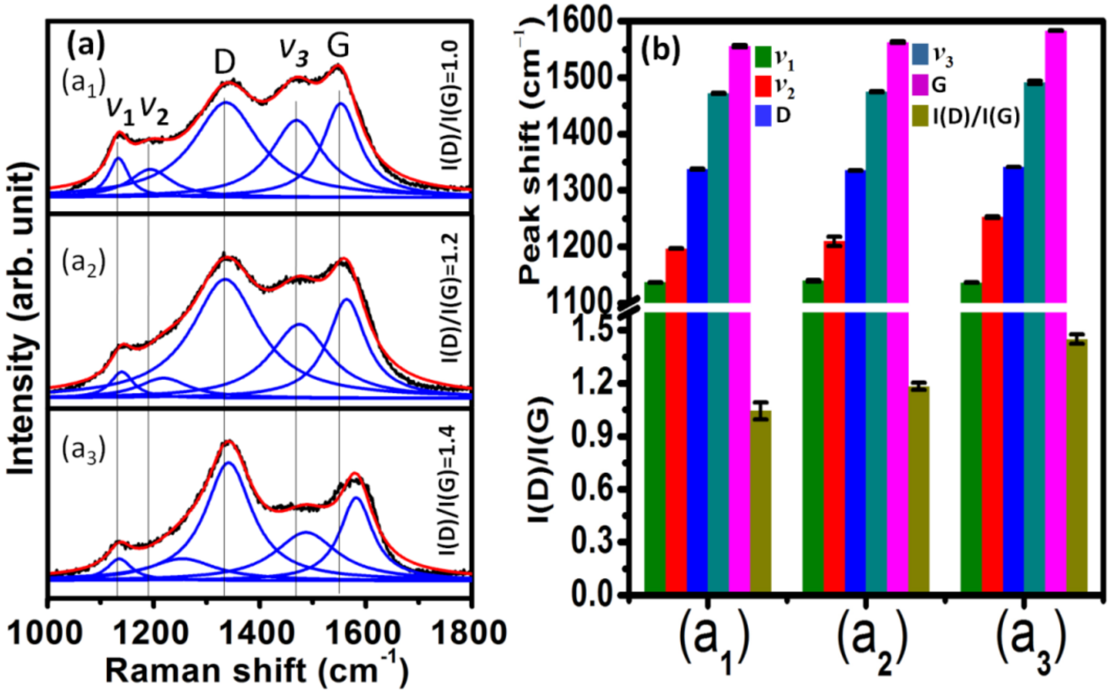

Fig. 4.4. *(a) Raman spectra of films and (b) peak position of* v_1, v_2, v_3, *D and G bands and I(D)/I(G) ratio: (*a_1*) as-deposited, (*a_2*)* F_{Ar}*_15 and (*a_3*)* F_{Ar}*_30 films*

The systematic peak intensity reduction and blue shift of v_1, v_2 and v_3 bands are observed in F_{Ar}_15 and F_{Ar}_30 films with reference to as-deposited films (Figs. 4.4a$_1$-a$_3$) which indicate about the change of long *t-PA* chains into shorter one after Ar$^+$-ion sputtering process [27]. Moreover, the blue shift of G band and increase in I(D)/I(G) ratio in sputtered films are fingerprint of small in-plane size of sp^2 phase [28]. Furthermore, the relative increase in D band intensity after sputtering process also indicates the decrease in graphite phase and increase in *a-C* and sp^3 phase in sputtered films. Moreover, the Raman analysis carried out at various locations in these films also supports these results as shown in Fig. 4.4b. It is reported that the sp^2 phase rich layer is formed at film surface during final steps of deposition process [29]. The depth-dependent variation in the chemical nature of UNCD films is supposed to be due to removal of sp^2-rich phase with long *t-PA* chain from as-deposited UNCD film surface during sputtering process. Moreover, Ar$^+$-ion sputtering induced conversion of sp^2 into sp^3 phase and vice versa needs very high activation energy which is not feasible in our present scenario [30].

4.3.4. The gas dependent friction and wear behavior of UNCD films

The friction analysis of as-deposited, F$_{Ar}$_15 and F$_{Ar}$_30 films is carried out while sliding against alumina Al_2O_3 ball in four distinct environmental conditions of Amt, N_2, Ar and CH_4 media as shown in Fig. 4.5. In all tribo-conditions, the friction coefficient gradually decreases and saturates to ultralow value 0.02-0.05 after initial run-in behavior (Figs. 4.5a-c). In all three sets of UNCD films, the highest friction coefficient value is observed in ambient condition.

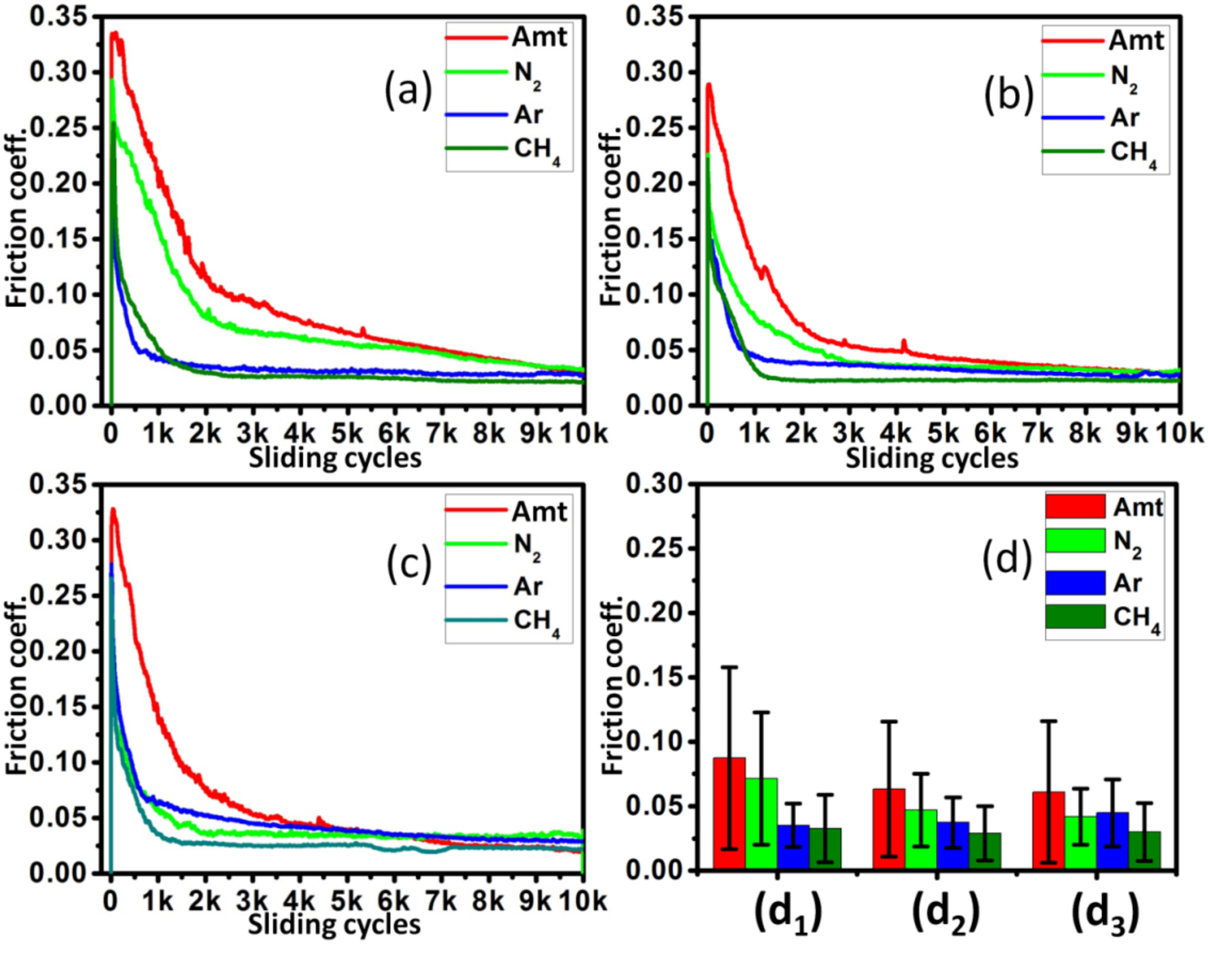

Fig. 4.5. *Friction coefficient vs sliding cycles (1k = 1000 cycles) of (a) as-deposited, (b) F$_{Ar}$_15 and (c) F$_{Ar}$_30 films and (d) friction coefficient with standard deviation of (d_1) as-deposited, (d_2) F$_{Ar}$_15 and (d_3) F$_{Ar}$_15 films in different tribo-atmospheric conditions: Amt, N_2, Ar, and CH_4 media*

However, the friction value is lowest in CH_4 tribo-environmental condition for all three sets of UNCD films (Fig. 4.5d). Moreover, moderate friction value is measured in inert Ar and N_2 atmospheres. The average values of friction coefficients are found to decrease in sputtered films compared to as-deposited UNCD films in all tribo-environmental conditions as shown in Fig. 4.5d. The wear tracks of as-deposited, F_{Ar}_15 and F_{Ar}_30 films and corresponding ball scars for all tribological conditions are shown in Fig. 4.6a. Highest wear resistance property is observed for CH_4 tribo-environmental condition for all three sets of UNCD films with lowest wear track width and ball scar size.

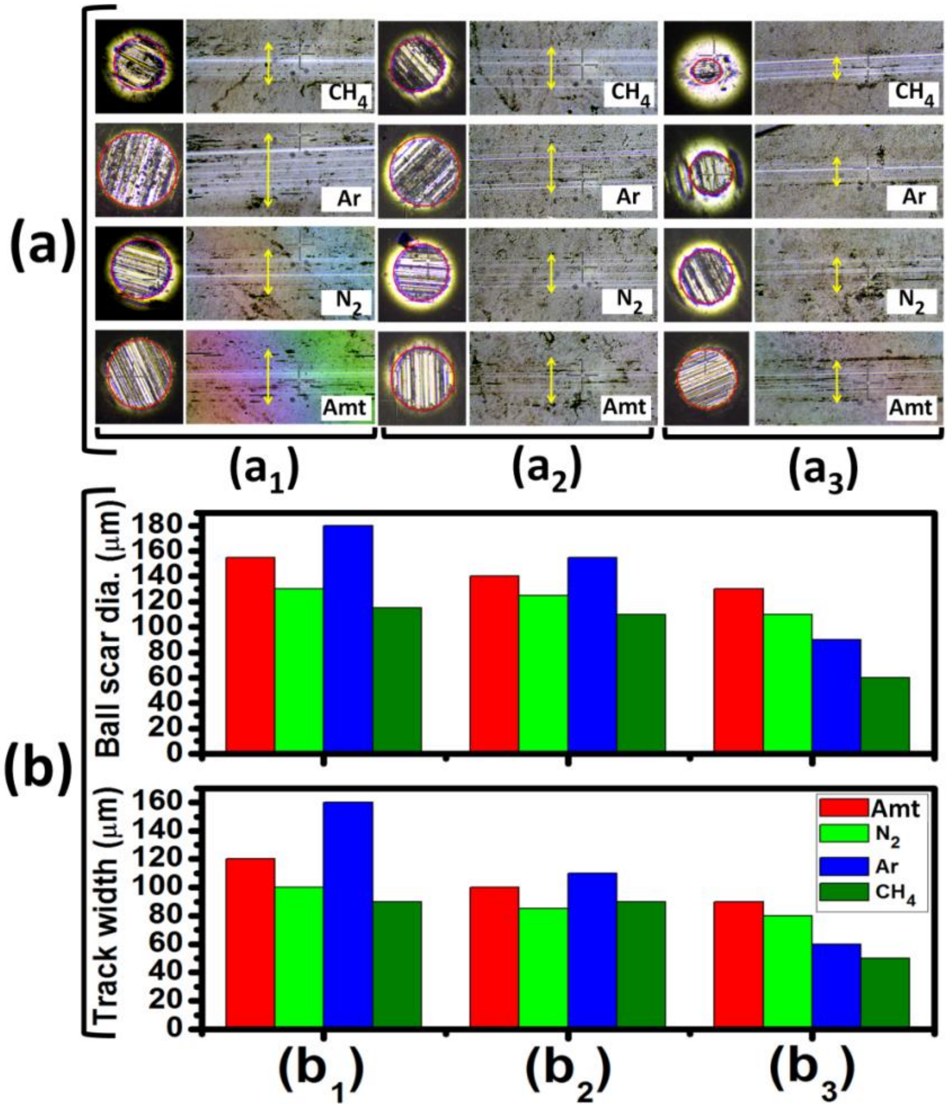

Fig. 4.6. *(a) Optical image of wear tracks and ball scars, (b) wear dimensions of sliding interfaces in bar graph: (a_1, b_1) as-deposited, (a_2, b_2) F_{Ar}_15 and (a_3, b_3) F_{Ar}_30 films in different tribo-atmospheric conditions: Amt, N_2, Ar, and CH_4 media*

The run-in regime and wear is found to decrease in sputtered films compared to as-deposited UNCD films in all tribo-conditions. It is reported that the friction and wear generally increase with the increase in roughness value of films [10,11]. Though, the roughness value is slightly higher in sputtered films compared to as-deposited films and therefore, the roughness parameter alone is not the ruling factor for observed friction and wear behavior. To understand the observed friction and wear results, the detailed elemental and surface chemical analysis of alumina ball scar is carried out in all four distinct tribological conditions as discussed below.

4.3.5. The chemical analysis of alumina ball scar

To establish the governing tribological mechanisms in all distinct tribo-media, the EDX and XPS analysis of alumina ball scar are carried out while sliding against F_{Ar}_30 films.

4.3.5.1. EDX analysis

The EDX elemental mapping of alumina ball scars is carried out to understand the chemical nature of transferfilm formed on these ball scars during tribological tests. EDX being bulk sensitive technique provides valuable information about the bulk chemical composition of given test sample. The superimposed images of all elements and also the corresponding EDX spectra are shown in Fig. 4.7 for all distinct tribo-conditions. Moreover, the detailed elemental mapping results for individual elements are also analyzed for each tribo-condition [25]. The EDX analysis clearly reveals that C at.% is highest at ball scar developed in ambient condition compared to all other tribo-conditions (Figs. 4.7a-d). Thus, carbon transferfilm formation on ball scar is more favorable in ambient condition. The small amount of N on alumina ball scar is clearly evident in N_2 tribo-atmospheric medium which suggests the adsorption of nitrogen on alumina ball scar as a result of sliding process (Fig. 4.7b).

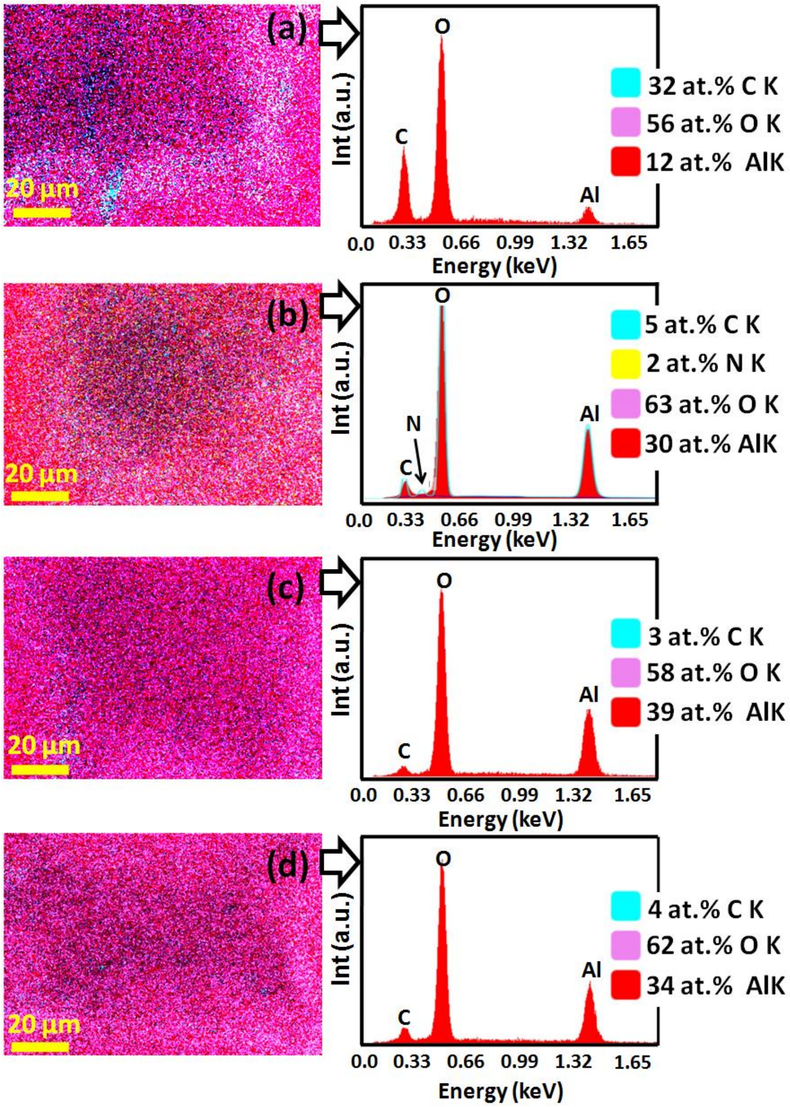

Fig. 4.7. *In the left panel: EDX elemental mapping of the alumina ball scar while sliding against* F_{Ar}*_30 films, In the right panel: EDX spectra of the whole area mapping of ball scar developed in (a) ambient, (b)* N_2*, (c) Ar and (d)* CH_4 *media*

4.3.5.2. XPS analysis

The detailed surface chemical analysis of alumina ball scars is carried out using XPS for all distinct tribo-conditions as shown in Fig. 4.8. The XPS survey spectra show well-resolved C1s peak in all four tribo-conditions which suggest the carbonaceous transferfilm formation on ball scars. Moreover, the C/(O+Al) ratio is highest in ambient condition [25] compared to N_2, Ar and CH_4 tribo-conditions which clearly indicates that carbonaceous transferfilm formation is high in ambient condition as studied by EDX analysis as well. Furthermore, the high-resolution XPS spectra are also obtained for local chemical bonding analysis of ball scars at locations marked as circle in Figs. 4.8a$_1$-d$_1$.

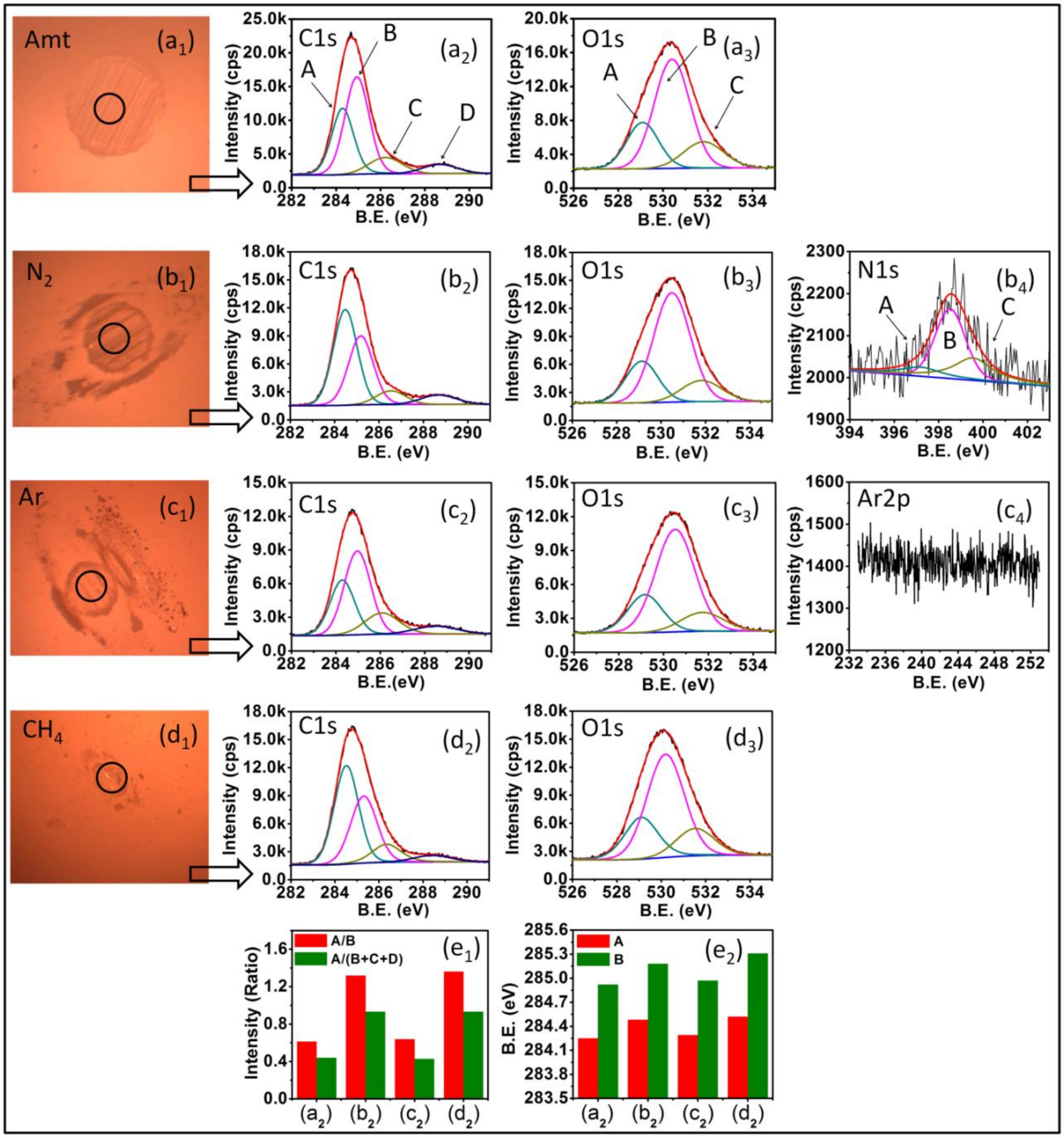

Fig. 4.8. *Optical image of alumina ball scar in (a$_1$) Amt, (b$_1$) N$_2$, (c$_1$) Ar and (d$_1$) CH$_4$ atmosphere, and corresponding high-resolution XPS spectra: (a$_2$−d$_2$) C1s spectra, (a$_3$−d$_3$) O1s spectra, (b$_4$) N1s spectra and (c$_4$) Ar2p spectra, (e$_1$) (A/B): sp^2/sp^3 and A/(B+C+D): sp^2/(sp^3+C−O/C−OH+C=O) ratio and (e$_2$) binding energy shift of sp^2 (A) and sp^3 (B) components: (a$_2$−d$_2$ in x-axis) in (e$_1$) and (e$_2$) correspond to (a$_2$) Amt, (b$_2$) N$_2$, (c$_2$) Ar and (d$_2$) CH$_4$ tribo-atmosphere*

In all tribo-conditions, the C1s band is deconvoluted into four individual components A, B, C and D as shown in Figs. 4.8a_2-d_2 which correspond to sp^2 and sp^3 hybridized carbon phases, C−O/C−OH and C=O functional groups, respectively [23]. It is clearly evident that these functional groups are more active at ball scar compared to F_{Ar}_30 film surface (Fig. 4.2a_7) which is supposed to be due to tribo-chemical reactions at contact sliding interface during tribological process [31]. The C1s spectra clearly suggest that sp^2/sp^3 ratio is tribo-atmospheric dependent. This ratio is low i.e. 0.61 and 0.63 in ambient and Ar gas media, respectively (Figs. 4.8a_2,c_2) and significantly increased to 1.31 and 1.35 in N_2 and CH_4 tribo-atmospheric conditions, respectively (Figs. 4.8b_2,d_2). The A/(B+C+D) ratio is lower i.e. 0.43 and 0.42 in ambient and Ar gas media, respectively. However, these values increased to 0.93 in both N_2 and CH_4 tribo-atmospheric conditions as shown in Fig. 4.8e_1. This clearly indicates relatively high sp^2 carbon phase fraction on ball scar in N_2 and CH_4 tribo-conditions. The electronic interaction of sp^2 and sp^3 carbon phases with static residual charge of alumina surface causes high binding energy shift of these phases (Fig. 4.8e_2). However, in the case of ambient and Ar gas media, the influence of static charge of alumina is not much significant due to relatively thick carbon transferfilm formation. Moreover, O1s spectra are quite similar in all four tribo-atmospheric media (Figs. 4.8a_3-d_3). The broad O1s spectra is deconvoluted into three components A, B and C which correspond to C=O, C−OH and C−O chemical groups, respectively. In O1s spectra, oxygen from both Al_2O_3 ball and ambient atmosphere contribute to form oxygen functional complexes.

The chemisorbed phases at sliding interface in N_2 gas media protect against the oxygen functional group formation during sliding process. This is well evident in N1s spectra as shown in Fig. 4.8b_4 where three well-resolved bands of A, B and C components are observed at energy shift of 397.2, 398.5 and 399.5 eV, respectively. The component A corresponds to C−N bonding phase which can occur only when N_2 gas molecule dissociates into isolated N atoms [32]. However, B and C components correspond to N_2 chemisorptions into sp^2 and sp^3 carbon phases, respectively, where the lone electron pair of N_2 molecule interacts with relatively less electronegative carbon atoms due to difference in the electronic charged dipole states of these atoms. The Ar gas being electrically neutral does not interact with sliding interface. However, physical adsorption of Ar at sliding interface is probable due to induced dipole interaction between carbon and Ar atoms. The evidence of chemisorbed Ar at ball scar is not noticed in

Ar2p spectra (Fig. 4.8c_4). Moreover, in ambient condition, the moisture and water vapor chemically interact with sliding interface and hence, more oxygen functional groups are formed.

4.3.6. The tribological mechanisms

The governing tribological mechanisms are established for UNCD films in all four distinct tribo-atmospheric conditions based on the experimentally obtained results.

4.3.6.1. Ambient tribo-atmospheric condition

In ambient condition, water molecules interact with the sp^2 and sp^3 carbon network of UNCD film forming COO, C−O and C−OH oxy-functional groups [33,34]. Furthermore, the single atom of dissociated oxygen molecule reacts with the unsaturated carbon atoms of UNCD film surface forming C−O−C covalent bonds and other functional complexes and thus, creating strong adhesion at sliding interface and cause increase in tangential shear force [35,36]. However, the density functional calculations predict that H_2 passivation mechanism is more effective in diamond films compared to dissociative H_2O passivation mechanism [37]. The EDX analysis confirms the carbonaceous transferlayer formation on ball scar (Fig. 4.7a). Moreover, the XPS analysis provides the evidence of more oxidized carbon and oxygen functional complexes on ball counterbody (Fig. 4.8a_2) and thus, high friction of UNCD films is observed in ambient condition. However, a gradual decrease of friction value in F_{Ar}_15 and F_{Ar}_30 films is noticed compared to as-deposited UNCD films. The average friction value is 0.08 in as-deposited films compared to to 0.06 and 0.05 in F_{Ar}_15 and F_{Ar}_30 films, respectively (Fig. 4.5). The standard deviation in the friction value is reduced to 26 and 22% of as-deposited films in F_{Ar}_15 and F_{Ar}_30 films, respectively, which indicates about the stable friction behavior in sputtered films. This is probably due to removal of the adsorbed oxygen and oxy-functional groups from as-deposited film surface after sputtering process which definitely reduced the oxidation and covalent-linking possibility of functional groups across the sliding interfaces [36] and thus, reduced the run-in regime also.

4.3.6.2. N_2 tribo-atmospheric conditions

The chemically inert N_2 and Ar gases provide physically/chemically adsorbed gaseous layer at sliding interface depending on their chemical affinity towards film surface and thus, reduce the strong covalent bonding possibility across sliding interface [21]. In N_2 tribo-atmosphere, electrostatic repulsion is possible at contact tribo-interface if two folds of N_2-terminated carbon film surfaces are brought into contact [21,38,39]. The EDX analysis indicates the carbonaceous transferlayer formation on ball scar in N_2 tribo-atmosphere (Fig. 4.7b). The evidence of adsorbed N_2 and C–N phase at ball scar is also clearly evident in XPS spectra (Fig. 4.8b$_4$) which validate the electrostatically repulsive mechanism for friction reduction in N_2 tribo-condition. Moreover, the experimental evidence of these chemically adsorbed phases is not available in literature yet. The mean value of friction coefficient is 0.05 and 0.04 for F_{Ar}_15 and F_{Ar}_30 films, respectively, compared to 0.07 in the as-deposited films (Fig. 4.5). The standard deviation in friction value is reduced to 45 and 57% of as-deposited films in F_{Ar}_15 and F_{Ar}_30 films, respectively. In run-in regime, the friction value is higher especially in as-deposited films mainly because of the oxygen and oxy-functional groups at film surface which interact with N_2 gas and destroy the electrostatic repulsion across the sliding interface and thus, cause the increase in frictional resistance [36].

4.3.6.3. Ar tribo-atmospheric condition

The carbon dangling bonds does not interact with inert Ar gaseous atoms chemically and hence provide no passivation mechanism at sliding interface which is supposed to be the main reason for high friction of diamond films in Ar condition compared to N_2 tribo-condition [39]. The friction value of UNCD films is less in Ar tribo-atmosphere compared to ambient condition. Moreover, the friction value in Ar atmosphere is less than that of N_2 as well in as-deposited and F_{Ar}_15 films. This is probably due to the physical adsorption of Ar at sliding interface which restricts the covalent interaction between dangling carbon bonds at sliding interface and thus, keeps the sliding surfaces apart. It is interesting to note that friction value in this condition does not change much in as-deposited and sputtered films which directly indicates the absence of chemical interaction of Ar with diamond films. Though in XPS spectra, the signature of Ar is absent (Fig. 4.8c$_4$) as because it is not chemically adsorbed at sliding interface. The mean value of friction coefficient slightly increases to 0.036 and 0.04 in F_{Ar}_15 and F_{Ar}_30 films, respectively, compared to 0.035 in as-deposited films (Fig. 4.5). The standard deviation in friction value is also found to increase by 15 and 55% of the as-deposited films in F_{Ar}_15 and F_{Ar}_30 films, respectively.

4.3.6.4. CH_4 tribo-atmospheric condition

The friction coefficient of UNCD films is significantly less in CH_4 tribo-atmospheric condition compared to other gaseous conditions. The mean value of friction is 0.033 in as-deposited films which reduces to 0.029 in F_{Ar}_15 and F_{Ar}_30 films (Fig. 4.5). Furthermore, the standard deviation in friction value is also similar in all three films. In this tribo-condition, the dangling carbon bonds at film surface are instantly saturated by hydrogen atoms/molecules, a dissociated product of CH_4 molecules [39]. It can be clearly understood by considering that one fold of hydrogenated carbon surface interacts with the other fold of sliding surface having the same hydrogenated carbon configuration and thus, generate weak repulsive Van der Waals force at sliding interface. This is a well known mechanism by which low friction is explained for carbon based films in CH_4 tribo-condition [16,39]. Moreover, this mechanism is more effective when oxygen and oxy-functional additives are absent or limited at film surface which may restrict the effective electrostatic repulsion of sliding interfaces. However, no such influence is observed on friction results in as-deposited films which suggest the excess adsorption of CH_4 molecules and its dissociative complexes at sliding interface.

4.4. Conclusions

The UNCD films are sputtered using low energy Ar^+-ion in ultrahigh vacuum condition to remove the oxygen/oxy-functional and excess *a-C*/graphitic phase contaminations from the film surface to address the run-in issue. Friction and wear properties of these films are studied in distinct environments of reactive and inert gaseous conditions and suitable tribological mechanisms are established based upon the experimentally observed results. High friction in ambient atmospheric condition is associated with the oxidation of the sliding interfaces. The low friction in N_2 tribo-atmosphere is due to the adsorption of dissociated N_2 gas molecules forming repulsive electrostatic interaction across the sliding interface. Moreover, low friction in chemically inert Ar atmosphere is possibly due to the adsorption of inert Ar gaseous species which avoid the covalent carbon bond formation across the sliding interface. Furthermore, the friction value in chemically reactive CH_4 tribo-atmosphere is lowest due to hydrogen-terminated carbon bond formation at the sliding interface. The friction trends of sputtered films show lower run-in regime in all tribo-atmospheric conditions which is due to the elimination of oxygen/oxy-functional additives and *a-C* contamination from film surface. Moreover, wear resistance is significantly improved in Ar^+-ion sputtered films in all tribo-atmospheric conditions.

4.5. References

1) P.W. May, Diamond thin films: A 21st-century material, Philos. Trans. R. Soc. A 358 (2000) 473–95.
2) O.A. Williams, Nanocrystalline diamond, Diam. Relat. Mater. 20 (2011) 621–40.
3) P.A. Nistor, P.W. May, Diamond thin films: Giving biomedical applications a new shine, J. R. Soc. Interface 14 (2017) 382–96.
4) R. Rani, N. Kumar, A.T. Kozakov, K.A. Googlev, K.J. Sankaran, P.K. Das, S. Dash, A.K. Tyagi, I.N. Lin, Superlubrication properties of ultra-nanocrystalline diamond film sliding against a zirconia Ball, RSC Adv. 5 (2015) 100663–73.
5) R. Rani, K.J. Sankaran, K. Panda, N. Kumar, K. Ganesan, S. Chakravarty, I.N. Lin, Tribofilm formation in ultrananocrystalline diamond film, Diam. Relat. Mater. 78 (2017) 12–23.
6) M.J. Marino, E. Hsiao, Y. Chen, O.L. Eryilmaz, A. Erdemir, S.H. Kim, Understanding run-in behavior of diamond-like carbon friction and preventing diamond-like carbon wear in humid air, Langmuir 27 (2011) 12702–08.
7) P. Manimunda, A. Al-Azizi, S.H. Kim, R.R. Chromik, Shear-induced structural changes and origin of ultralow friction of hydrogenated diamond-like carbon (DLC) in dry environment, ACS Appl. Mater. Interfaces 9 (2017) 16704−14.
8) R. Zhang, Z. Lu, L. Wang, Understanding the run-in tribological behavior of amorphous carbon films against Al_2O_3 balls under high vacuum, RSC Adv. 5 (2015) 32690–97.
9) A. Erdemir, C. Donnet, Tribology of diamond-like carbon films: Recent progress and future prospects, J. Phys. D: Appl. Phys. 39 (2006) 311–27.
10) I.P. Hayward, I.L. Singer, L.E. Seitzman, Effect of roughness on the friction of diamond on CVD diamond coatings, Wear 157 (1992) 215–27.
11) A. Erdemir, G.R. Fenske, A.R. Krauss, D.M. Gruen, T. McCauley, R.T. Csencsits, Tribological properties of nanocrystalline diamond films, Surf. Coat. Technol. 120–121 (1999) 565–72.
12) R.R. Chromik, A.L. Winfrey, J. Luning, R.J. Nemanich, K.J. Wahl, Run-in behavior of nanocrystalline diamond coatings studied by in situ tribometry, Wear 265 (2008) 477–89.
13) A.R. Konicek, D.S. Grierson, A.V. Sumant, T.A. Friedmann, J.P. Sullivan, P.U.P.A. Gilbert, W.G. Sawyer, R.W. Carpick, Influence of surface passivation on the friction and

wear behavior of ultrananocrystalline diamond and tetrahedral amorphous carbon thin films, Phys. Rev. B 85 (2012) 155448–60.

14) N. Kumar, R. Ramadoss, A.T. Kozakov, K.J. Sankaran, S. Dash, A.K. Tyagi, N.H. Tai, I.N. Lin, Humidity-dependent friction mechanism in an ultrananocrystalline diamond film, J. Phys. D: Appl. Phys. 46 (2013) 275501–08.
15) W. Qin, W. Yue, C. Wang, Understanding integrated effects of humidity and interfacial transfer film formation on tribological behaviors of sintered polycrystalline diamond, RSC Adv. 5 (2015) 53484–96.
16) S.R. Polaki, N. Kumar, K. Madapu, K. Ganesan, N.G. Krishna, S.K. Srivastava, S. Abhaya, M. Kamruddin, S. Dash, A.K. Tyagi, Interpretation of friction and wear in DLC film: Role of surface chemistry and test environment, J. Phys. D: Appl. Phys. 49 (2016) 445302–14.
17) H. Miki, N. Yoshida, K. Bando, T. Takeno, T. Abe, T. Takagi, Atmosphere dependence of the frictional wearing properties of partly-polished polycrystalline diamonds, Diam. Relat. Mater. 17 (2008) 868–72.
18) A.R. Konicek, D.S. Grierson, P.U.P.A. Gilbert, W.G. Sawyer, A.V. Sumant, R.W. Carpick, Origin of ultralow friction and wear in ultrananocrystalline diamond, Phys. Rev. Lett. 100 (2008) 235502–05.
19) M.I.D.B. Bouchet, G. Zilibotti, C. Matta, M.C. Righi, L. Vandenbulcke, B. Vacher, J.M. Martin, Friction of diamond in the presence of water vapor and hydrogen gas. Coupling gas-phase lubrication and first-principles studies, J. Phys. Chem. C 116 (2012) 6966−72.
20) J. Shi, Z. Gong, C. Wang, B. Zhang, J. Zhang, Tribological properties of hydrogenated amorphous carbon films in different atmospheres, Diam. Relat. Mater. 77 (2017) 84–91.
21) C. Wang, B. Li, X. Ling, J. Zhang, Superlubricity of hydrogenated carbon films in a nitrogen gas environment: Adsorption and electronic interactions at the sliding interface, RSC Adv. 7 (2017) 3025–34.
22) D.A. Shirley, High-resolution X-ray photoemission spectrum of the valance bands of gold, Phys. Rev. B 5 (1972) 4709–14.
23) P. Merel, M. Tabbal, M. Chaker, S. Moisa, J. Margot, Direct evaluation of the sp^3 content in diamond-like-carbon films by XPS, Appl. Surf. Sci. 136 (1998) 105–10.

24) B. Ren, J. Huang, H. Yu, W. Yang, L. Wang, Z. Pan, L. Wang, Thermal stability of hydrogenated diamond films in nitrogen ambience studied by reflection electron energy spectroscopy and X-ray photoelectron spectroscopy, Appl. Surf. Sci. 388 (2016) 565–70.

25) R. Rani, K. Panda, N. Kumar, K.J. Sankaran, K. Ganesan, I-Nan Lin, Tribological properties of ultrananocrystalline diamond films in inert and reactive tribo-atmospheres: XPS depth-resolved chemical analysis, J. Phys. Chem. C 122 (2018) 8602−13.

26) K.K. Mishra, R. Rani, N. Kumar, T.R. Ravindran, K.J. Sankaran, I.N. Lin, High pressure Raman spectroscopic sudies on ultrananocrystalline diamond thin films: Anharmonicity and thermal properties of the grain boundary, Diam. Relat. Mater. 80 (2017) 45–53.

27) M. Rybachuk, J.M. Bell, Electronic states of trans-polyacetylene, poly (p-phenylene vinylene) and sp-hybridised carbon species in amorphous hydrogenated carbon probed by resonant Raman scattering, Carbon 47 (2009) 2481–90.

28) A.C. Ferrari, J. Robertson, Interpretation of Raman spectra of disordered and amorphous carbon, Phys. Rev. B 61 (2000) 14095–107.

29) M.I.D.B. Bouchet, C. Matta, B. Vacher, T.L. Magne, J.M. Martin, J.V. Lautz, T. Ma, L. Pastewka, J. Otschik, P. Gumbsch, M. Moseler, Energy filtering transmission electron microscopy and atomistic simulations of tribo-induced hybridization change of nanocrystalline diamond coating, Carbon (2015) 87 317–29.

30) J. Narayan, A. Bhaumik, Direct conversion of amorphous carbon into diamond at ambient pressures and temperatures in air, APL Mater. 3 (2015) 100702–12.

31) G. Zilibotti, S. Corni, M.C. Righi, Load-induced confinement activates diamond lubrication by water, Phys. Rev. Lett. 111 (2013) 146101–05.

32) I. Kusunoki, M. Sakai, Y. Igari, S. Ishidzuka, T. Takami, T. Takaoka, M.N. Gamo, T. Ando, Nitridation of a diamond film using 300–700 eV N_2^+ ion beams, Diam. Relat. Mater. 9 (2000) 698–702.

33) A. Alazizi, A.J. Barthel, N.D. Surdyka, J. Luo, S.H. Kim, Vapors in the ambient–A complication in tribological studies or an engineering solution of tribological problems?, Friction 3 (2015) 85–114.

34) E. Desimoni, G.I. Casella, A. Morone, A.M. Salvi, XPS determination of oxygen-containing functional groups on carbon-fibre surfaces and the cleaning of these surfaces, Surf. Interface Anal. 15 (1990) 627–34.

35) S. Dag, S. Ciraci, Atomic scale study of superlow friction between hydrogenated diamond surfaces, Phys. Rev. B 70 (2004) 241401−04.

36) L. Wang, L. Cui, Z. Lu, H. Zhou, Understanding the unusual friction behavior of hydrogen-free diamond-like carbon films in oxygen atmosphere by first-principles calculations, Carbon 100 (2016) 556–63.

37) Y. Qi, E. Konca, A.T. Alpas, Atmospheric effects on the adhesion and friction between non-hydrogenated diamond-like carbon (DLC) coating and aluminum−A first principles investigation, Surf. Sci. 600 (2006) 2955−65.

38) J.A. Heimberg, K.J. Wahl, I.L. Singer, A. Erdemir, Superlow friction behavior of diamond-like carbon coatings: Time and speed effects, Appl. Phys. Lett. 78 (2001) 2449–51.

39) N. Kumar, N. Sharma, S. Dash, C. Popov, W. Kulisch, J.P. Reithmaier, G. Favaro, A.K. Tyagi, B. Raj. Tribological poperties of ultrananocrystalline diamond films in various test atmosphere, Tribol. Int. 44 (2011) 2042–49.

Chapter 5

High Temperature and High Vacuum Tribological Properties of UNCD Films

5.1. Introduction

The crystalline diamond films are future potential candidate for space and high temperature tribological application areas due to their unique chemical and microstructural properties. The tribological behavior of UNCD films depend on environmental tribo-test conditions e.g. humidity, vacuum and temperature etc. in addition to their microstructural parameters [1-3]. The passivation and graphitization tribological mechanisms explain the observed friction and wear behavior of UNCD and DLC films most of the times [1,4-12]. But phase transformation at sliding interface makes it complex to understand the governing tribo-mechanisms under different set of environmental conditions [5,6,7,9,13]. The improvement in tribological properties of diamond and DLC films is challenging at high temperature conditions mainly due to phase transformation possibility of carbon phases. The low friction in NCD/UNCD films in ambient humid tribo-conditions is generally explained by the passivation mechanism of sliding interface by atmospheric water dissociated species [1,2,14,15]. In low humid conditions, the passivation mechanism still explains the low friction in diamond films even if graphitization happens at sliding interface [7]. In high vacuum conditions, friction and wear value of diamond films is reported to be high which is basically due to graphitization process at sliding interface and lack of external passivating media [16,17]. The ultralow friction and high wear resistance is reported in UNCD films at 200ºC which is supposed to be due to formation of the chemically passivated sliding interface. Though at further high temperature, tribological failure happens mainly due to oxidation and amorphization/polymerization mechanism at sliding interface [18].

The phase stability of UNCD films is studied at high temperature and high vacuum conditions using Raman spectroscopy technique and crystal structure of these films is found to be stable at temperature up to ~613 K [19]. Thus, in this chapter, the tribological properties of UNCD films are studied at high temperature condition of 350ºC (623 K). Novel UNCD films are deposited on Si substrate to improve high temperature and high vacuum tribological response of these films employing unique deposition parameters. Tribo-tests are conducted in three different sets of environmental conditions e.g. ambient, high vacuum (HV), high temperature and high vacuum (HTHV). The underlying tribo-mechanisms are established to explain the observed friction and wear behavior of these films by carrying out comprehensive characterization of sliding interfaces using Raman spectroscopy, XPS, FESEM, EDX etc. for all cases.

5.2. Experimental

The UNCD films are deposited on silicon substrate (100) using MPECVD system using optimised set of deposition parameters with gas mixtures of CH_4, H_2 and N_2 with total flow rate of 328 sccm, microwave power of 1300 W, process pressure of 50 Torr, microwave radiation frequency of 2.45 GHz and substrate temperature of 700°C [20]. The morphological and microstructural analysis of these films is carried out by FESEM and HRTEM, respectively. The chemical phase structure and local bonding nature of film surface and sliding interface are studied using micro-Raman spectrometer and XPS, respectively. Moreover, deformation behavior and chemical composition of sliding interface are analyzed using FESEM and EDX, respectively. The friction and wear behaviors of UNCD films are studied using ball-on-disc geometry high temperature and high vacuum tribometer operating in circular motion mode. The normal load, sliding speed and diameter of sliding contact are kept fixed as 0.5 N, 50 rpm and 5 mm, respectively, for all friction tests. The tribological tests are run for sliding cycles of 15,000 for all cases. Alumina Al_2O_3 ball (6 mm dia., R_a: 45 nm) is used as sliding counterbody. The tribo-tests are conducted in three different environmental conditions: (a) ambient atmosphere and room temperature (b) High vacuum (HV) of $\sim5\times10^{-6}$ mbar and room temperature; (c) high temperature and high vacuum (HTHV) with vacuum level $\sim5\times10^{-6}$ mbar and UNCD sample test temperature of 623 K. Two-dimensional wear profiles are measured by profilometer for wear analysis.

5.3. Results and discussion

5.3.1. Morphological, microstructural and chemical analysis of UNCD films

The homogeneously distributed nanowall like morphological feature is observed in UNCD films (Fig. 5.1a). Each nanowall is comprised of diamond grains of size ~5 nm as core embedded with sp^2-bonded amorphous carbon as shell as clearly shown in HRTEM image (Fig. 5.1b). The FT_1 and FT_2 Fourier transformed diffractograms confirm that the core and shell consists of diamond and sp^2- bonded amorphous carbon, respectively.

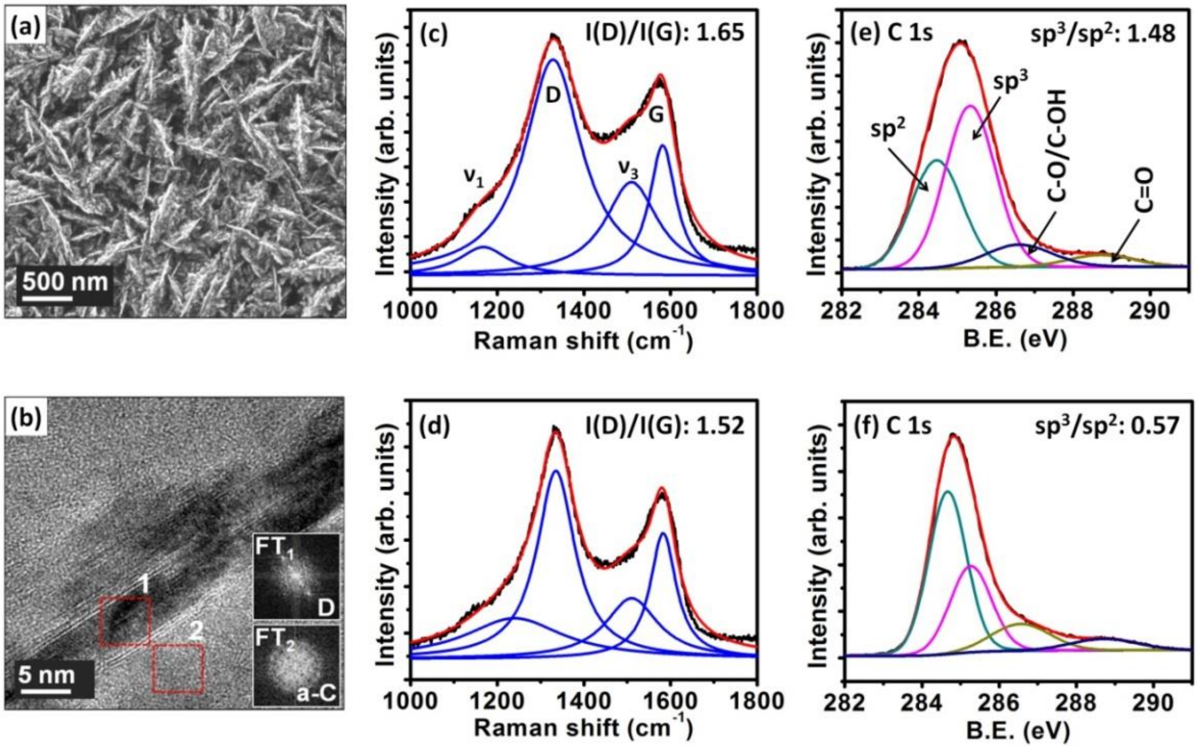

Fig. 5.1. *(a) SEM image of UNCD film surface and (b) HRTEM image of typical nanowall feature of film surface, (c & d) Raman spectra and (e & f) XPS: (c & e) UNCD film surface at RT and (d & f) UNCD film surface exposed to temperature of ~623 K*

The chemical bonding structure of UNCD films are examined by Raman spectroscopy and XPS at room temperature and high temperature of 623 K (Figs. 5.1c-f). In Raman spectra, the v_1 (1168 cm^{-1}) and v_3 (1510 cm^{-1}) bands correspond to transpolyacetylene (*t-PA*) phases and D (1329 cm^{-1}) and G (1582 cm^{-1}) bands are signature of *a-C* and graphitic phases, respectively (Figs. 5.1c,d). These Raman bands are fingerprint of UNCD films [21-24]. The I(D)/I(G) ratio of UNCD film at room temperature (RT) is 1.65 which decreases to 1.52 while film is exposed to temperature of 623 K. Furthermore, local bonding characteristics of film surface is studied by high-resolution XPS as shown in Figs. 5.1e,f. The broad C1s photoelectron emission spectrum is deconvoluted into four peaks at binding energies of 284.46, 285.3, 286.6 and 288.7 eV (Figs. 5.1e,f). The first two peaks correspond to sp^2 and sp^3 hybridized carbon and third and fourth one correspond to oxygen functional groups i.e. carboxylic (C-O/C-OH) and carbonyl (C=O) groups, respectively [2,25,26]. The sp^3/sp^2 ratio for UNCD film surface is 1.48 at RT and decreased to 0.57 while film is exposed to temperature of 623 K.

5.3.2. Friction and wear properties of UNCD films

The Friction and wear behavior of UNCD films are studied in three different conditions of ambient, HV and HTHV while sliding against alumina ball as shown in Fig. 5.2a. The friction trend distinctly differs depending upon the tribo-test environment. The friction gradually saturates to ultralow value ~0.023 (curve a_1) in ambient condition. However, it significantly increases to ~0.17 in HV tribo-condition (curve a_2) and early film failure is also noticed. The friction is further decreased to superlow value ~0.002 in HTHV tribo-condition (curve a_3) which is even lower than the ambient case.

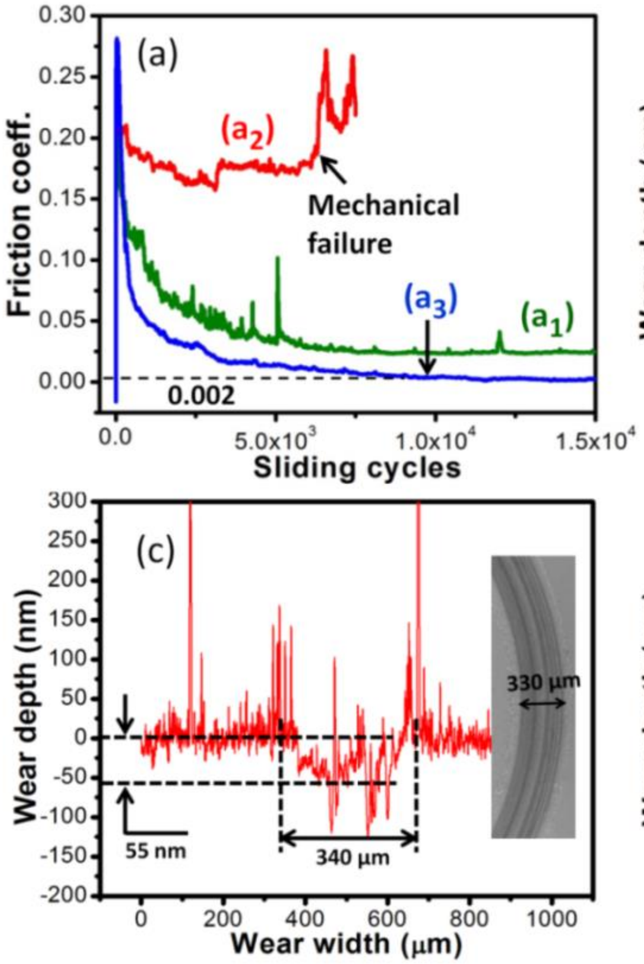

Fig. 5.2. *(a) Friction coefficient vs sliding cycles of UNCD films: (a_1) ambient, (a_2) HV and (a_3) HTHV tribo-conditions, two-dimensional wear track profile in (b) ambient, (c) HV and (d) HTHV tribo-conditions, SEM images of the corresponding wear tracks are embedded for each condition*

The 2D wear profile is plotted in Figs. 5.2b-d for all three tribo-environmental conditions. The wear dimension is found directly proportional to the friction value, being lowest in HTHV compared to other two conditions (Fig. 5.2d). Four wear profile measurements are recorded at random locations in each wear track and the data is found repeatable. The SEM images of wear tracks are also embedded in Figs. 5.2b-d. In HTHV condition, films are highly wear resistant with wear loss of mere 0.0016 nm/cycles. However, wear loss of films in ambient and HV tribo-conditions are 0.002 and 0.006 nm/cycle, respectively. This clearly indicates that the wear resistance of films is improved in HTHV i.e. 17 and 55% of ambient and HV tribo-conditions, respectively.

5.3.3. The morphological and elemental compositional analysis of sliding interface

The morphological and elemental compositional analysis of sliding interface is carried out using FESEM and EDX as shown in Figs. 5.3-5.5 to have understanding about the governing mechanisms for observed friction and wear behavior in UNCD films in all distinct tribological conditions. The deformation behavior of sliding interface is studied using high-resolution SEM as shown in Figs. 5.3a,c-5.5a,c. Furthermore, the elemental compositional analysis of tribo-contact interface is also carried out using EDX as shown in Figs. 5.3b,d-5.5b,d. The morphological analysis of wear track shows that the nanostructured feature of UNCD films is sustained in ambient condition (Fig. 5.3a). However, plastically deformed nanostructured morphology is observed in wear track in HV tribo-condition. In this case, the wear dimension and extent of deformation of counterbody ball are much higher compared to ambient condition (Figs. 5.4a,c). In HTHV, layered deformed patches are observed and wear track dimensions and the extent of ball deformation is significantly less compared to other two conditions (Figs. 5.5a,c).

The EDX analysis inside wear track in ambient condition shows the localized patch formation made up of O and Al entities which are wear product of Al_2O_3 ball as clearly shown in Figs. 5.3a_2,b_2. The C signature is observed on Al_2O_3 ball scar i.e. carbonaceous transferlayer is also formed. These are indicated in EDX mapping spots of c_1-c_3 on ball scar and corresponding EDX spectra as d_1-d_3 in Figs. 5.3c,d.

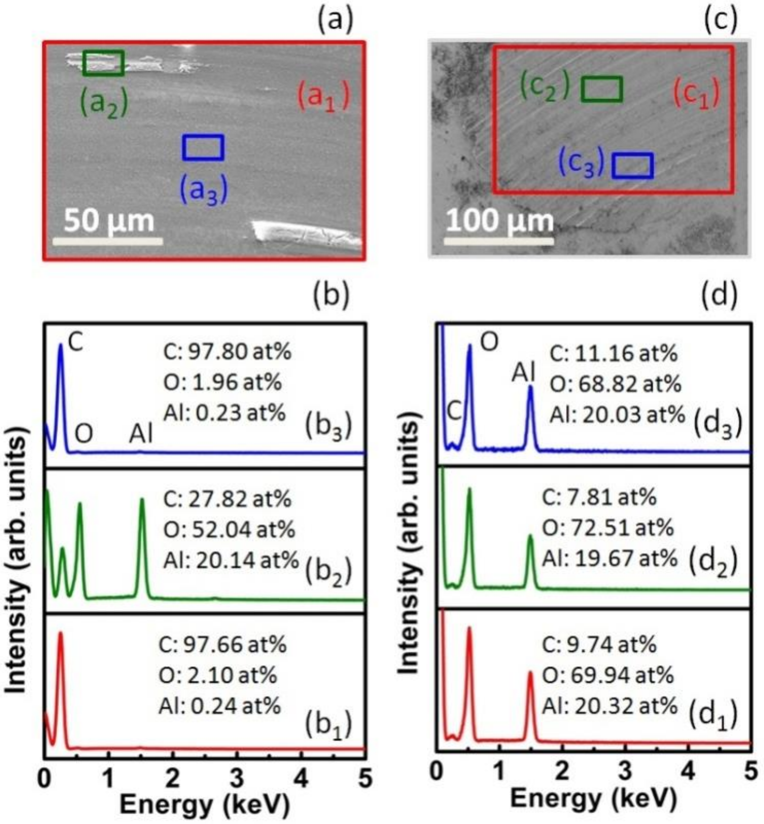

Fig. 5.3. *(a) SEM image of wear track and EDX locations a_1-a_3 with (b) corresponding EDX spectra b_1-b_3 of each location, (c) SEM image of ball scar and selected locations c_1-c_3 with (d) corresponding EDX spectra d_1-d_3 of each location; in ambient condition*

The EDX spectra of whole region (a) in wear track shows the negligible atomic fraction of Al and O in HV tribo-condition because the oxidation process is restricted (Figs. 5.4a,b). Moreover, the C signal is strong on ball scar which indicates the formation of carbonaceous transferlayer (Figs. 5.4c,d). Furthermore, the negligible fraction of Al and O is observed in wear track in HTHV tribo-condition. The EDX mapping spots are shown as a_1 and a_2, and corresponding spectra are presented in b_1 and b_2 in Figs. 5.5a,b. The atomic fraction of C is high at ball scar due to transferlayer formation. This is shown in spots c_1 and c_2, and corresponding spectra in d_1 and d_2 in Figs. 5.5c,d. It is clearly evident that carbonaceous transferfilm is present on ball scar in all three tribo-conditions. The atomic percentage of carbon is more in HV and HTHV tribology conditions compared to ambient condition.

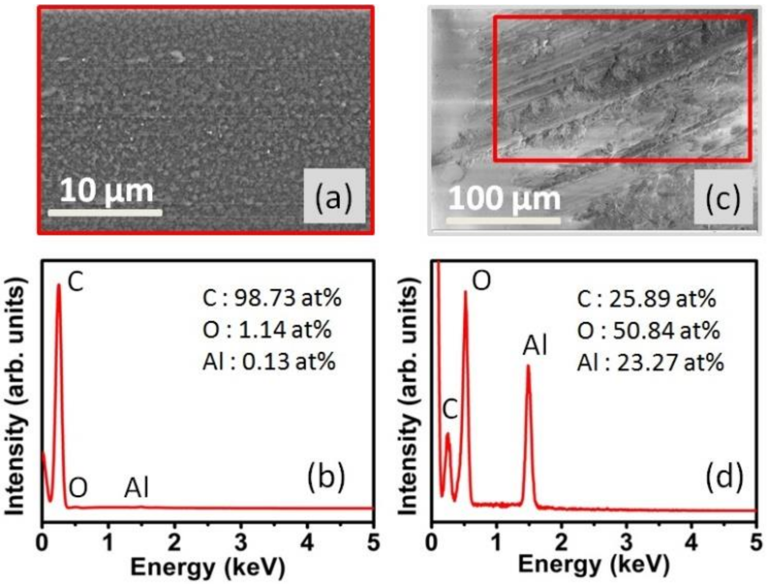

Fig. 5.4. *(a) SEM image of wear track and EDX location in red rectangle with (b) corresponding EDX spectra of whole image selected in red rectangle, (c) SEM image of ball scar and (d) corresponding EDX spectra; in HV condition*

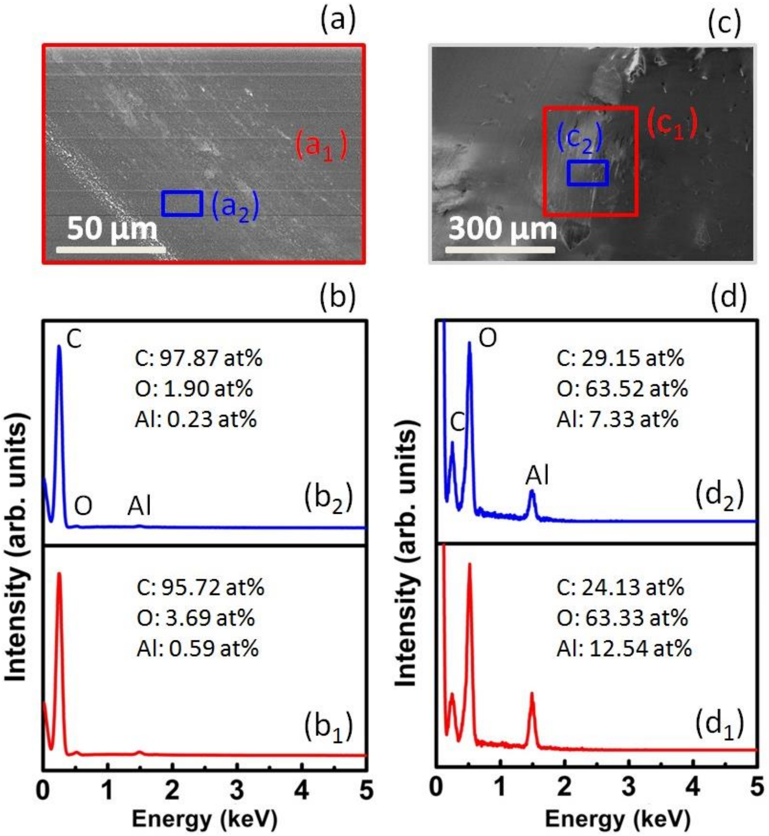

Fig. 5.5. *(a) SEM image of wear track and EDX locations a_1-a_2 with (b) corresponding EDX spectra b_1-b_2 of each locations, (c) SEM image of ball scar and selected locations c_1-c_2 with (d) corresponding EDX spectra d_1-d_2 of each location; in HTHV condition*

5.3.4. The chemical phase structural analysis of sliding interface

The chemical phase structural analysis of sliding interface is carried out in UNCD films using Raman spectroscopy for all three tribo-tests conditions. The deconvoluted Raman spectra and I(D)/I(G) ratio of wear tracks and ball scars are shown in Fig. 5.6 for all three distinct tribo-conditions. The I(D)/I(G) ratio is an important parameter for the determination of chemical structure of carbon phase [24]. For comparison purpose, all parameters of the Raman spectrometer are kept same. The chemical structure and I(D)/I(G) ratio of wear track is similar to UNCD film surface in ambient condition (Fig. 5.6a). In this case, the chemical stability of UNCD structure can be possibly explained by passivation mechanism of sliding surfaces by ambient atmospheric chemical species. Similar Raman shift at ball scar clearly indicates carbonaceous transferfilm formation (Fig. 5.6b). Moreover, decrease in I(D)/I(G) ratio from 1.66 to 1.39 and blue shift in D and G bands are observed at the ball scar area compared to the wear track. These observations point towards the shear induced *a-C* to graphitization in ambient condition [27].

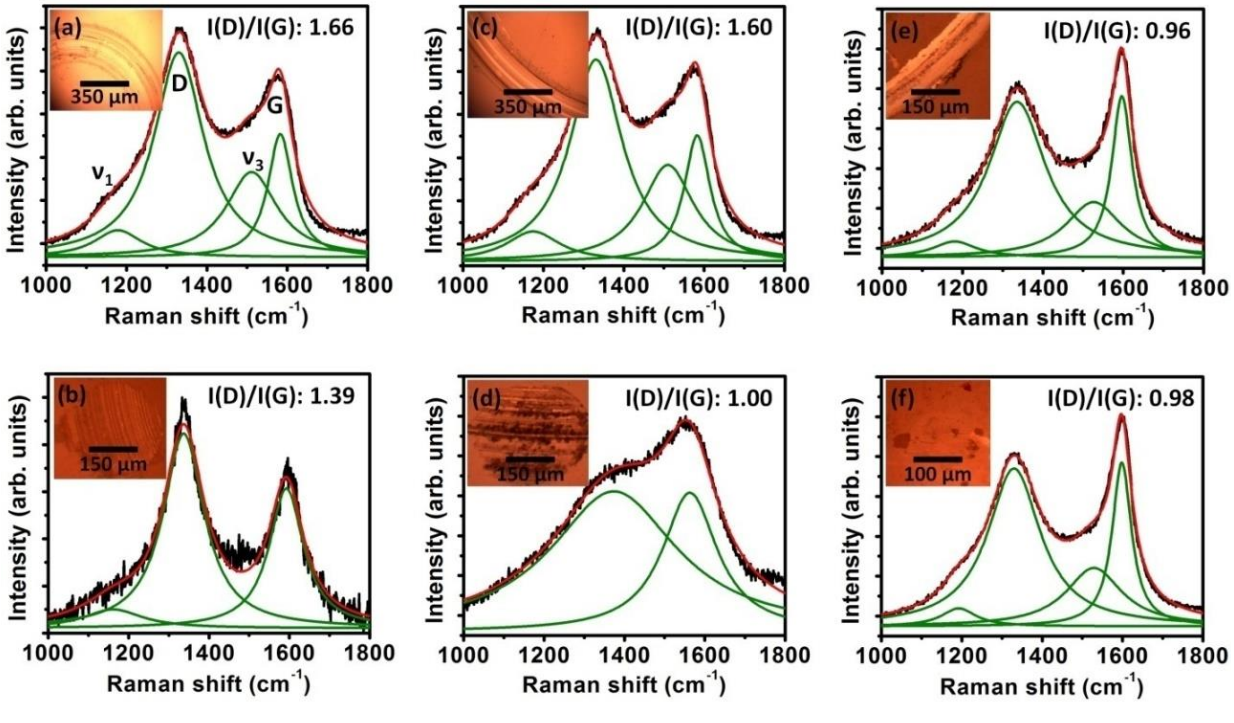

Fig. 5.6. *Raman spectra: (a & b) ambient, (c & d) HV (e & f) HTHV, (a, c & e) inside the wear track of UNCD films and (b, d & f) corresponding alumina ball scars, optical images of wear tracks and corresponding alumina ball scars are also embedded for each tribo-condition*

The Raman peak parameters such as peak shape, peak position, I(D)/I(G) ratio and *t-PA* phase of UNCD structure in wear track in HV are also quite similar to the wear track formed in ambient condition (Fig. 5.6c). However, the chemical structure of carbonaceous transferfilm formed at the ball scar is completely transformed into *a-C* and *t-aC* structure [28]. This is noticed by the significant changes in peak shape, peak position and modified I(D)/I(G) ratio of Raman spectra as shown in Fig. 5.6d. In this condition, the blue shift in D and red shift in G band is observed compared to the carbon structure of the corresponding wear track. Here, *t-PA* phase has completely disappeared which is probably a strong indication for conversion of UNCD into *a-C* and *t-aC* structure. This is probably due to high frictional energy which provides the required activation energy for such conversion. Therefore, in HV, the ball scar is fully covered with transferfilm of *a-C* and *t-aC* phases. Thus, in this particular condition, sliding occurs between UNCD film and *a-C/t-aC* structure formed on the ball side. Distinct changes in Raman spectra of sliding surfaces in HTHV are observed (Figs. 5.6e,f). The I(D/I(G) ratio of UNCD film exposed to temperature of 623 K is 1.52 which is slightly less than the UNCD film at RT as shown earlier (Figs. 5.1c,d). Moreover, at HTHV, the D and G bands are blue shifted, indicating temperature induced annealing which tends to reorient the carbon structure into more ordered sp^2 phase. The I(D)/I(G) ratio significantly decreases to 0.96 in wear track compared to film surface (Fig. 5.6e) and it describes bulk graphitization of the contact surface [27] which is contrasting to wear track formed in ambient and HV conditions. This indicates that the contact pressure aided by temperature at HTHV tribo-condition is deterministic factor to reorient *a-C* into ordered sp^2 phase. Moreover, sp^3 to sp^2 phase conversion is also possible depending upon the activation energy which can be provided by both temperature and contact pressure. For quantitative analysis, Raman spectra are obtained at several locations of the wear track in all three different tribology conditions (Fig. 5.7). The Raman analysis shows the shift in D and G bands to higher wave number and a decrease in the I(D)/I(G) ratio in HTHV tribo-condition compared to other two cases.

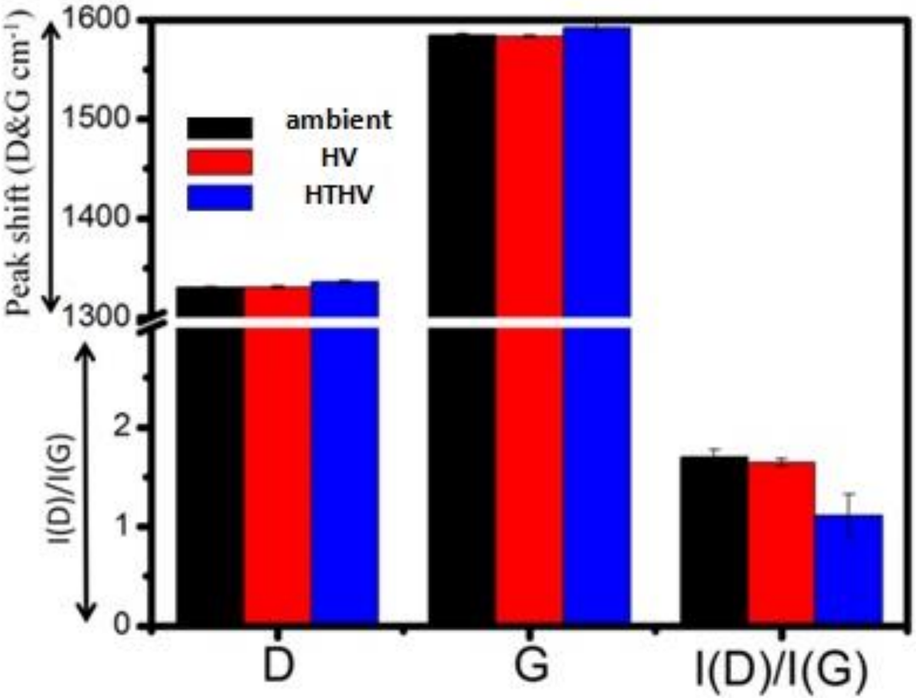

Fig. 5.7. *D, G and I(D)/I(G) ratio of wear track in three different tribo-conditions, first half and second half panel in x-axis describes peak shift of D and G bands and I(D)/I(G) ratio, respectively; in each wear track more than 20 Raman spectra are obtained and error bar is also given*

5.3.5. The local chemical bonding nature of sliding interface

The XPS study is carried out for more insightful surface chemical analysis of transferfilm formed on ball contact area during sliding process as studied by Raman analysis as well (Fig. 5.8). The 50 µm spatial resolution of XPS makes it possible to focus X-ray spot at specific locations on ball scar area. Moreover, the XPS analysis is carried out at two different locations of ball scar for repetitive purpose. The survey XPS spectra shows well resolved C1s and O1s photoelectron shifts on ball scar region in all three distinct tribo-conditions which is a signature of carbonaceous transferfilm formation with adsorbed oxygen functional groups (Figs. 5.8a,c,e). In survey spectra, the C/O ratio is 0.51 in ambient condition and intensity of the alumina peaks Al2p and Al2s is also strong (Fig. 5.8a). The HR-XPS of C1s photoelectron shift shows well-resolved sp^2 and sp^3 carbon peaks with contribution of oxygen functional groups (Fig. 5.8b). The sp^3/sp^2 carbon ratio is 0.65 which is much lower compared to virgin film surface i.e. 1.48 (Fig. 5.1e) which is indicative of tribo-chemical conversion of sp^3 to sp^2 phase.

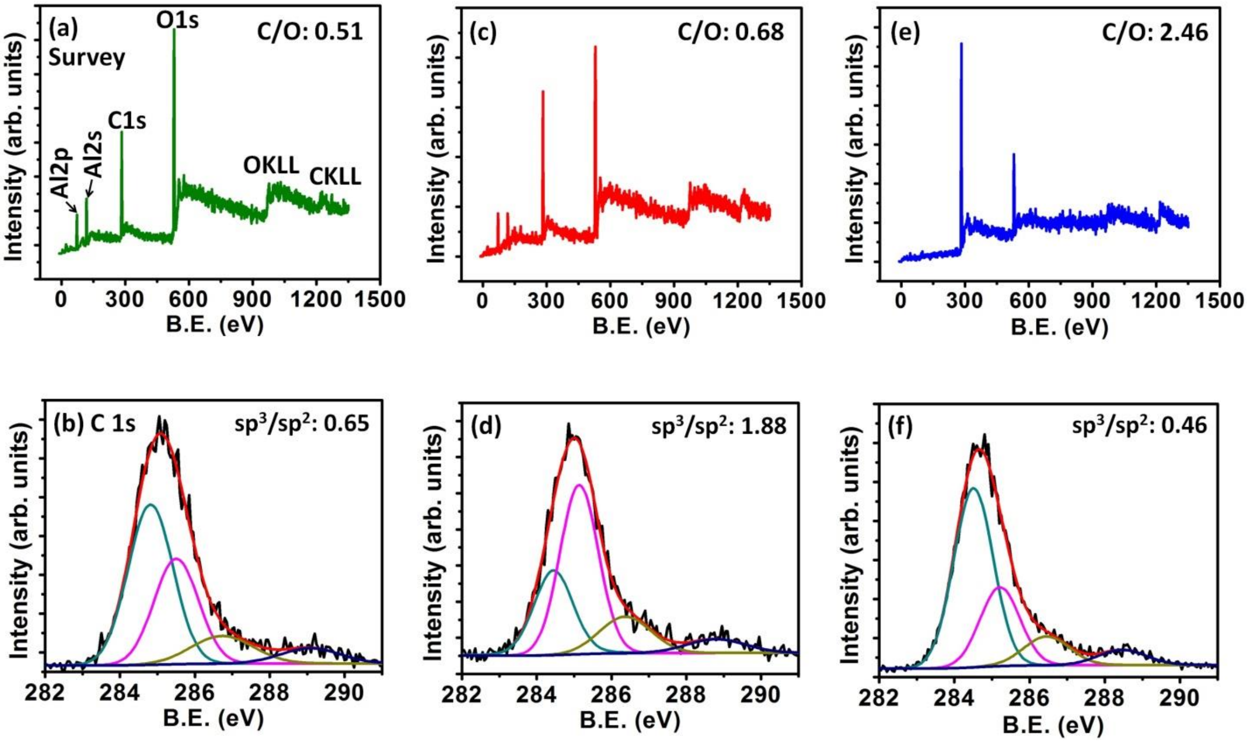

Fig. 5.8. *XPS spectra: (a & b) ambient, (c & d) HV and (e & f) HTHV, (a, c & e) survey XPS and (b,d & f) corresponding C1s HR-XPS spectra of alumina ball scars*

In survey spectra, C/O ratio is 0.68 on ball scar in HV tribo-condition (Fig. 5.8c). In this case, the contribution of oxygen contamination is mainly due to exposure of film sample to ambient atmosphere after conducting the tribo-tests. Moreover, HR-XPS C1s spectra shows significant increase in sp^3/sp^2 ratio to 1.88 (Fig. 5.8d) which is much higher compared to ambient condition i.e. 0.65. Furthermore, the sp^3/sp^2 ratio is even higher than the virgin film surface i.e. 1.48 (Fig. 5.1e). This is probably associated to the sp^2 carbon phase conversion into amorphous carbon (*a-C*) and disordered sp^3 (*t-aC*) phase in HV condition which is supported by Raman spectroscopy as well (Fig. 5.6d). The high frictional energy in HV condition provides necessary activation energy for this phase transformation.

In XPS survey spectra, the C/O ratio is much higher i.e. 2.46 on ball scar area in HTHV condition compared to other two tribo-conditions (Fig. 5.8e) which indicates the thermal desorption of residual oxygen contamination in high temperature and high vacuum conditions probably due to weakening of cohesive barrier. Moreover, the sp^3/sp^2 ratio of transferfilm on ball scar is 0.46 in HTHV tribo-condition (Fig. 5.8f) which is lower than the film surface when exposed to high temperature of 623 K i.e. 0.57 (Fig. 5.1f). This directly indicates the significant tribo-induced conversion of sp^3 into sp^2 phase in HTHV condition. Though this conversion is also evident in ambient case to some extent but high temperature is energetically favorable for such transformation [29]. The tribo-stress induced conversion of sp^3 into sp^2 phase is dominating in ambient condition while stress and thermal energy both are driving factors for this conversion in HTHV condition. The chemical characteristics of transferfilm in ambient and HTHV conditions are contrasting to HV case. The amorphization is dominated in HV condition while graphitization occurs in ambient and HTHV tribo-conditions. The tribo-induced conversion of amorphized state to ordered sp^2 and sp^3 phases is restricted in HV condition. However, nucleation of ordered sp^2 carbon phase is realistic in ambient and HTHV conditions due to favorable activation energy.

5.3.6. The tribological mechanism

The friction and wear behavior of UNCD films distinctly differ depending upon the tribology test conditions as shown in Figs. 5.2a-d. The friction value is lower in ambient and HTHV tribo-conditions compared to HV condition. This distinct tribological behavior can be possibly understood by considering either (a) passivation mechanism of carbon dangling bonds [1,14] or (b) passivated graphitization mechanism at sliding interface. One study on Density functional theory calculations clearly reports that it is energetically favorable for H_2 and H_2O dissociated products to passivate the dangling bonds at sliding interface in diamond films which reduce the surface energy [30]. The same passivation mechanism is also experimentally established for UNCD films in ambient atmosphere and room temperature tribological conditions using spectroscopic technique [1]. The passivation of dangling bonds by atmospheric H_2O dissociated products i.e. -OH or -H results in low friction coefficient and high wear resistance in ambient tribo-condition [1,14,30]. Our experimental results show the relative increase in oxygen and its functional groups on ball scar in ambient condition (Figs. 5.8a,b). Thus, the low friction and high wear resistance of UNCD film in ambient condition are governed by passivation mechanism of dangling bonds and partial graphitization of transferlayer formed on alumina ball scar as supported by Raman spectroscopy (Figs. 5.6a,b).

The dissociative passivation mechanism of dangling bonds by ambient atmospheric species is restricted in HV tribo-condition. But the transformation of diamond and graphitic phase into *a-C* and *t-aC* structures is energetically favorable which is mainly associated with tribo-contact stress and high frictional energy. This is clearly analyzed by Raman spectroscopy which shows increase in *a-C* and *t-aC* structures and termination of *t-PA* phase on ball scar area in HV conditions (Fig. 5.6d). Furthermore, the XPS analysis shows a large amount of sp^3 fraction on ball contact area in this condition (Fig. 5.8d). Thus, the sliding takes place between *a-C* and *t-aC* structures which occupy the large fraction of dangling bonds in HV condition [31]. The dangling bonds of these carbon species form covalent bonds across sliding interfaces which enhance the shear resistance and wear to high value which ultimately leads to the partial mechanical failure of film (Figs. 5.2a,c).

The friction coefficient and wear almost vanish in HTHV condition which is in contrast to HV tribo-condition. In this case also, the passivation mechanism of dangling bonds at contact interface is restricted. The tribological properties of UNCD films at high temperature and ambient atmospheric condition significantly degraded due to the oxidation mechanism which increases the shear resistance [18]. The evidence of graphitized sliding interfaces is well supported by Raman spectroscopy (Figs. 5.6e,f) and XPS analysis as well (Figs. 5.8e,f). Thus, the graphitization of sliding interfaces can be considered for significantly improved tribological properties in HTHV condition [32]. The hydrogen passivation of graphitized phases is intrinsically carried out by *t-PA* phase as clearly observed in Raman analysis. The basic mechanism is governed by unique lamellar lattice structure of hydrogenated sp^2 phase which improves the tribological properties [33]. Here, frictional shear occurs between hydrogenated graphitized interface that leads to ultralow friction coefficient and high wear resistance behavior.

5.4. Conclusions

The tribological properties of UNCD films are studied in three distinct tribo-environments conditions of ambient, HV and HTHV. These films exhibit randomly oriented nanowall like morphology. The friction and wear behavior of films distinctly differ depending upon the tribology test conditions. The tribo-environment dependent chemical characteristic of transferfilm formation at contact interface is analyzed using spectroscopic tools. The passivation and graphitization are energetically favorable mechanisms for low friction and wear in ambient tribo-condition. The friction coefficient is high and wear induced film failure is observed in HV condition. In this case, passivation mechanism is restricted and frictional shear transforms the diamond sp^3 into *a-C* and *t-aC* phases. However, significant conversion of diamond sp^3 into hydrogenated graphitized phase is predominant mechanism for amazingly superlow friction value and ultrahigh wear resistance in HTHV tribo-condition.

5.5. References

1) A.R. Konicek, D.S. Grierson, P.U.P.A. Gilbert, W.G. Sawyer, A.V. Sumant, R.W. Carpick, Origin of ultralow friction and wear in ultrananocrystalline diamond, Phys. Rev. Lett. 100 (2008) 235502–05.
2) N. Kumar, R. Ramadoss, A.T. Kozakov, K.J. Sankaran, S. Dash, A.K. Tyagi, N.H. Tai, I.N. Lin, Humidity-dependent friction mechanism in an ultrananocrystalline diamond film, J. Phys. D: Appl. Phys. 46 (2013) 275501–08.
3) J. Li, W. Yue, W. Qin, C. Wang, Approach to controllable tribological properties of sintered polycrystalline diamond compact through annealing treatment, Carbon 116 (2017) 103–12.
4) N. Kumar, K. Panda, S. Dash, C. Popov, J.P. Reithmaier, B.K. Panigrahi, A.K. Tyagi, B. Raj, Tribological properties of nanocrystalline diamond films deposited by hot filament chemical vapor deposition, AIP Adv. 2 (2012) 032164–77.
5) X. Lei, B. Shen, S. Chen, L. Wang, F. Sun, Tribological behavior between micro– and nano–crystalline diamond films under dry sliding and water lubrication, Tribol. Int. 69 (2014) 118–27.
6) R. Rani, K.J. Sankaran, K. Panda, N. Kumar, K. Ganesan, S. Chakravarty, I.N. Lin, Tribofilm formation in ultrananocrystalline diamond film, Diam. Relat. Mater. 78 (2017) 12–23.
7) M.I.D.B. Bouchet, C. Matta, B. Vacher, T. Le-Magne, J.M. Martin, J. von Lautz, T. Ma, L. Pastewka, J. Otschik, P. Gumbsch, M. Moseler, Energy filtering transmission electron microscopy and atomistic simulations of tribo-induced hybridization change of nanocrystalline diamond coating, Carbon 87 (2015) 317–29.
8) S.R. Polaki, N. Kumar, K. Madapu, K. Ganesan, N.G. Krishna, S.K. Srivastava, S. Abhaya, M. Kamruddin, S. Dash, A.K. Tyagi, Interpretation of friction and wear in DLC film: Role of surface chemistry and test environment, J. Phys. D: Appl. Phys. 49 (2016) 445302–14.
9) S.R. Polaki, N. Kumar, K. Ganesan, K. Madapu, A. Bahuguna, M. Kamruddin, S. Dash, A.K. Tyagi, Tribological behavior of hydrogenated DLC film: Chemical and physical transformation at nano-scale, Wear 338–339 (2015) 105–13.

10) L. Bai, G. Zhang, Z. Lu, Z. Wu, Y. Wang, L. Wang, P. Yan, Tribological mechanism of hydrogenated amorphous carbon film against pairs: A physical description, J. Appl. Phys. 110 (2011) 033521–28.

11) L. Cui, Z. Lu, L. Wang, Probing the low–friction mechanism of diamond–like carbon by varying of sliding velocity and vacuum pressure, Carbon 66 (2014) 259–66.

12) T.B. Ma, L.F. Wang, Y.Z. Hu, X. Li, H. Wang, A shear localization mechanism for lubricity of amorphous carbon materials, Sci. Rep. 4 (2014) 3662–67.

13) T. Kunze, M. Posselt, S. Gemming, G. Seifert, A.R. Konicek, R.W. Carpick, L. Pastewka, M. Moseler, Wear, plasticity, and rehybridization in tetrahedral amorphous carbon, Tribol. Lett. 53 (2014) 119–26.

14) M.I.D.B. Bouchet, G. Zilibotti, C. Matta, M.C. Righi, L. Vandenbulcke, B. Vacher, J.M. Martin, Friction of diamond in the presence of water vapor and hydrogen gas. Coupling gas-phase lubrication and first-principles studies, J. Phys. Chem. C 116 (2012) 6966−72.

15) W. Qin, W. Yue, C. Wang, Understanding integrated effects of humidity and interfacial transfer film formation on tribological behaviors of sintered polycrystalline diamond, RSC Adv. 5 (2015) 53484–96.

16) K. Miyoshi, Considerations in vacuum tribology (adhesion, friction, wear, and solid lubrication in vacuum), Tribol. Int. 32 (1999) 605–16.

17) Z. Feng, Y. Tzeng, J.E. Field, Friction of diamond on diamond in ultra-high vacuum and low-pressure environments, J. Phys. D: Appl. Phys. 25 (1992) 1418–24.

18) R. Ramadoss, N. Kumar, K.J. Sankaran, P. Das, T.R. Ravindran, S. Dash, A.K. Tyagi, N.H. Tai, I.N. Lin, Temperature dependent tribological studies and phase transformation in ultra-nanocrystalline diamond films, Sci. Adv. Mater. 6 (4) (2014) 751–59.

19) K.K. Mishra, R. Rani, N. Kumar, T.R. Ravindran, K.J. Sankaran, I.N. Lin, High pressure Raman spectroscopic studies on ultrananocrystalline diamond thin films: Anharmonicity and thermal properties of grain boundary, Diam. Relat. Mater. 80 (2017) 45–53.

20) R. Rani, K. Panda, N. Kumar, K.J. Sankaran, R. Pandian, M. Ficek, R. Bogdanowicz, K.Haenen, I.N. Lin, Triboenvironment dependent chemical modification of sliding interfaces in ultrananocrystalline diamond nanowall film: Correlation with friction and wear, J. Phys. Chem. C 122 (2018) 945−56.

21) J. Birrell, J.E. Gerbi, O. Auciello, J.M. Gibson, J. Johnson, J.A. Carlisle, Interpretation of the Raman Spectra of Ultrananocrystalline Diamond, Diam. Relat. Mater. 14 (2005) 86–92.

22) R. Pfeiffer, H. Kuzmany, P. Knoll, S. Bokova, N. Salk, B. Gunther, Evidence for trans-polyacetylene in nano-crystalline diamond films, Diam. Relat. Mater. 12 (2003) 268–71.

23) T. López-Rı´os, É. Sandré, S. Leclercq, É. Sauvain, Polyacetylene in diamond films evidenced by surface enhanced Raman scattering, Phy. Rev. Lett. 76 (1996) 4935–38.

24) A.C. Ferrari, J. Robertson, Resonant Raman spectroscopy of disordered, amorphous, and diamondlike carbon, Phys. Rev. B 64 (2001) 75414–26.

25) P. Merel, M. Tabbal, M. Chaker, S. Moisa, J. Margot, Direct evaluation of the sp^3 content in diamond-like-carbon films by XPS, Appl. Surf. Sci. 136 (1998) 105–10.

26) B. Ren, J. Huang, H. Yu, W. Yang, L. Wang, Z. Pan, L. Wang, Thermal stability of hydrogenated diamond films in nitrogen ambience studied by reflection electron energy spectroscopy and X-ray photoelectron spectroscopy, Appl. Surf. Sci. 388 (2016) 565–70.

27) A.C. Ferrari, J. Robertson, Interpretation of Raman spectra of disordered and amorphous carbon, Phys. Rev. B 61 (2000) 14095–107.

28) J. Schwan, S. Ulrich, V. Batori, H. Ehrhardt, S.R.P. Silva, Raman spectroscopy on amorphous carbon films, J. Appl. Phys. 80 (1996) 440–47.

29) F. Mangolini, F. Rose, J. Hilbert, R.W. Carpick, Thermally induced evolution of hydrogenated amorphous carbon, Appl. Phys. Lett. 103 (2013) 161605–09.

30) Y. Qi, E. Konca, A.T. Alpas, Atmospheric effects on the adhesion and friction between non-hydrogenated diamond-like carbon (DLC) coating and aluminum – A first principles investigation, Surf. Sci. 600 (2006) 2955–65.

31) A. Erdemir, C. Donnet, Tribology of diamond-like carbon films: Recent progress and future prospects, J. Phys. D: Appl. Phys. 39 (2006) 311–27.

32) Y. Liu, W. Yue, W. Qin, C. Wang, Improved vacuum tribological properties of sintered polycrystalline diamond compacts treated by high temperature annealing, Carbon 124 (2017) 651–61.

33) B.K. Yen, Influence of water vapor and oxygen on the tribology of carbon materials with sp^2 valence configuration, Wear 192 (1996) 208–15.

Chapter 6

The Role of Intrinsic Hydrogen on the Tribological Properties of UNCD Films in High Vacuum Tribo-Conditions

6.1. Introduction

The simultaneous improvement in the tribological properties of diamond films in ambient and high vacuum environmental conditions for inter-atmospheric tribological applications is quite challenging task. As discussed in previous chapter, the UNCD films showed good tribological response i.e. low friction value and high wear resistance properties in ambient conditions. But high friction and wear properties were observed in high vacuum tribology conditions. Thus, there is still a need to improve the tribological properties of UNCD films in high vacuum tribo-conditions as well. The non-hydrogenated DLC films also show high friction and wear properties in vacuum tribology conditions [1]. But DLC films with intrinsic hydrogen concentration exhibit improved tribological properties in high vacuum conditions where intrinsic hydrogen atoms passivate the dangling carbon bonds at sliding contact interface [2,3]. The phase transformation of carbon species and modification in the chemical nature of transferfilm at sliding interface is also dependent on tribo-atmospheric media [4]. Moreover, the interfacial properties change during sliding process due to change in roughness, deformation process, chemical reactions, oxidation and tribofilm formation etc. [5-7]. The passivation mechanism and conversion of tetrahedral DLC and crystalline diamond phase into amorphous carbon (*a-C*) and graphitic tribolayer formation are important governing mechanisms for enhancement in friction and wear resistance properties of DLC and diamond films in humid atmospheric conditions [1-4,8,9]. Though the passivation mechanism by ambient atmospheric species is restricted in high vacuum tribology conditions and thus, NCD films deposited on Ti-alloys showed high friction value in high vacuum conditions [10].

In this chapter, two distinct UNCD films with the change in intrinsic hydrogen concentration are deposited on Ti–6Al–4V substrate by employing optimized deposition parameters using MPECVD system for improvement in tribological properties of UNCD films in high vacuum conditions and understanding of underlying tribo-mechanisms. The hydrogen concentration is varied in these films to investigate the role of intrinsic hydrogen concentration on the tribological properties of UNCD films in high vacuum condition. The friction and wear behavior of these films are studied in two distinct tribo-atmospheric conditions of ambient and high vacuum (3×10^{-6} mbar) tribology conditions. The comprehensive chemical investigation of sliding interface is carried out by employing characterization tools e.g. FESEM, EDX and Raman spectroscopy etc. to understand the underlying friction and wear mechanism in these films.

6.2. Experimental

Two distinct UNCD films are grown on mirror polished Ti-alloy Ti–6Al–4V substrate in H_2(6%)/CH_4(2%)/Ar(rest) and H_2(0%)/CH_4(2%)/Ar(rest) plasma media at pressure of 150 Torr and 130 Torr, respectively, using MPECVD system. These films will be designated as UNCD(6%H_2) and UNCD(0%H_2) films, respectively. The microwave power of 1200 W and substrate temperature of 550°C is used for the deposition process. The surface topography of these films is analyzed by AFM. The elemental depths profile analysis of C, H and Ti in both films is carried out by secondary ion mass spectroscopy (SIMS) (TOF-SIMS5, ION-TOF GmbH) using Bismuth (Bs^+) ion source. Detailed microstructure and local bonding nature of both films is analyzed by HRTEM and EELS, respectively. The film morphology and tribo-induced deformation behavior of sliding interface is studied using FESEM. The chemical phase structure of films and wear tracks/ball scars is examined by micro-Raman spectrometer. The elemental analysis on ball scars is carried out using EDX technique.

The friction and wear behaviors of these films are measured in high-vacuum tribometer operating in circular rotation mode of ball-on-disc configuration. The tribology tests are conducted for sliding cycles of 5×10^4 along the circular path of 2 mm diameter. The Al_2O_3 ball (6 mm diameter, average roughness $R_a \sim 45$ nm) is used as sliding counterbody. The tribo-tests are carried out in ambient and high vacuum (3×10^{-6} mbar) tribology conditions.

6.3. Results and discussion

6.3.1. The topographical and chemical analysis of UNCD films

The surface topography of UNCD(6%H_2) and UNCD(0%H_2) films is studied using AFM as shown in Figs. 6.1a_i,a_{ii}. The roughness value for UNCD(6%H_2) and UNCD(0%H_2) films is almost similar i.e. 11.8 and 9.3 nm, respectively. Densely packed and homogeneously distributed

UNCD structure is observed in both films. The chemical phase structure of both films is analyzed using micro-Raman spectroscopy. The Raman spectra are deconvoluted into five well resolved individual bands for both films as shown in Figs. 6.1b_i,b_{ii}. The v_1, v_2 and v_3 Raman peaks correspond to trans-polyacetylene *(t-PA)* phase at grain boundary and considered as the fingerprint for UNCD structure [11-13]. These bands are prominent in UNCD(6%H_2) compared to UNCD(0%H_2) films which indicates the extensive hydrogenated network in the grain boundaries. The D and G bands correspond to disordered carbon and graphitic domains, respectively, occupying the grain boundaries [11,14-16]. The elemental depth profile analysis for C, H and Ti elements is carried out using SIMS and thickness of both films is approximately 1 μm as shown in Figs. 6.1c_i,c_{ii}. The ratio of H/C is 1:7.5 and 1:13.2 in UNCD(6%H_2) and UNCD(0%H_2) films which clearly indicate the high hydrogen concentration in UNCD(6%H_2) compared to UNCD(0%H_2) films. The hydrogen presence in plasma media during deposition process is the main reason for increased hydrogen concentration in UNCD(6%H_2) films. Moreover, the gradual change of C^+, H^+ and Ti^+ at film-substrate interface indicates the reactive layer formation.

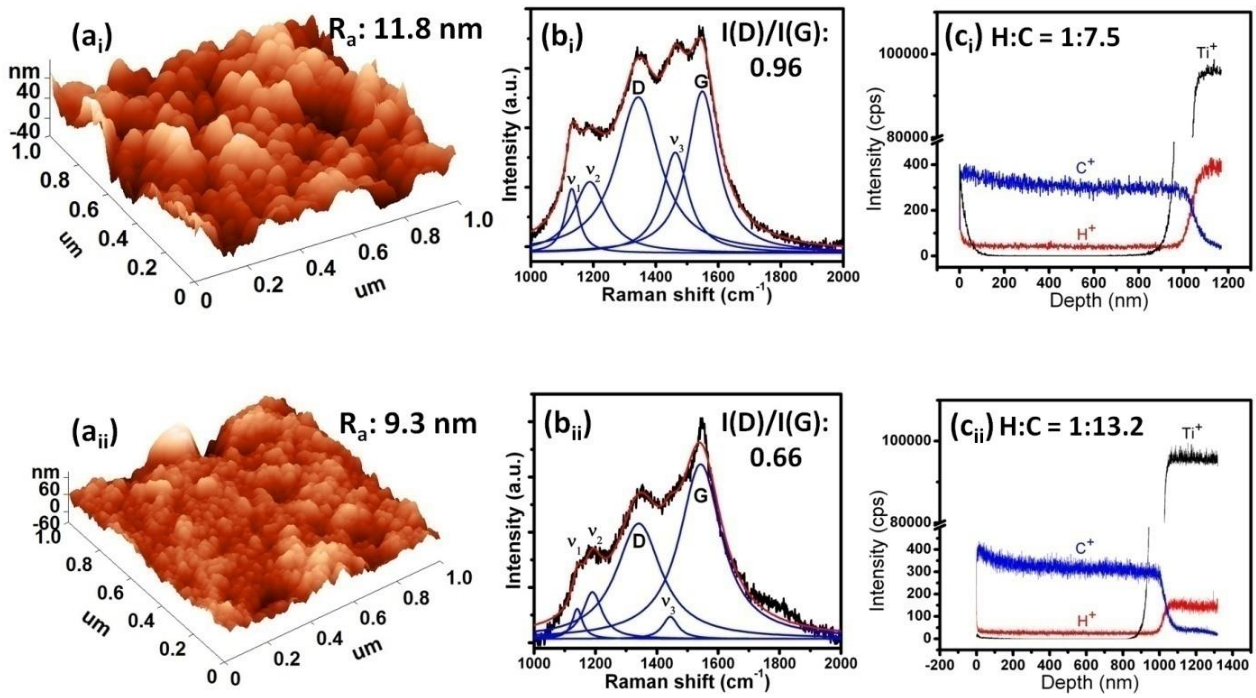

Fig. 6.1. *(a_i, a_{ii}) Surface topography, (b_i, b_{ii}) Raman spectra and (c_i, c_{ii}) SIMS depth profile of: (a_i, b_i, c_i) UNCD(6%H_2) and (a_{ii}, b_{ii}, c_{ii}) UNCD(0%H_2) films*

6.3.2. The morphological and microstructural analysis of UNCD films

The morphological analysis of UNCD films is carried out using FESEM as shown in Figs. 6.2a,b. The diamond grains are embedded in nanowire like feature in UNCD(6%H_2) films while UNCD(0%H_2) films show equiaxed morphology.

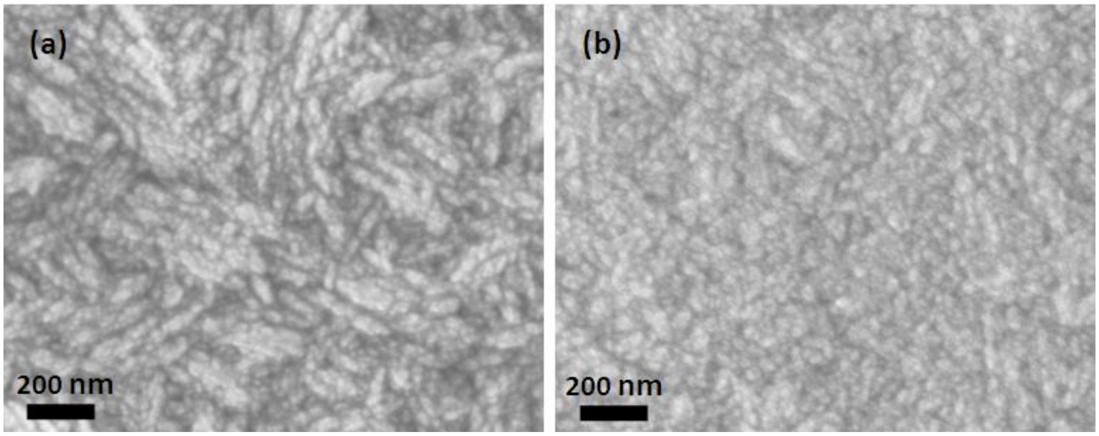

Fig. 6.2. *Surface morphology of (a) UNCD(6%H_2) films and (b) UNCD(0%H_2) films*

The detailed microstructural analysis of both UNCD films is carried out using TEM and EELS. The BF(TEM) micrograph and corresponding SAED patterns of UNCD(6%H_2) films are shown in Fig. 6.3a_i. The BF(TEM) micrograph contains some dark regions which are diamond aggregates and distributed among the matrix of ultra-small diamond grains. The SAED pattern contains (111), (220) and (311) diffraction rings, confirming that these films are predominately diamond. Moreover, diffuse ring in the center implies the existence of some sp^2-bonded carbon (*a-C*/graphitic phase). The distribution of large diamond aggregates, ultra-small diamond grains and sp^2 bonded clusters is best illustrated by the composed dark field (c-DF) micrograph as shown in Fig. 6.3a_{ii}, corresponding to the dashed square region in Fig. 6.3a_i. The c-DF micrograph is the superposition of dark-field TEM micrographs obtained using different segments of diffraction ring (designated in inset of Fig. 6.3a_{ii}).

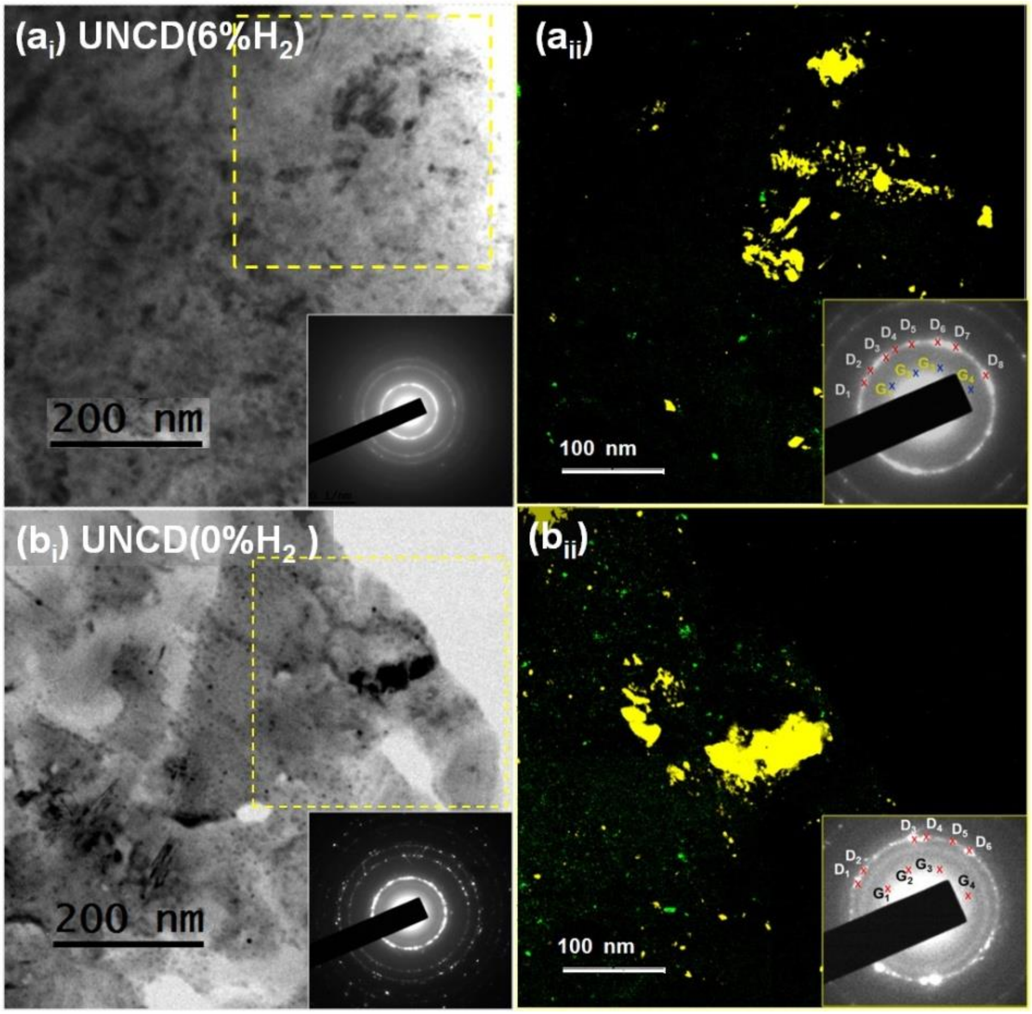

Fig. 6.3. *(a_i, b_i) BF(TEM) micrograph and (a_{ii}, b_{ii}) c-DF micrograph: (a_i, a_{ii}) UNCD(6%H_2) and (b_i, b_{ii}) UNCD(0%H_2) films with SAED pattern shown in inset*

The yellow colored large and small grain regions in Fig. 6.3a$_{ii}$ are diamond which correspond to the diffraction spots D_1, D_2, …D_8 in inset, whereas the green colored tiny clusters are sp^2 bonded phase which correspond to the diffraction spots G_1, G_2…G_4 in the inset. The microstructure of UNCD(0%H_2) films is shown in Figs. 6.3b$_i$,b$_{ii}$ as BF(TEM) and c-DF micrographs, respectively. The BF(TEM) micrograph of UNCD(0%H_2) films is very much similar to UNCD(6%H_2) films, indicating that the microstructure of the both UNCD films are similar i.e. both films contain large diamond aggregates dispersed in the matrix of ultra-small diamond grains except that the proportion of diamond aggregates in UNCD(0%H_2) films is slightly less abundant than UNCD(6%H_2) films.

The HRTEM structure image of typical small grain regions shown in Fig. 6.4 reveals the existence of ultra-small diamond grains of size around 5 nm and relatively wide grain boundaries in both films. However, the microstructure of the large diamond aggregates in UNCD(6%H_2) films are distinctly different from UNCD(0%H_2) films. Figure 6.4a shows the structure image of large diamond aggregates in UNCD(6%H_2) films, indicating that the parallel fringes corresponding to (111) lattice planes of grain 1 lie almost in parallel with those for grain 2 (i.e. two grains are aligned) and boundaries between them is completely eliminated. This is further supported by the fact that ft_1 and ft_2 images corresponding to regions 1 and 2 are oriented in the same direction i.e. the adjacent diamond grains are merged into single large diamond grain resulting into diamond aggregates in UNCD(6%H_2) films.

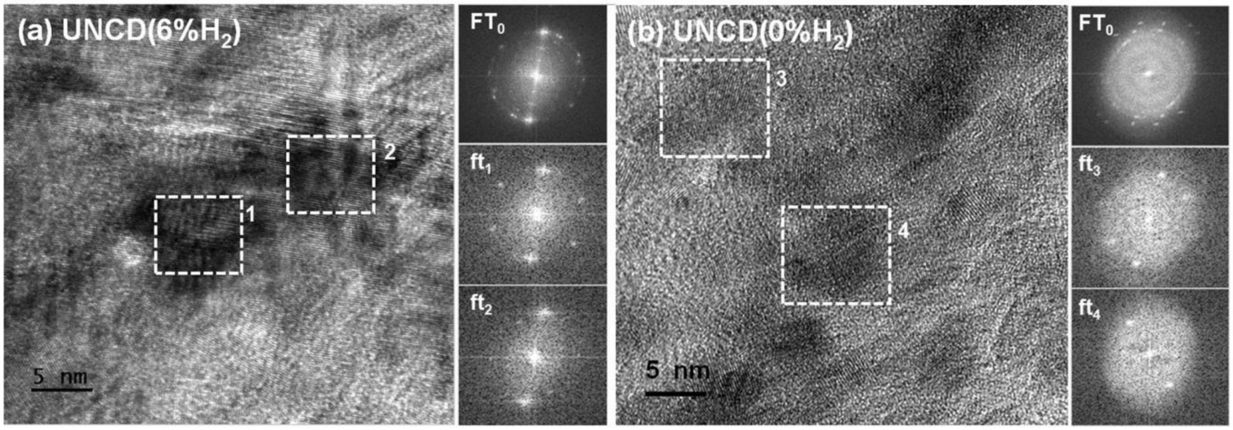

Fig. 6.4. *HRTEM image of (a) UNCD(6%H_2) and (b) UNCD(0%H_2) films, The FT_0 image in 'a' and 'b' shows the Fourier transformed diffractogram corresponding to entire structure image in 'a' and 'b', whereas FT_1 to FT_4 are FT images corresponding to areas 1 to 4, respectively*

In contrast, Fig. 6.4b shows the structure image of UNCD(0%H_2) films. The FT_0 image contains diffraction spots arranged in ring geometry indicating that the ultra-small diamond grains are randomly oriented. The FT_0 image contains a large central diffuse ring indicating the presence of more amorphous sp^2 bonded carbon in UNCD(0%H_2) films. The existence of ultra-small diamond grains is highlighted by ft_3 and ft_4 images which correspond to the regions 3 and 4, respectively. Notably, the diamond aggregates for UNCD(0%H_2) films contain ultra-small diamond grains which are still isolated from each other by grain boundary phases.

Curve I in Figs. 6.5a,b show the core-loss and plasmon-loss EELS spectra of UNCD(6%H_2) films, respectively which correspond to BF(TEM) micrographs in Fig. 6.3a_i.

These curves indicate that the UNCD(6%H_2) films are predominantly diamond (sp^3-bonded carbons) with very small content of sp^2-bonded carbons, as the core-loss EELS contains σ^*-band at 289.5 eV and secondary dip at 302 eV (curve I, Fig. 6.5a) with essentially no hump (π^*-band) at 284.5 eV [17-20].

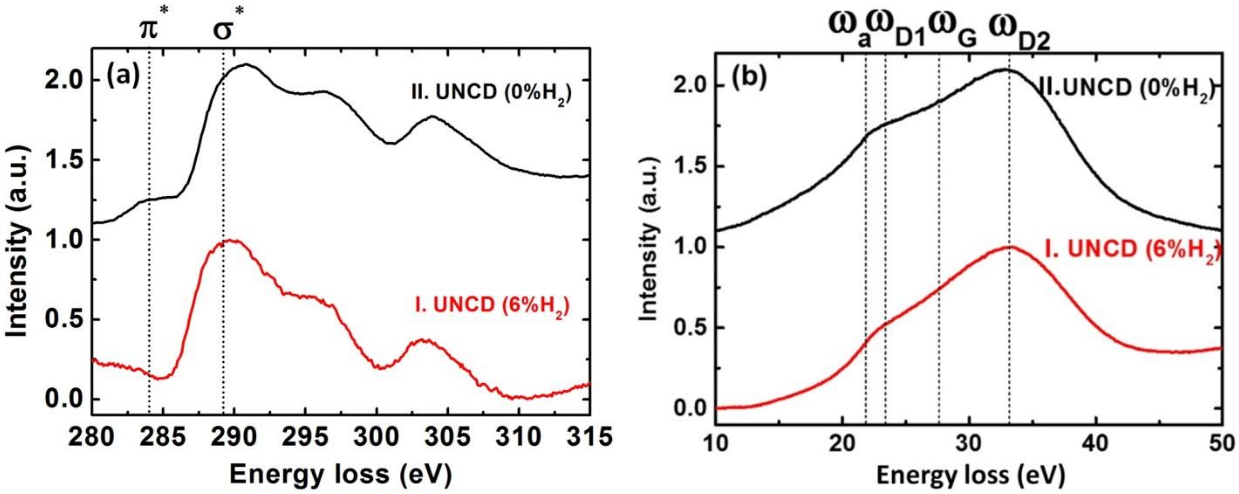

Fig. 6.5. *(a) Carbon edge core-loss EELS and (b) plasmon-loss EELS of (I) UNCD (6%H_2) and (II) UNCD (0%H_2) films, respectively*

Moreover, the plasmon-loss EELS contains ω_{D1}- and ω_{D2}-bands with $I\omega_{D1}/I\omega_{D2}$ ratio nearly $1/\sqrt{2}$ (curve I, Fig. 6.5b), which implies again the content of sp^2-bonded carbon in UNCD(6%H_2) films is very small. In contrast, curve II in Figs. 6.5a,b shows the core-loss and plasmon-loss EELS spectra of UNCD(0%H_2) films, respectively, which correspond to BF(TEM) micrographs in Fig. 6.3b$_i$. These curves indicate that UNCD(0%H_2) films are also predominantly diamond. The core-loss EELS of UNCD(0%H_2) films contain small hump (π^*-band) at 284.5 eV, implying that these films contain more sp^2-bonded carbon compared to UNCD(6%H_2) films. Furthermore, the plasmon-loss EELS of UNCD(0%H_2) films (curve II, Fig. 6.5b) contains ω_{D1}- and ω_{D2}-bands with the $I\omega_{D1}/I\omega_{D2}$ ratio slightly larger than $1/\sqrt{2}$. This implies that there exists some *a-C* phase besides diamond as denoted by ω_a-band. The observations in EELS spectroscopy for UNCD(6%H_2) and UNCD(0%H_2) films are in accord with those of TEM. Furthermore, XPS and Auger electron spectroscopy (AES) also indicated more sp^2-bonded carbon phase in UNCD(0%H_2) compared to UNCD(6%H_2) films [21].

6.3.3. Friction and wear properties of UNCD films

The friction coefficient values are found similar for both UNCD films in ambient tribo-conditions and it gradually decreases with the sliding process (Fig. 6.6). However, two distinct i.e. low and high friction regimes are observed in high vacuum tribo-conditions (3×10^{-6} mbar). In UNCD(6%H_2) films, the friction coefficient is low in the beginning of the sliding process and gradually increases to high value. On the other side, for UNCD(0%H_2) films, the friction coefficient is high from the beginning itself and does not change much afterwards.

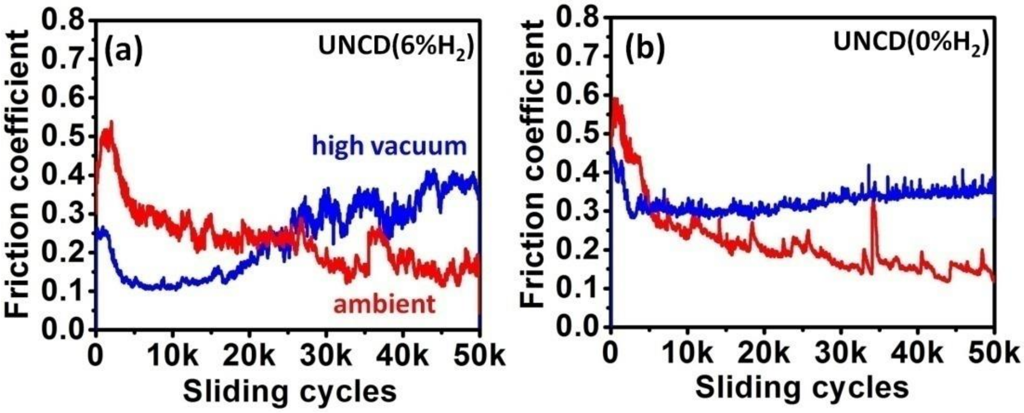

Fig. 6.6. *Friction coefficient of (a) UNCD(6%H_2) and (b) UNCD(0%H_2) films in ambient and high vacuum (3×10^{-6} mbar) tribology conditions*

6.3.4. Tribo-induced deformation behavior of UNCD films

The tribo-induced deformation analysis of wear tracks for both UNCD films i.e. UNCD(6%H_2) and UNCD(0%H_2) is studied using FESEM in both tribology conditions of ambient and high vacuum (3×10^{-6} mbar) as shown in Fig. 6.7 and Fig. 6.8. The nanostructured diamond feature is clearly preserved in both wear tracks in ambient condition being more noticeable for UNCD(6%H_2) films (Fig. 6.7a). However, transferlayer is locally formed in both wear tracks as indicated by arrows in high-resolution FESEM image. This is more evident at the edge of wear tracks where cracks within thick transferlayer are observed. More deformed wear track with severe plowing wear is observed for UNCD(6%H_2) films in high vacuum tribology condition (Fig. 6.8a). The wear track is plastically deformed and nanostructured diamond feature disappears as shown in high-resolution FESEM image. However, abrasive wear mechanism is governed in UNCD(0%H_2) films at HV tribology conditions (Fig. 6.8b).

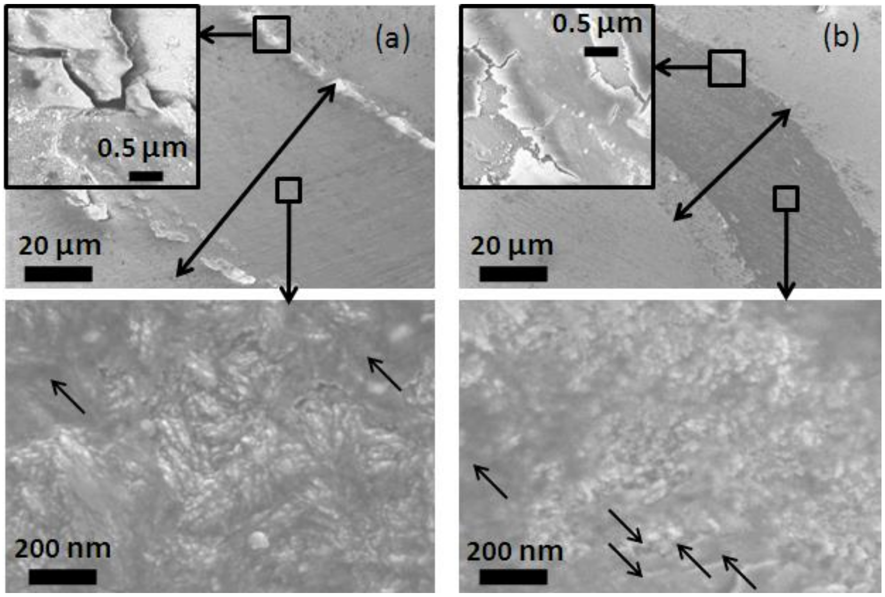

Fig. 6.7. *Wear track morphology of (a) UNCD(6%H_2) and (b) UNCD(0%H_2) films; tribology condition: ambient*

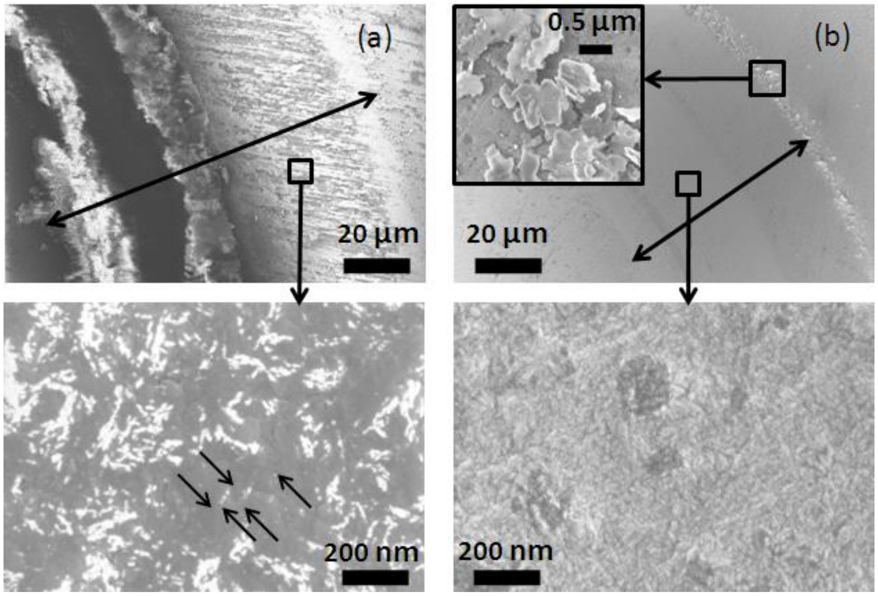

Fig. 6.8. *Wear track morphology of (a) UNCD(6%H_2) and (b) UNCD(0%H_2) films; tribology condition: high vacuum (3×10^{-6} mbar)*

In both films, the Ti-alloy substrate is not exposed to deformation process in both tribology conditions and the extent of deformation is well within the film surface only. This shows the extremely high wear resistance property of these films in both ambient and high vacuum conditions even after covering 5×10^{4} sliding cycles.

6.3.5. The chemical phase structural analysis of sliding interface

The chemical phase structural analysis of wear tracks and ball scars is carried out in ambient and high vacuum (3×10^{-6} mbar) tribology conditions using micro-Raman spectroscopy technique for both UNCD(6%H_2) and UNCD(0%H_2) films as shown in Fig. 6.9 and Fig. 6.10.

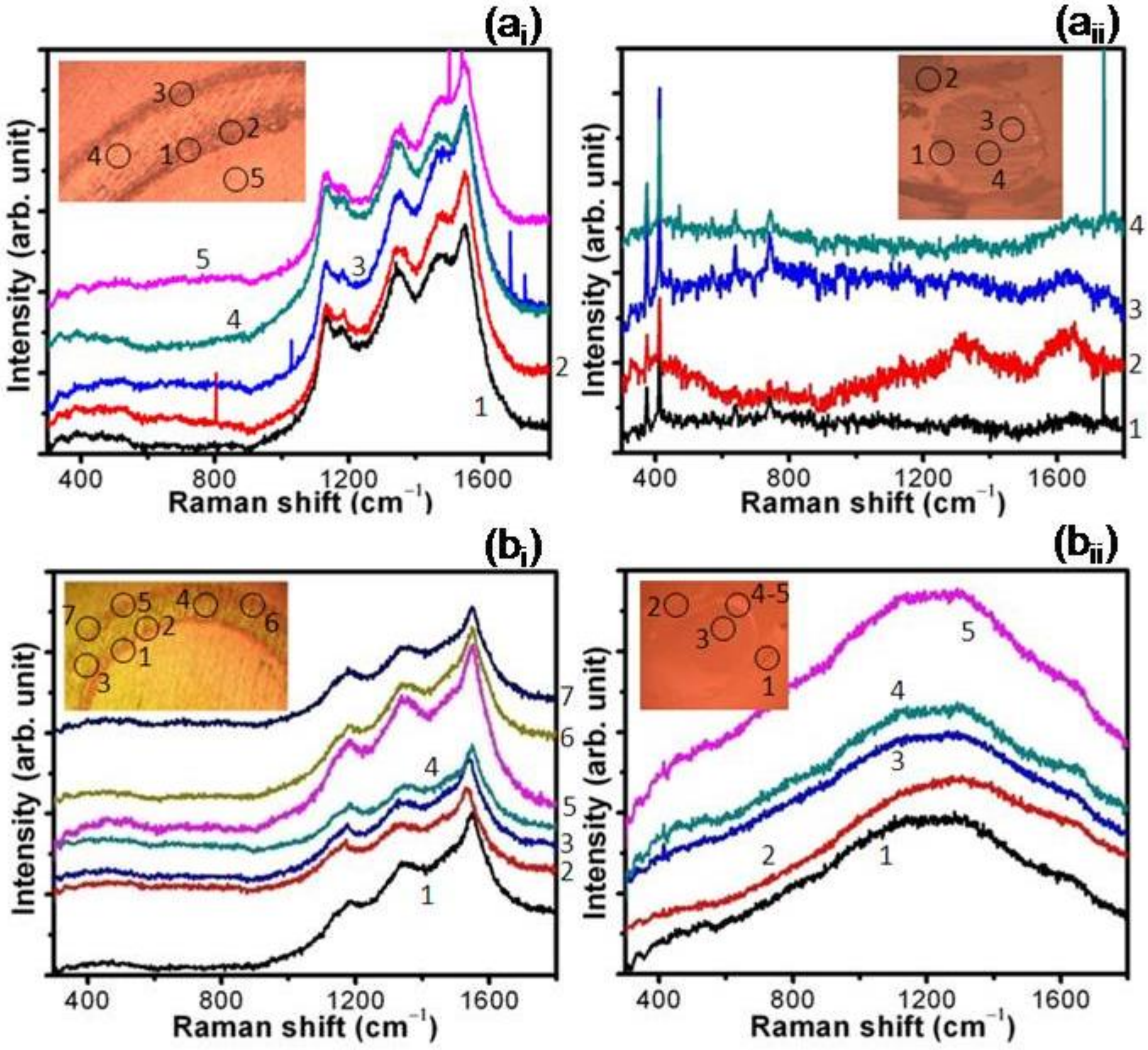

Fig. 6.9. *Raman spectra at various locations of: (a_i, b_i) wear track and (a_{ii}, b_{ii}) ball scar in the sliding combination of: (a_i, a_{ii}) UNCD(6%H_2)/Al_2O_3) and (b_i, b_{ii}) UNCD(0%H_2)/Al_2O_3; tribology condition: ambient*

The chemical structure of wear tracks is stable in both films and does not transform into *a-C*/graphite phase in ambient tribology conditions (Figs. 6.9a_i,b_i). However, weak signal of broad peaks is observed at 1320 cm^{-1} (D band) and 1620 cm^{-1} (G band), indicating the *a-C* structure formation [22] at the edge of ball scar for UNCD(6%H_2) films (Fig. 6.9a_{ii}). The carbon transferlayer is possibly quite thin in the sliding combinations of UNCD(0%H_2)/Al_2O_3 and strong luminescence signal of alumina with large background is observed (Fig. 6.9b_{ii}). In contrast, the chemical structure of wear track is largely transformed into carbonaceous *a-C*/graphite phase in high vacuum conditions in both films (Fig. 6.10).

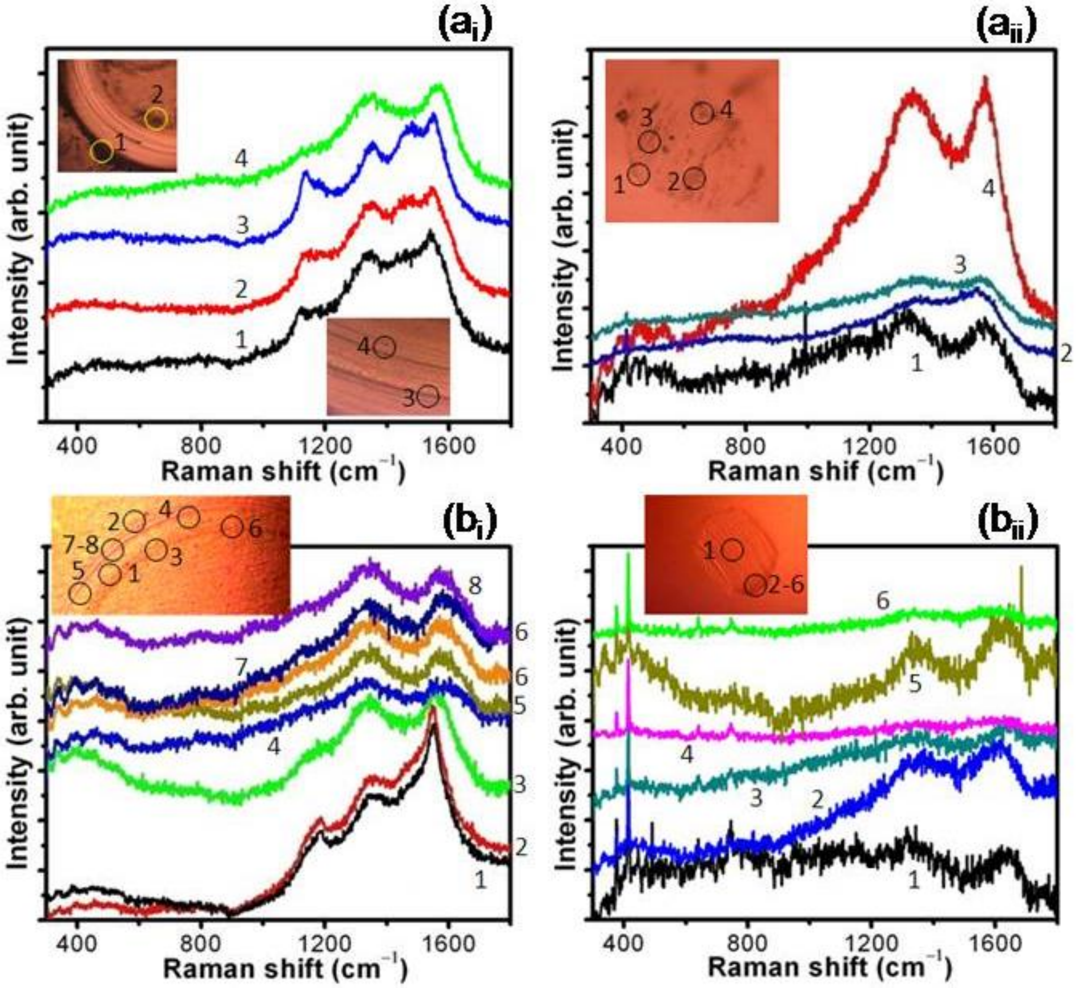

Fig. 6.10. *Raman spectra at various locations of: (a_i, b_i) wear track and (a_{ii}, b_{ii}) ball scar in the sliding combination of: (a_i, a_{ii}) UNCD(6%H_2)/Al_2O_3 and (b_i, b_{ii}) UNCD(0%H_2)/Al_2O_3; tribology condition: high vacuum (3×10^{-6} mbar)*

Though, this transformation is more prominent in UNCD(0%H_2) films compared to UNCD(6%H_2) films where the combination of five peaks are transformed to strong broad doublet around 1345 cm^{-1} and 1570 cm^{-1} with the disappearance of *t-PA* peaks (Fig. 6.10b_i). The evidence of *a-C* transferlayer is clearly observed on ball scars as well in high vacuum conditions which is associated to unstable UNCD structure at contact interface in the absence of passivation media (Figs. 6.10a_{ii},b_{ii}). Moreover, well resolved and strong peak of *a-C* (Fig. 6.10a_{ii}, curve 4) is related to intense localized amorphization process. The Raman signature of virgin Al_2O_3 ball lies in the range of 350 cm^{-1} to 800 cm^{-1} [23] and these bands are clearly seen on ball scars. Though weak feature of Al_2O_3 peaks is observed at wear track as well, indicating alumina transferlayer formation on wear tracks during sliding process. These results are in good agreement with FESEM analysis also as discussed in previous section.

6.3.5.1. The dynamics of transferlayer formation with sliding process

To study the evolution of transferlayer formation process, the micro-Raman spectra are recorded for sliding combination of UNCD(6%H_2)/Al_2O_3 at sliding cycles of 2×10^3, 5×10^3 and 1×10^4 in high vacuum tribology conditions as shown in Fig. 6.11. The gradual *a-C* transferlayer formation process on ball scars is clearly evident with the increasing number of sliding cycles.

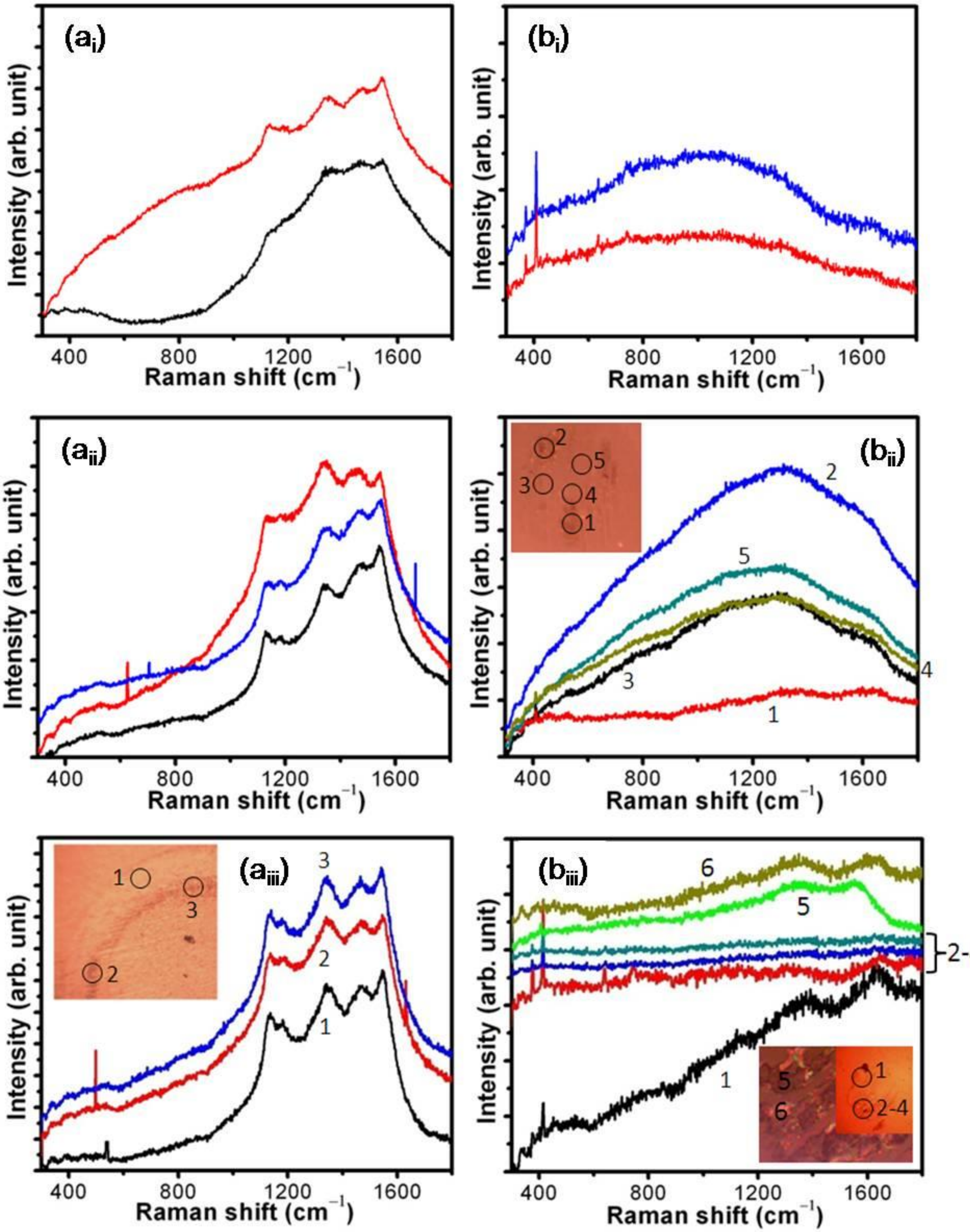

Fig. 6.11. *Raman spectra at various locations of: (a_i-a_{iii}) wear track and (b_i-b_{iii}) ball scar in the sliding combination of UNCD(6%H_2)/Al_2O_3 at sliding cycles of: (a_i, b_i) 2×10^3, (a_{ii}, b_{ii}) 5×10^3 and (a_{iii}, b_{iii}) 1×10^4; tribology condition: high vacuum (3×10^{-6} mbar)*

6.3.6. The elemental analysis of sliding interface

The EDX elemental mapping is also carried out for quantitative chemical analysis of transferlayer formation process on alumina ball scar for sliding combination of UNCD(0%H_2)/Al_2O_3 in both ambient and high vacuum tribology conditions (Fig. 6.12). The EDX mapping analysis clearly indicates that carbon concentration is high while oxygen and Al concentrations are low, suggesting significantly carbon enriched transferlayer formation on ball scar in high vacuum condition (Figs. 6.12a_{ii}-c_{ii}) compared to ambient (Figs. 6.12a_i-c_i). Moreover, XPS analysis also clearly indicates sp^2 rich transferlayer formation on ball scar in high vacuum condition compared to ambient tribo-conditions [21].

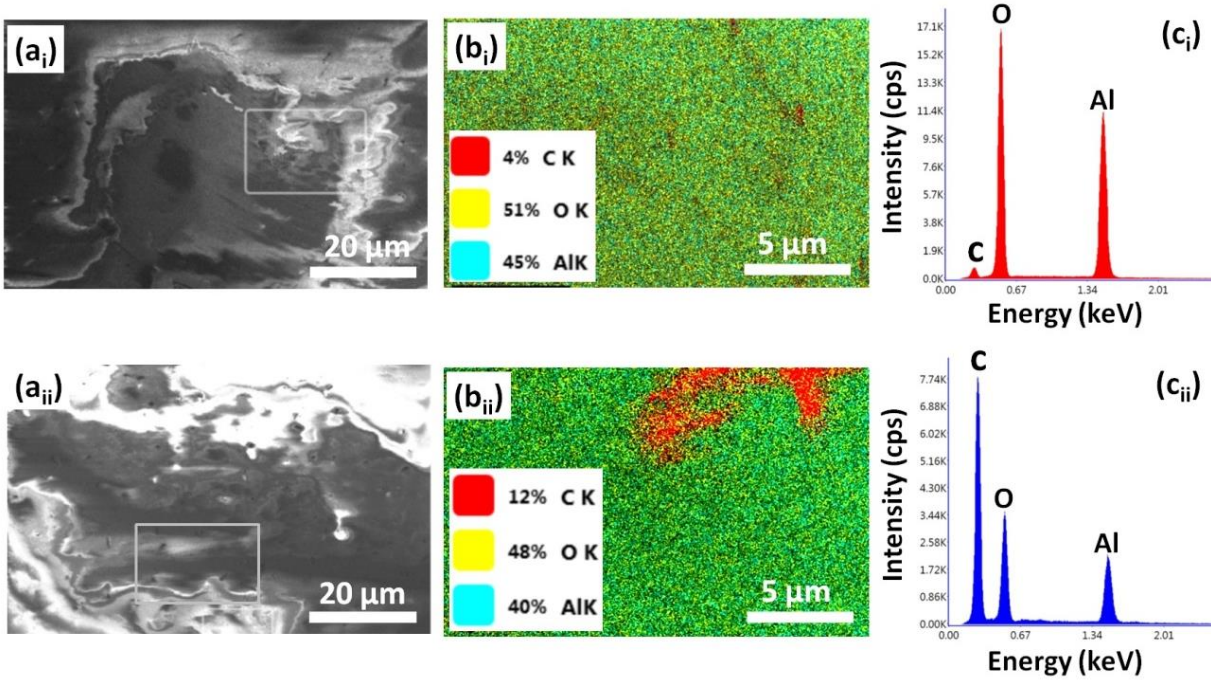

Fig. 6.12. *(a_i,a_{ii}) Backscattered diffraction (BSD) image, (b_i,b_{ii}) EDX elemental mapping image of square area indicated in panel (a_i, a_{ii}) and (c_i, c_{ii}) EDX spectra of alumina ball scar sliding against UNCD(0%) films; (a_i, b_i, c_i) for ambient and (a_{ii}, b_{ii}, c_{ii}) for high vacuum tribology conditions*

6.3.7. The tribology mechanism

In ambient atmosphere, both UNCD films show almost similar trend of friction coefficient. The diamond structural conversion into *a-C* and graphite phases is reported earlier for NCD films at mild tribo-contact conditions [10]. Even in DLC films, one possible mechanism is sliding induced fatigue where structural conversion takes place by micro-cracking [24]. The other mechanism in DLC films is related to flash temperature at contact interface due to kinetic energy of sliding bodies [25]. The water molecules/vapor passivate the unoccupied carbon dangling bonds of sp^3/sp^2 phases at tribo-contact area, forming carbon-oxygen complexes in ambient condition. The carbon transferlayer formation is not much significant on ball scar but strong oxygen signal is observed as evident from EDX analysis (Fig. 6.12c_i). The FESEM study indicates about the stability of wear track (Fig. 6.7). The micro-Raman analysis of wear track also clearly indicates stable chemical feature of UNCD structure which is almost similar to virgin film surface (Fig. 6.9a_i,b_i). However, very weak signal of *a-C* transferlayer is observed on ball scar in UNCD(6%H_2) case (Fig. 6.9a_{ii}). Furthermore, this layer coverage on ball scar is even less in UNCD(0%H_2) case as shown by micro-Raman (Fig. 6.9b_{ii}) and EDX analyses (Fig. 6.12a_i-c_i). Generally, such stability of UNCD structure in tribo-stressed condition is derived by passivation effect in ambient and moist conditions [26-29]. In stressful sliding, plastic deformation may take place and some of the sp^3 and sp^2 phases may collapse due to fatigue. However, these phases are instantaneously passivated by carbon-hydrogen and carbon-oxygen complexes which further restrict the UNCD transformation to *a-C*/graphite phases. Therefore, low friction and wear behavior of UNCD films is governed by passivation effect in ambient tribo-conditions.

The friction coefficient of UNCD(6%H_2) films is less up to 1×10^4 sliding cycles and gradually increases to high magnitude in high vacuum condition. The SIMS analysis shows large amount of hydrogen in these films (Fig. 6.1c_i). Here, low friction region is derived by intrinsic hydrogen present in these films which provides passivation of carbon dangling bonds in high vacuum condition. This fact is well reported in hydrogenated DLC and hydrogenated diamond nanostructured materials [30,31]. The UNCD(6%H_2) films show improved friction behavior in high vacuum condition as these contain small fraction of *a-C*/sp^2 phase as evident from HRTEM and Raman analyses. In the beginning of sliding cycles (2×10^3), no change in chemical structure of UNCD(6%H_2) films is observed in wear track and carbon signal on ball scar is negligible (Figs. 6.11a_i,b_i). However, *a-C* layer is gradually formed on ball scar with increasing sliding cycles (Figs. 6.11a_{ii},b_{ii}). Furthermore, at 1×10^4 cycles, the *a-C* signal (broad peak of D and G band) evolves on ball scar and other peaks related to UNCD structure are disappeared (Figs 6.11a_{iii},b_{iii}). At low friction regime, the spectral changes showing *a-C* transferlayer formation are localized at few locations of ball scar which are densely distributed at the end i.e. 5×10^4 sliding cycles (Fig. 6.10a_{ii}). Therefore, the conversion of UNCD to *a-C*/graphite phase is observed in high friction regime. In DLC films, it is reported that amorphization and graphitization do not assist in reducing the friction in high vacuum condition [30,32]. The reason for the gradual formation of *a-C* phase and increase in friction value is possibly explained by desorption of hydrogen under continuous tribo-stressed condition in high vacuum. The similar mechanism i.e. desorption of hydrogen after longer sliding cycles is reported in hydrogenated DLC films in high vacuum tribo-condition [2].

In contrast, stable high friction value is observed in UNCD(0%H_2) films in high vacuum conditions throughout the whole sliding process. Here, carbon transferlayer is significantly formed on ball scar as evident from micro-Raman spectroscopy (Fig. 6.10b_{ii}) and EDX (Figs. 6.12a_{ii}-c_{ii}) analyses. This can induce strong adhesive interaction between the sliding surfaces and thus, results in high friction value. The intrinsic hydrogen is limited in these films to passivate the sliding interfaces in vacuum conditions. Therefore, the friction value is higher during the initial sliding cycles and does not change further with time. It is well known that the low friction mechanism of graphite takes place in ambient conditions [33,34]. However, in high vacuum conditions, shear resistance of graphite plane increases due to lack of passivation which results in high friction and wear.

6.4. Conclusions

Two distinct UNCD films are deposited on Ti-alloy substrate by varying hydrogen concentration in MPECVD system. The tribological properties of these UNCD films are analyzed in ambient and high vacuum conditions. Friction coefficient of UNCD films containing excess hydrogen is less in high vacuum tribology condition up to limited number of sliding cycles. This is explained by the intrinsic hydrogen passivation mechanism of dangling carbon bonds. However, UNCD films with less hydrogen concentration show high friction value in high vacuum condition which is due to the limited intrinsic hydrogen passivation mechanism which results in extensive *a-C*/graphitic transferlayer formation on ball scar as evident from Raman spectroscopy and EDX analyses. Moreover, the chemical structure of wear track is largely transformed into carbonaceous *a-C*/graphite phase in high vacuum condition. This ultimately leads to increase in frictional resistance due to strong bond formation between *a-C*/graphitic phases across sliding interface. However, both UNCD films show less friction values with similar trend in ambient tribology conditions which is explained by the natural passivation mechanism of sliding interface by atmospheric chemical species.

6.5. References

1) E. Konca, Y.T. Cheng, A.M. Weiner, J.M. Dasch, A.T. Alpas, Effect of test atmosphere on the tribological behaviour of the non-hydrogenated diamond-like carbon coatings against 319 aluminum alloy and tungsten carbide, Surf. Coatings Technol. 200 (2005) 1783–91.
2) F. Gao, A. Erdemir, W.T. Tysoe, The tribological properties of low-friction hydrogenated diamond-like carbon measured in ultrahigh vacuum, Tribol. Lett. 20 (2005) 221–27.
3) Z. Feng, Y. Tzeng, J.E. Field, Friction of diamond on diamond in ultra-high vacuum and low-pressure environments, J. Phys. D Appl. Phys. 25 (1992) 1418–24.
4) J.D. Schall, G. Gao, J.A. Harrison, Effects of adhesion and transfer film formation on the tribology of self-mated DLC contacts, J. Phys. Chem. C 114 (2010) 5321–30.
5) K. Holmberg, A. Matthews, H. Ronkainen, Coatings tribology—Contact mechanisms and surface design, Tribol. Int. 31 (1998) 107–20.
6) H. So, The mechanism of oxidational wear, Wear 184 (1995) 161–67.
7) A. Mahato, A. Sachdev, S.K. Biswas, Lubricated tribology of a eutectic aluminium-silicon alloy in the ultra-mild wear and mild wear regimes for long sliding times, ACS Appl. Mater. Interfaces 2 (2010) 2870–79.
8) Y. Liu, A. Erdemir, E.I. Meletis, A study of the wear mechanism of diamond-like carbon films, Surf. Coatings Technol. 82 (1996) 48–56.
9) W. Qin, W. Yue, C. Wang, Understanding integrated effects of humidity and interfacial transfer film formation on tribological behaviors of sintered polycrystalline diamond, RSC Adv. 5 (2015) 53484–96.
10) M.I.D.B. Bouchet, C. Matta, B. Vacher, T.L. Mogne, J.M. Martin, J.V. Lautz, T. Ma, L. Pastewka, J. Otschik, P. Gumbsch, M. Moseler, Energy filtering transmission electron microscopy and atomistic simulations of tribo-induced hybridization change of nanocrystalline diamond coating, Carbon 87 (2015) 317–29.
11) I.I. Vlasov, V.G. Ralchenko, E. Goovaerts, A.V. Saveliev, M.V. Kanzyuba, Bulk and surface-enhanced raman spectroscopy of nitrogen-doped ultrananocrystalline diamond films, Phys. Stat. Sol. 203 (2006) 3028–35.
12) A.C. Ferrari, J. Robertson, Origin of the 1150 cm^{-1} Raman mode in nanocrystalline diamond, Phys. Rev. B 63 (2001) 121405–08.

13) A.C. Ferrari, J. Robertson, Raman spectroscopy of amorphous, nanostructured, diamond-like carbon, and nanodiamond, Philos. Trans. R. Soc. Lond. A 362 (2004) 2477–512.

14) K.J. Sankaran, N. Kumar, J. Kurian, R. Ramadoss, H.C. Chen, S. Dash, A.K. Tyagi, C.Y. Lee, N.H. Tai, I.N. Lin, Improvement in tribological properties by modification of grain boundary and microstructure of ultrananocrystalline diamond films, ACS Appl. Mater. Interfaces 5 (2013) 3614–24.

15) R. Arenal, G. Montagnac, P. Bruno, D.M. Gruen, Multiwavelength Raman spectroscopy of diamond nanowires present in n-type ultrananocrystalline films, Phys. Rev. B 76 (2007) 245316–21.

16) J. Birrell, J.E. Gerbi, O. Auciello, J.M. Gibson, J. Johnson, J.A. Carlisle, Interpretation of the Raman spectra of ultrananocrystalline diamond, Diam. Relat. Mater. 14 (2005) 86–92.

17) S. Prawer, R. Kalish, Ion-beam-induced transformation of diamond, Phys. Rev. B 51 (1995) 15712–22.

18) P. Kovarik, E.B.D. Bourdon, R.H. Prince, Electron-energy-loss characterization of laser-deposited a-C, a-C:H, and diamond films, Phys. Rev. B 48 (1993) 12123–29.

19) S.S. Chen, H.C. Chen, W.C. Wang, C.Y. Lee, I.N. Lin, J. Guo, C.L. Chang, Effects of high energy Au-ion irradiation on the microstructure of diamond films, J. Appl. Phys. 113 (2013) 113704–13.

20) S.D. Berger, D.R. McKenzie, P.J. Martin, EELS analysis of vacuum arc-deposited diamond like films, Philos. Mag. Lett. 57 (1988) 285–90.

21) R. Rani, K. Panda, N. Kumar, K.A. Titovich, K.V. Ivanovich, S.A. Vyacheslavovich and I.N. Lin, Tribological properties of ultrananocrystalline diamond films: Mechanochemical transformation of sliding interfaces, Sci. Rep. 8 (2018) 283−98.

22) A.C. Ferrari, Interpretation of Raman spectra of disordered and amorphous carbon, Phys. Rev. B 61 (2000) 14095–107.

23) R.S. Krishnan, Raman spectrum of alumina and the luminescence and absorption spectra of ruby, Nature 160 (1947) 26–26.

24) K.A. Laux, A.J. Fulcrand, H.J. Sue, T. Bremner, J.S.S. Wong, The Influence of surface properties on sliding contact temperature and friction for polyetheretherketone (PEEK), Polymer 103 (2016) 397–404.

25) R. Wei, P.J. Wilbur, M.J. Liston, G. Lux, Rolling-contact-fatigue wear characteristics of diamond-Like hydrocarbon coatings on steels, Wear 162–164 (1993) 558–68.

26) N. Kumar, R. Ramadoss, A.T. Kozakov, K.J. Sankaran, S. Dash, A.K. Tyagi, N.H. Tai, I.N. Lin Humidity-dependent friction mechanism in an ultrananocrystalline diamond film, J. Phys. D Appl. Phys. 46 (2013) 275501–08.

27) A.R. Konicek, D.S. Grierson, P.U.P.A. Gilbert, W.G. Sawyer, A.V. Sumant, R.W. Carpick, Origin of ultralow friction and wear in ultrananocrystalline diamond, Phys. Rev. Lett. 100 (2008) 235502–05.

28) A.R. Konicek, D.S. Grierson, A.V. Sumant, T.A. Friedmann, J.P. Sullivan, P.U.P.A. Gilbert, W.G. Sawyer, R.W. Carpick, Influence of surface passivation on the friction and wear behavior of ultrananocrystalline diamond and tetrahedral amorphous carbon thin films, Phys Rev. B 85 (2012) 155448–60.

29) A.V. Sumant, D.S. Grierson, J.E. Gerbi, J. Carlisle, O. Auciello, R.W. Carpick, Surface chemistry and bonding configuration of ultrananocrystalline diamond surfaces and their effects on nanotribological properties, Phys. Rev. B 76 (2007) 235429–39.

30) A. Grill, Review of the tribology of diamond-like carbon, Wear 168 (1993) 143–153.

31) S. Dag, S. Ciraci, Atomic scale study of superlow friction between hydrogenated diamond surfaces, Phys. Rev. B 70 (2004) 241401–04.

32) J. Andersson, R.A. Erck, A. Erdemir, Friction of diamond-like carbon Films in different atmospheres, Wear 254 (2003) 1070–75.

33) R.H. Savage, Graphite lubrication, J. Appl. Phys. 19 (1948) 1–10.

34) J.K. Lancaster, J.R. Pritchard, The influence of environment and pressure on the transition to dusting wear of graphite, J. Phys. D Appl. Phys. 14 (1981) 747–62.

Chapter 7

Summary and Future Scope

7.1. Summary of the thesis

The motivation behind the current thesis work is primarily to improve the friction and wear resistance properties of UNCD films in high temperature and controlled atmospheric tribo-conditions and comprehensive understanding of the respective governing tribo-mechanisms. With this purpose, the UNCD films are grown on Si substrate using optimized deposition parameters in MPECVD system. The microstructural, morphological and chemical characterization of UNCD films is carried out using HRTEM, EELS, FESEM, EDX, AFM, XPS and Raman spectroscopic techniques. The detailed tribological properties of UNCD films are studied using ball-on-disc geometry high temperature high vacuum micro-tribometer in ambient, distinct gaseous media, HV and HTHV tribo-conditions. It is evident from this work that the best tribological properties of UNCD films come from films where hard nanocrystalline diamond is embedded in a graphitic or sp^2 phase. The important findings of the entire thesis work can be summarized as below:

- Comprehensive understanding of effect of local phase composition on the tribological behavior of UNCD films and governing tribo-mechanisms is carried out. In CH_4/Ar plasma media, equiaxed morphology of UNCD films is observed while in CH_4/N_2 media, needle like morphology is observed. The graphitic tribofilm formation mechanism is established for low stable friction coefficient value in UNCD films where hard nanocrystalline diamonds are embedded in a graphitic or sp^2 phase in needle like morphology in ambient tribo-conditions.
- High run-in regime issue in UNCD films is addressed employing low energy (1 keV) Ar$^+$-ion sputtering process. The friction and wear resistance properties of surface modified UNCD films are found to improve with sputtering depth in all distinct tribo-environmental conditions of reactive and inert gaseous media. The tribological passivation mechanism across the sliding interface is established for observed low friction value in inert N_2 and chemically reactive CH_4 tribo-conditions. High friction in

ambient condition is associated with the oxidation of the sliding interfaces. The low friction in chemically inert Ar atmosphere is possibly due to the adsorption of inert Ar gaseous species at the sliding interface.

- The superlow friction value and ultrahigh wear resistance properties of UNCD films are studied in high temperature and high vacuum tribo-conditions. The passivation and graphitization/amorphization mechanisms are established for observed tribological response in UNCD films in distinct tribo-conditions of ambient, HV and HTHV.
- Novel hydrogenated UNCD films are deposited on Ti alloy substrate to address high friction response in high vacuum tribo-conditions. The intrinsic hydrogen passivation mechanism of dangling carbon bonds is established for low friction coefficient of UNCD films up to limited number of sliding cycles in high vacuum tribology condition. The interaction of carbonaceous *a-C* phase at sliding interface results in high friction value of UNCD films in high vacuum tribo-conditions once intrinsic hydrogen supply is exhausted.

7.2. Future scope

In this present thesis work, the underlying tribological mechanisms for improved friction and wear properties of UNCD films are established using experimental characterization techniques. However, several issues still need to be addressed to have better understanding about underlying tribological mechanisms as mentioned below:

- The study of the dynamics of transferlayer formation on contact interface with sliding process using depth-resolved XPS in distinct tribo-environmental conditions of high temperature, high vacuum etc. and its correlation with friction and wear trend.
- The correlation of friction and wear properties of UNCD films having nanowall morphology with wide tribo-test temperature range.
- Understanding the effect of Ti–6Al–4V substrate on observed high friction value of UNCD films in ambient conditions compared to UNCD films deposited on Si substrate.
- The enhancement in tribological properties of UNCD films in HV conditions for longer duration of sliding cycles by tuning the hydrogen concentration in deposition plasma media.

LIST OF ABBREVIATIONS

2D	two-dimensional
a_o	lattice constant
a-C	amorphous Carbon
AES	Auger Electron Spectroscopy
AFM	Atomic Force Microscopy
Ar	Argon gas
BF	Bright Field
BSE	Back Scattered Electron Image
CH_4	Methane gas
CMOS	Complimentary Metal Oxide Semiconductor
CVD	Chemical Vapor Deposition
DLC	Diamond like Carbon
ECR	Electrical Contact Resistance
EDX	Energy-Dispersive X-ray Spectroscopy
EELS	Electron Energy Loss Spectroscopy
eV	electron Volt
FCC	Face Centered Cubic
FESEM	Field Emission Scanning Electron Microscopy
FT	Fourier Transform
FWHM	Full Width at Half Maxima
HFCVD	Hot Filament Chemical Vapor Deposition
HRTEM	High-Resolution Transmission Electron Microscopy
HTHV	High Temperature High Vacuum
IC	Integrated Circuits
LIB	Lithium Ion Batteries
LVDT	Linear Variable Differential Transformer/Transducer
MCD	Microcrystalline Diamond
MEMS/NEMS	Micro/Nano Electromechanical Systems
MPECVD	Microwave Plasma Enhanced Chemical Vapor Deposition

NCD	Nanocrystalline Diamond
N_2	Nitrogen gas
NEXAFS	Near Edge X-ray Absorption Fine Structure Spectroscopy
NFC	Near Frictionless Carbon
PEEM	Photoelectron Emission Microscopy
PZT	Lead Zirconate Titanate
R_a	average Roughness
RH	Relative Humidity
RMS (R_q)	Root Mean Square Roughness
RT	Room Temperature
SAED	Selected Area Electron Diffraction
SIMS	Secondary Ion Mass Spectroscopy
t-PA	transpolyacetylene
UNCD	Ultrananocrystalline Diamond
XPS	X-ray Photoelectron Spectroscopy

Conference papers/presentations

1) ***Revati Rani***, N. Kumar, I-Nan Lin "Tribological properties of ultrananocrystalline diamond nanowire thin film: Influence of sliding counterbodies" International Conference on Thin Films ***ICTF-2017***, 13–17 Nov, 2017 at NPL-CSIR, New Delhi, India. [**Oral** presentation] https://arxiv.org/abs/1806.10765
2) ***Revati Rani***, N. Kumar, I-Nan Lin "Ultrananocrystalline diamond film: Tribological studies against metal and ceramic balls" 9th International Conference on Industrial Tribology ***ICIT-2017***, 6–9 Dec, 2017 at Vedic Village Spa Resort, Kolkata, India. [**Oral** presentation] https://arxiv.org/abs/1806.10302
3) ***Revati Rani***, N. Kumar, I-Nan Lin "Ultrahigh wear resistance of ultrananocrystalline diamond nanowall thin film" International Nanotribology Forum: Nanoscale Effects in Macrotribology ***INF NanoGoa-2018***, 8–12 Jan, 2018 at Dona Sylvia Beach Resort, Goa, India. [**Poster** presentation & awarded **full scholarship** for conference participation]
4) ***Revati Rani***, N. Kumar, I-Nan Lin "Tribological properties of ultrananocrystalline diamond thin films: Role of intrinsic hydrogen" International Conference on Nano Science and Technology ***ICONSAT-2018***, 21–23 March, 2018 at IISc, Bengaluru, India organised by CeNS, Bengaluru. [**Poster** presentation]
5) ***Revati Rani***, N. Kumar, I-Nan Lin "Smart ultrananocrystalline diamond thin films for tribological applications" 5th International Conference on Nanoscience and Nanotechnology ***ICONN-2019***, 28–30 January, 2019 at SRM Institute of Science and Technology, Chennai, India. [**Oral** presentation]
6) ***Revati Rani***, N. Kumar, I-Nan Lin "Tribological studies of surface modified ultrananocrystalline diamond thin films under inert and reactive gaseous tribo-atmospheric media" 26th International Symposium on Metastable, Amorphous and Nanostructured Materials ***ISMANAM-2019***, 08–12 July 2019 at Raintree, Annasalai, Chennai, India organized by IIT-Madras. [**Poster** presentation]

IGC report/article

- Invited article "High temperature and vacuum tribological properties of ultrananocrystalline diamond thin films" under the category of "***Young Officer Forum***" ***IGC Newsletter***, ISSN 0972-5741, Volume 116 April, 2018.

ICTF 2017

17th International Conference on Thin Films

November 13th-17th, 2017

Certificate of participation

This is to certify that Prof./Dr./Mr./[✓ Ms.] Revati Rani, (Oral Presentation)

from Indira Gandhi Centre for Atomic Research - Kalpakkam

has attended ICTF 2017 held during 13th-17th November 2017 at CSIR-National Physical Laboratory, New Delhi, India in collaboration of Indian Vacuum Society.

Dr. Sushil Kumar
Convener

Srikrishan Gupta
President IVS

Dr. D.K. Aswal
Conference Chair

TSI

बामर लॉरी एण्ड कं० लिमिटेड
(भारत सरकार का एक उद्यम)
Balmer Lawrie & Co. Ltd.
(A Government of India Enterprise)
SINCE 1867

CERTIFICATE

This is to certify that Revati Rani of IGCAR, HBNI Kalpakkam has participated in the 9th International Conference on Industrial Tribology organized by Balmer Lawrie & Co Ltd under the aegis of Tribology Society of India during 6-9 December 2017 at Kolkata India. She had presented a paper titled *Ultrananocrystalline Diamond Film: Tribological Studies Against Metal and Ceramic Balls* during this conference.

TRIBOLOGY SOCIETY OF INDIA
c/o Indian Oil Corporation Limited
Research & Development Centre
Sec.-13, Faridabad-121 007, Haryana, India
E-mail: info@tribologyindia.org

(Amit Kumar Basak)
Organising Secretary ICIT 2017

(Ajay Kumar Harinarain)
Secretary, TSI

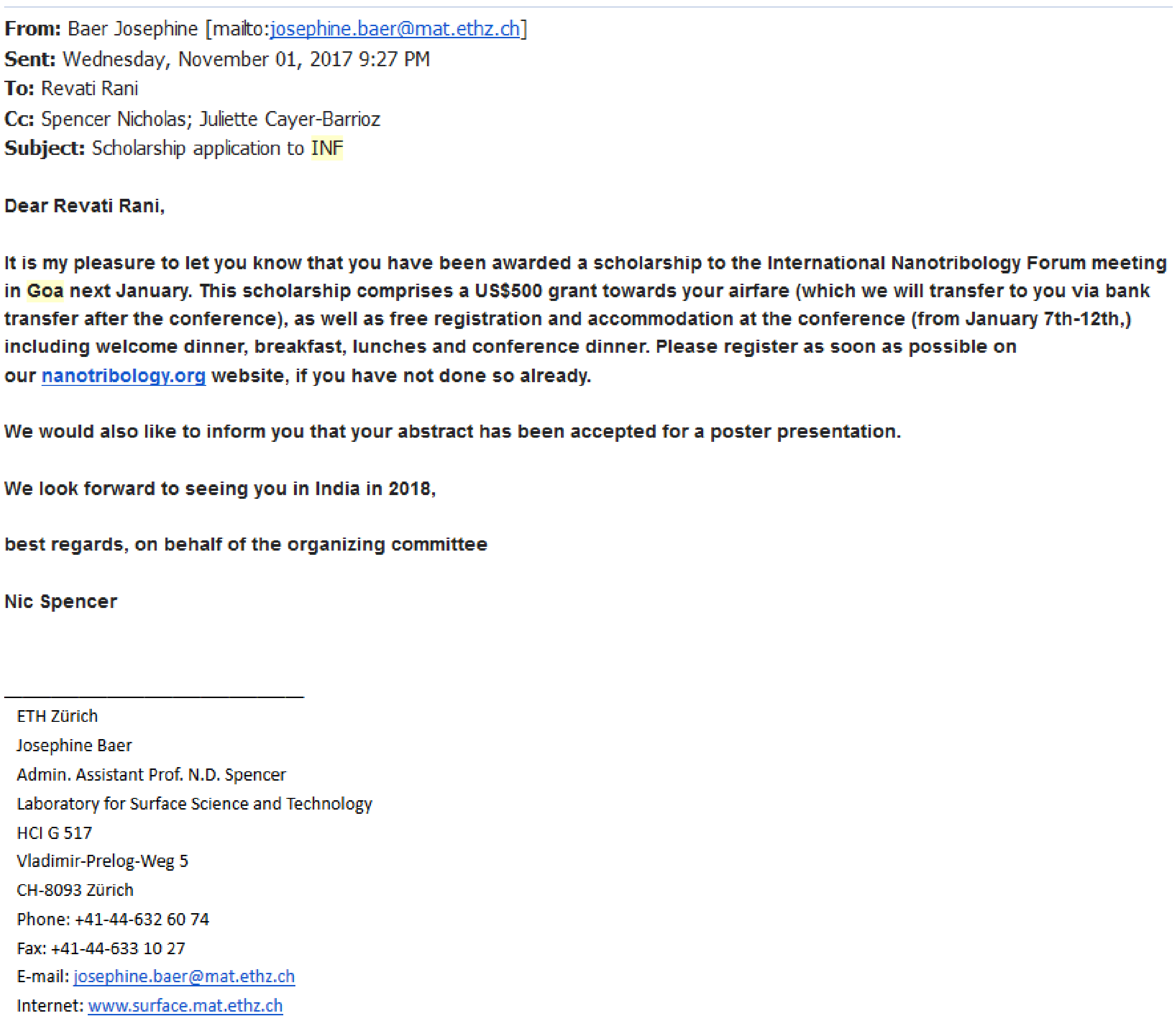

From: Baer Josephine [mailto:josephine.baer@mat.ethz.ch]
Sent: Wednesday, November 01, 2017 9:27 PM
To: Revati Rani
Cc: Spencer Nicholas; Juliette Cayer-Barrioz
Subject: Scholarship application to INF

Dear Revati Rani,

It is my pleasure to let you know that you have been awarded a scholarship to the International Nanotribology Forum meeting in Goa next January. This scholarship comprises a US$500 grant towards your airfare (which we will transfer to you via bank transfer after the conference), as well as free registration and accommodation at the conference (from January 7th-12th,) including welcome dinner, breakfast, lunches and conference dinner. Please register as soon as possible on our nanotribology.org website, if you have not done so already.

We would also like to inform you that your abstract has been accepted for a poster presentation.

We look forward to seeing you in India in 2018,

best regards, on behalf of the organizing committee

Nic Spencer

ETH Zürich
Josephine Baer
Admin. Assistant Prof. N.D. Spencer
Laboratory for Surface Science and Technology
HCI G 517
Vladimir-Prelog-Weg 5
CH-8093 Zürich
Phone: +41-44-632 60 74
Fax: +41-44-633 10 27
E-mail: josephine.baer@mat.ethz.ch
Internet: www.surface.mat.ethz.ch

ICONSAT 2018
INTERNATIONAL CONFERENCE ON
NANOSCIENCE AND TECHNOLOGY
MARCH 21-23, 2018 BENGALURU

Supported by
Nano Mission
Department of
Science and Technology
Government of India

Organized by
CeNS
Centre for Nano and
Soft Matter Sciences

CERTIFICATE OF PARTICIPATION

This is to certify that

Ms. Revati Rani

IGCAR, Kalpakkam

participated and made a poster presentation at the

International Conference on Nanoscience and Technology

(ICONSAT-2018) held during 21-23 March 2018, Bengaluru.

P. K. Santra

Dr. Pralay K. Santra
Convenor, ICONSAT-2018

Prof. G. U. Kulkarni
Chairman, ICONSAT-2018

SRM
INSTITUTE OF SCIENCE & TECHNOLOGY
(Deemed to be University u/s 3 of UGC Act, 1956)

5th International Conference on Nanoscience and Nanotechnology (ICONN 2019)

ICONN 2019

SRM INSTITUTE OF SCIENCE AND TECHNOLOGY

Kattankulathur - 603 203

CERTIFICATE

This is to certify that Mr. / Ms. / Dr. Revati Rani *has* ***Participated / Presented a Paper*** *entitled* Smart Ultrananocrystalline Diamond Thin-films for Tribological Application *in the International Conference on Nanoscience and Nanotechnology (ICONN 2019) organized by Department of Physics and Nanotechnology, SRM IST - India during 28 - 30th January 2019, in association with Shizuoka University, Japan; National Chiao Tung University, Taiwan; GNS Science, New Zealand; CSIR - National Physical Laboratory, India; Asian Consortium on Computational Materials Science and The Institution of Engineering and Technology, co-sponsored by Science & Engineering Research Board (DST-SERB) & CSIR India.*

Head, Dept. of Physics and Nanotechnology
SRM IST

Dean (Sciences)
SRM IST

Shizuoka University, Japan · NCTU, Taiwan · GNS, New Zealand · CSIR-NPL · ACCMS · IET (The Institution of Engineering and Technology)

ISMANAM - 2019

26th International Symposium on Metastable, Amorphous and
Nanostructured Materials
8-12, July 2019, Chennai, India

This is to certify that Mr./Ms./Dr. *Revati Rani, IGCAR Kalpakkam*

has participated and presented a paper titled *Tribological studies of surface modified ultra-nanocrystalline diamond thin films under inert and reactive gaseous tribo-atmospheric media* at the **"26th International Symposium on Metastable, Amorphous and Nanostructured Materials",** organized by the Department of Metallurgical and Materials Engineering, Indian Institute of Technology Madras, Chennai during 8-12, July 2019.

N. K. Mukhopadhyay

Prof. V. Sampath
Chair, Technical Committee
ISMANAM - 2019

Prof. B.S. Murty
Co – Chair
ISMANAM - 2019

Prof. N. K. Mukhopadhyay
Co – Chair
ISMANAM - 2019

Young Officer's FORUM

Ms Revati Rani is working as Scientific Officer in Materials Science Group. She is from 8th batch of BARC Training school at IGCAR campus. She has completed her M.Sc. (Physics) from Kurukshetra University, Haryana in 2012. She is currently pursuing her Ph.D (Physical Sciences) from HBNI under the guidance of Dr. Niranjan Kumar. Her research interest includes tribo-chemical investigation of low friction mechanisms in nanocrystalline diamond films under high-temperature and high-vacuum conditions.

High Temperature and Vacuum Tribological Properties of Ultrananocrystalline Diamond Thin Films

Tribology is derived from the Greek word *tribos*, which means "rubbing" and it is defined as the study of two surfaces in relative motion under the application of load, leading to friction and wear. The coefficient of friction is defined as the ratio of frictional force to normal load. Fundamentally, it is proportional to the normal load and depends on the real area of contact. Low friction and high wear resistance properties of materials are desirable for efficient and durable sliding devices. The carbon based materials are attractive for tribological purposes due to tunable hybridization state of carbon atom. The deposition of crystalline diamond films onto the the transformation of sp^3 crystalline diamond into sp^2 and α-C phases is responsible for the deformation of the sliding surfaces. The tribo-test environment including the internal chemical structure of films are governing factors for determining passivation and/or graphitization mechanisms. The tribological properties of UNCD thin films are investigated in (a) ambient atmosphere and room temperature (AART) (b) high vacuum $\sim 5\times10^{-6}$ mbar and room temperature (HVRT) and (c) high-temperature $\sim$623 K and high-vacuum $\sim 5\times10^{-6}$ mbar (HTHV) tribo-environmental conditions. Raman spectroscopy and X-ray photoelectron

Homi Bhabha National Institute

Ph.D. PROGRAMME

PRE SYNOPSIS RECOMMENDATION REPORT

1. **Name of the Student :** REVATI RANI
2. **Name of the Constituent Institution :** IGCAR-Kalpakkam
3. **Enrolment No. and Date of Enrolment :** PHYS02201604002 and 1st Aug, 2016
4. **Title of the Thesis :** Tribological properties of ultrananocrystalline diamond films at high temperature and controlled atmosphere
5. **Board of Studies :** Physical Sciences

Report of Doctoral Committee

Ms Revati Rani gave detailed Pre-synopsis public viva presentation, outlining her PhD thesis work and brought out salient results. Her thesis consists of four core chapters apart from the introduction, experimental details and summary & future direction chapters. She has published four journal publications and presented her work in total six international conferences. She has answered all queries from the audience and DC members. In view of this, DC recommends submission of Synopsis by the candidate.

Doctoral Committee:

S. No.	Name	Designation	Signature	Date
1.	Dr. N. V. Chandra Shekar	Chairman	N.V. Chandra Sk	26/9/19
2.	Dr. M. Kamruddin	Guide & Convener		26/9/19
3.	Dr. T. R. Ravindran	Member		26/9/2019
4.	Dr. B. Sundaravel	Member	B. Sundaravel	26/9/2019
5.	Dr. Shaju K Albert	Member		26/9/19

Signature
Dean-Academic
30/09/19

To

Dean, HBNI

Homi Bhabha National Institute

Proposed List of Ph.D Thesis Reviewers*

1. **Name of the Student:** REVATI RANI
2. **Name of the Constituent Institution:** IGCAR-Kalpakkam
3. **Enrolment No. :** PHYS02201604002
4. **Title of the Thesis:** Tribological properties of ultrananocrystalline diamond films at high temperature and controlled atmosphere
5. **Board of Studies:** Physical Sciences

S. No.	Name, postal & email address of proposed reviewers	Field of specialization	Give details if he/she reviewed thesis of your student(s) in previous one year
1.	**Prof. C S Ramesh** Dean, Research & Innovations, Department of Mechanical Engineering, Presidency University, Bangalore 560 064, India Email: rameshcs@presidencyuniversity.in	Tribology, Mechanical properties, Coatings, Mechanical behavior of materials, Metallurgical engineering, Composites, Materials characterization	
2.	**Prof. Rajnesh Tyagi** Department of Mechanical Engineering, Indian Institute of Technology, Banaras Hindu University, Varanasi 221005, India Phone: +917607384674 Email: rtyagi.mec@itbhu.ac.in	Tribology, Materials development, Composite materials, High temperature wear and self lubrication, Surface engineering	

3.	**Prof. Manish Roy** Defence Metallurgical Research Laboratory, Defence Research and Development Organization, Defence Research Complex, P.O. Kanchanbagh, Hyderabad 500058, India Email: manish@dmrl.drdo.in	Tribology, Friction, Wear testing, Nanoindentation, Tribo-corrosion, Surface characterization, Surface modification, Surface science, Materials and surface engineering for ambient temperature and elevated temperature tribological applications, Metallurgical engineering	
4.	**Prof. M. Kamaraj** Associate Professor Office : MSB 105 Lab : Mechanical Testing Lab & High Temperature Lab, Indian Institute of Technology Madras, Chennai 600036, India Phone : (91)-44-2257-4769 Email: kamaraj@iitm.ac.in	Surface engineering, Tribology, Wear behavior of coatings, and Inter-metallic reinforced PM base composites, High temperature deformation behavior of advanced materials	
5.	**Prof. Vikram Jayaram** **Chair, Division of Mechanical Sciences,** Department of Materials Engineering, Indian Institute of Science, Bangalore 560 012, India Phone: +91 80 2293 3243 Email: qjayaram@iisc.ac.in qjayaram@materials.iisc.ernet.in	Mechanical testing, Thin film mechanical characterization, Materials, Metallurgy, Ceramics, Phase transformations, Electron microscopy, Materials characterization	
6.	**Prof. Om P Khatri** Indian Institute of Petroleum, Tribology and Combustion Division, Mohkampur, Dehradun 248 005, India Phone: +91 135 2525 767 Email: opkhatri@iip.res.in	Micro/nano-tribology, Friction reduction practice**,** Extreme thin lubricating film**,** Tribochemistry**,** Micro/nano structure	

7.	**Prof. Noritsugu Umehara** Department of Mechanical Science & Engineering, Graduate School of Engineering, Nagoya University, Furo-cho, Chikusa-ku, Nagoya-City, Aichi 464-8603, Japan Phone: +81-52-789-2785 Email: ume@mech.nagoya-u.ac.jp	Micro/nano-tribology, Material effects, Surface texturing, Adhesion, Surface temperature, Micro/nano structure, DLC, Composite materials, Surface treatments/coatings	
8.	**Prof. Zahrul Fuadi** Department of Mechanical Engineering, Syiah Kuala University, Jl. T. Syech Abdul Rauf No. 7 Darussalam, Banda Aceh 23111, Indonesia Phone: +62-651-7552222 Email: zahrulfuadi@gmail.com	Lubricant effects, Wear of specific materials, Extreme thin lubricating film, Adsorption/adsorbed film, Micro/nano structure, Automotive/marine/aircraft lubricating oils, Mineral oils, Steel, DLC	
9.	**Prof. Shahira Liza Kamis** Senior Lecturer Tribology Precision and Machining (TriPreM) *i*-khoza, Department of Mechanical Precision Engineering (MPE), Malaysia-Japan International Institute of Technology, Universiti Teknologi Malaysia (UTM), Kuala Lumpur 54100, Kuala Lumpur, Malaysia Phone Office:03- 2203 1315 Email: shahiraliza@utm.my shahiraliza@gmail.com	Tribology, Surface modification, Thin films, Biomaterials	

Doctoral Committee:

S. No.	Doctoral Committee	Name	Signature	Date
1.	Chairman	Dr. N. V. Chandra Shekar		26/9/19
2.	Guide/ Convener	Dr. M. Kamruddin		26/9/19
4.	Member-1	Dr. T. R. Ravindran	T R Ravindran	26/9/2019
5.	Member-2	Dr. B. Sundaravel	B. Sundaravel	26/9/2019
6.	Member-3	Dr. Shaju K Albert		26/9/19.

Dean-Academic, CI
30/09/19

To
Dean, HBNI